NASA CR-
ERIM 1193-3-F

Final Report

ATMOSPHERIC MODELING RELATED TO THEMATIC MAPPER SCAN GEOMETRY

W.A. MALILA, J.M. GLEASON and R.C. CICONE
Infrared and Optics Division

APRIL 1976

(NASA-CR-147792) ATMOSPHERIC MODELING RELATED TO THEMATIC MAPPER SCAN GEOMETRY Final Report, 6 Feb. - 31 Mar. 1976 (Environmental Research Inst. of Michigan) 132 p HC $6.00 CSCL 04A G3/43

N76-26675

Unclas
44736

Prepared for
NATIONAL AERONAUTICS AND SPACE ADMINISTRATION
Earth Resources Program Office, Code HA
Johnson Space Center
Houston, Texas 77058
and
Earth Resources Branch, Code 920
Goddard Space Flight Center
Greenbelt, Maryland 20771

Contract NAS9-14319, Task II

ENVIRONMENTAL
BOX 618 ANN ARBOR MICHIGAN 48107

Sponsorship. The work reported herein was conducted by the Environmental Research Institute of Michigan for the National Aeronautics and Space Administration's Johnson Space Center (JSC), Houston, Texas 77058, and Goddard Space Flight Center (GSFC), Greenbelt, Maryland 20771, under Task II of Contract NAS9-14819 with the JSC. Mr. Jay Harnage/HC is Technical Monitor for JSC and Dr. Louis Walker/920 is Technical Monitor for GSFC.

This report comprises the final report for the Task II effort under the contract. Results for the major task (Task 1) of the contract will be reported separately.

Contracts and grants to the Institute for the support of sponsored research are administered through the Office of Contracts Administration.

TECHNICAL REPORT STANDARD TITLE PAGE

1. Report No. NASA CR-ERIM 119300-5-F	2. Government Accession No.	3. Recipient's Catalog No.
4. Title and Subtitle FINAL REPORT ON ATMOSPHERIC MODELING RELATED TO THEMATIC MAPPER SCAN GEOMETRY		5. Report Date April 1976 6. Performing Organization Code
7. Author(s) W. A. Malila, J. M. Gleason, and R. C. Cicone		8. Performing Organization Report No. 119300-5-F
9. Performing Organization Name and Address Environmental Research Institute of Michigan Infrared and Optics Division P. O. Box 618 Ann Arbor, Michigan 48107		10. Work Unit No Task II 11. Contract or Grant No. NAS9-14819
12. Sponsoring Agency Name and Address National Aeronautics and Space Administration Johnson Space Center Earth Resources Program Office/HA Houston, Texas 77058		13. Type of Report and Period Covered Final Report 6 February through 31 March 1976 14. Sponsoring Agency Code

15. Supplementary Notes
Mr. Jay Harnage/HC is Technical Monitor for NASA JSC. Task II was jointly sponsored by the JSC and the NASA Goddard Space Flight Center, Greenbelt, Md. 20771, with Dr. Louis Walter/920 as GSFC Technical Monitor. Results under Task I are being reported separately.

16. Abstract

A simulation study was carried out to characterize atmospheric effects in LANDSAT-D Thematic Mapper data. In particular, the objective was to determine if any differences would result from using a linear vs. a conical scanning geometry. Insight also was gained about the overall effect of the atmosphere on Thematic Mapper signals, together with the effects of time of day. An added analysis was made of the geometric potential for direct specular reflections (sun glint).

The ERIM multispectral system simulation model was used to compute inband Thematic Mapper radiances, taking into account sensor, atmospheric, and surface characteristics. Separate analyses were carried out for the thermal band and seven bands defined in the reflective spectral region. Reflective-region radiances were computed for 40°N, 0°, and 40°S latitudes; June, Mar., and Dec. days; and 9:30 and 11:00 AM solar times for both linear and conical scan modes. Also, accurate simulations of solar and viewing geometries throughout Thematic Mapper orbits were made.

It was shown that the atmosphere plays an important role in determining Thematic Mapper radiances, with atmospheric path radiance being the major component of total radiances for short wavelengths and decreasing in importance as wavelength increases. Path radiance was shown to depend heavily on the direct radiation scattering angle and on haze content. Scan-angle-dependent variations were shown to be substantial, especially for the short-wavelength bands.

17. Key Words	18. Distribution Statement
Thematic Mapper Atmospheric Effects Simulation Multispectral Scanner	Initial distribution is listed at the end of this document.

19. Security Classif. (of this report)	20. Security Classif. (of this page)	21. No. of Pages	22. Price
UNCLASSIFIED	UNCLASSIFIED	132	

16. Abstract (Continued)

Surface bidirectional reflectance effects were found to be of significance in total radiances only for the longest wavelength reflective band for which they were computed for a sparse and a dense green wheat canopy.

It was concluded that no major differences should be expected between overall atmospheric effects from 70°N to 70°S latitude for the linear and conical scan modes, based on a qualitative extrapolation of radiance simulation results to key latitudes through their relationship to scattering angle. Specific differences would exist for sub-ranges of latitudes. No significant difference was found between sizes of geometric sun glint potential zones for linear, forward-looking conical, and rearward-looking conical scan modes; those for the forward-looking conical mode were slightly smaller.

An 11:00 AM orbit would have a greater dynamic range of signal levels, greater variance due to scan angle and other effects, and a greater geometric potential for sun glints than a 9:30 AM orbit. However, the important quantity, ratio of ground signal to path radiance, is roughly the same for comparable conditions for the two orbit times. Consideration of the important factor of effect of orbit time on crop discrimination was not within the scope of this study.

Radiances for the 0.74–0.80-μm and 0.80–0.91-μm bands were found to be highly correlated ($\geq$0.9993) lending support to the earlier decision to combine them into a single band.

Recommended steps are given to follow in a more quantitative comparison of the relative effects of scan mode on the usefulness of Thematic Mapper signals, if required. To support system design efforts, more complete simulation and quantitative analysis of Thematic Mapper radiances, atmospheric effects, and crop discrimination are recommended. Also recommended are additional analyses to relate geometric sun glint potentials to actual sea surface conditions for a more complete assessment of the problem, and to study comparable effects on land surfaces.

PREFACE

This report describes efforts on Task II of a project studying system specifications for the LANDSAT-D Thematic Mapper (multispectral scanning system). The contract management resides with NASA's Lyndon B. Johnson Space Center, Houston, Texas. Task II was jointly sponsored by NASA's Goddard Space Flight Center, Greenbelt, Maryland.

The Task II effort was a "quick-response" effort in which simulation parameters were defined in the first few days and radiance simulations were carried out soon thereafter. The major question addressed in Task II was the effect of scan mode (linear vs. conical) on atmospheric effects in Thematic Mapper signals. Initial results were provided as generated. A relaxation in the time schedule according to which final results were required enabled (a) a more accurate calculation and simulation of Thematic Mapper orbit and scanning geometry relative to the sun position, (b) more thorough analyses of the simulation results, and (c) the examination of additional questions such as time of orbit and geometric potential for sun glint.

The research covered in this report was performed under Contract NAS9-14819, Task II, during the period 6 February 1976 through 31 March 1976. Technical Monitors were Mr. Jay Harnage, Code HC, JSC, and Dr. Louis Walter, Code 920, GSFC. The task was directed by Mr. R. R. Legault, a Vice-President of the Environmental Research Institute of Michigan (ERIM), and Dr. J. D. Erickson, Principal Investigator and Head of the ERIM Information Systems and Analysis Department. Dr. W. A. Malila was Task Leader. The ERIM report number is 119300-5-F. The Task I effort is being reported separately.

The authors acknowledge the use of mathematical models for atmospheric effects developed by Dr. R. E. Turner and for vegetation canopy bidirectional reflectance by Dr. G. H. Suits, both of ERIM. Mr. J. L. Beard contributed the derivation of Eq. (6), an initial analysis of the sun glint problem, and the basic mathematical analysis presented in Sec. 4. Secretarial services of Miss D. Dickerson are also acknowledged.

CONTENTS

FIGURES

FIGURES (Cont'd)

FIGURES (Cont'd)

FIGURES (Cont'd)

TABLES

TABLES (Cont'd)

1
SUMMARY, CONCLUSIONS, AND RECOMMENDATIONS

There are a great number of sensor, atmospheric, and surface factors which interact to produce the radiances observed by a sensor such as the LANDSAT-D Thematic Mapper. In this study, radiance simulations with the ERIM multispectral system simulation model were carried out in which most of the major factors were varied and their relative importances determined and/or demonstrated. The major objective of the effort was to characterize any differences between atmospheric effects in Thematic Mapper data that would result from using a linear vs. a conical scanning mode. In addition, a realistic simulation of scanning and solar geometries throughout orbital passes was accomplished and an analysis of the geometric potential for specular reflection (sun glint) was carried out.

Based on these simulations and analyses, the following conclusions were drawn and recommendations are made.

1.1 CONCLUSIONS

(1) Atmospheric effects have been shown to play an important role in determining Thematic Mapper radiances.

(a) Atmospheric path radiance is by far the major component of radiances in the short-wavelength Thematic Mapper bands, but decreases in importance as wavelength increases.

(b) Substantial variations in path radiance occur that depend on scan angle.

(c) Path radiance effects are intensified by an increase in atmospheric haze content.

(d) A strong dependence between path radiance and the direct radiation scattering angle was demonstrated.

(e) One important factor which was not varied in this study, but which affects reflective-region path radiance, is background albedo.

(f) In the thermal band, there is nearly complete compensation between path transmittance and path radiance effects, so changes in path length and/or atmosphere condition produce only very minor changes in total inband radiance.

(2) Surface bidirectional reflectance effects for the two (sparse and dense green wheat) canopies examined were found to produce significant variations in total inband radiances only for the longest wavelength band for which calculations were made (0.74-0.91 μm); in this band, path radiance was a relatively minor component of total radiance.

(3) The positions of the sun and the comparable satellite headings and scanner geometry also are important factors for reflective-band radiances.

(a) Total irradiance depends directly on solar zenith angle.

(b) Solar azimuth angle, satellite heading, and scanner geometry also help determine scattering angles and conditions for which there is potential for sun glint.

(4) No major differences should be expected between overall atmospheric effects for the linear and conical scan modes, based on a comparison of the geometric and radiance simulations.

(a) Essentially the same range of scattering angles applies to each scan mode, although the latitudes at which peak angles occur differ between modes.

(b) Reflective-region path radiance is highly correlated with scattering angle.

(c) The latitudes for which radiances were simulated are not sufficient of themselves to permit a definitive comparison of radiances for the two scan modes for the full range of the orbits, but can be qualitatively extrapolated to the key latitudes through the scattering angle relationship.

(d) Indications from the scattering angle analysis are that a forward-looking scanner might have slightly less atmospheric effects than a linear scanner, and slightly more than a rearward-looking conical scanner.

(e) If one were to restrict the range of latitudes of interest, e.g., to the mid-northern latitudes, substantial differences in atmospheric effects between scan modes could be expected.

(f) In the thermal band, there was essentially no difference in radiances for the two scan modes.

(5) No significant difference was found between potential sun glint zones for the linear and conical scanners in the reflective spectral region.

(a) Zones for the conical scanner were slightly smaller than comparable zones for the linear scanner, but shifted in latitude.

(b) Zones for the rearward-looking conical scanner were comparable in size to those of the linear, but shifted the opposite direction in latitude.

(6) The following observations regarding the two possible orbit times for Thematic Mapper can be made from the analysis of the radiance and geometric simulations.

(a) A greater range of sun zenith angles would be encountered for the 11:00 AM orbit than for the 9:30 AM orbit; consequently, greater changes in average reflective-region signal amplitude would occur throughout the 11:00 AM orbit.

(b) Both maximum and average scattering angles are higher for 11:00 AM, which would give rise to greater path radiance effects.

(c) The fact that the average range of scattering angle at a given latitude is smaller for 11:00 than for 9:30 AM tends to lessen the impact of (b). The important quantity, ratio of ground radiance to path radiance, is roughly the same for both orbit times for comparable conditions.

(d) An important factor that should enter into the choice of orbit time was not considered in this study, namely the effects of orbit time on the discriminability of representative sets of scene classes; sun angle does affect surface reflectances, apart from its influence on the atmospheric components of received radiances.

(7) The following observations regarding orbit times can be made from the analysis of geometric sun glint potential:

(a) Potential glint zones for the 11:00 AM orbit, for any given severity level and scan mode, are always larger than and include the comparable potential glint zones for the 9:30 AM orbit.

(b) The 11:00 AM orbit, therefore, is more susceptible to glints from smoother sea states than is the 9:30 AM orbit.

(c) Time of year and scan mode cause shifts in both the latitude location and severity of the potential glint patterns. The glint potential is greatest in June for both times and all three scan modes.

(8) The existence of very high correlation coefficients between 0.74-0.80-μm and 0.80-0.91-μm radiances, computed for the two vegetation canopies under the full range of atmospheric and observation conditions, lends support to the decision to combine the two bands for the Thematic Mapper, but of itself is not full justification.

1.2 RECOMMENDATIONS

(1) If required, a more quantitative comparison should be made of the relative effects of scan mode on the usefulness of Thematic Mapper data. This comparison would involve:

(a) Calculation of atmospheric effects for the critical latitudes for each scan mode.

(b) Inclusion of more surface cover classes.

(c) Quantitative comparison of the comparable sets of data, including statistical measures and estimates of the probability of misclassification.

(2) For system design purposes, a more complete simulation and quantitative analysis should be made of Thematic Mapper radiances and atmospheric effects within them, including more surface cover types, several background albedo spectra, and a more complete coverage of latitudes. Also, definitive studies of the effect of orbit time on crop discrimination should be carried out.

(3) Additional studies should be made to relate the geometric sun glint potential maps and refinements thereof to actual sea states and surface characteristics for a more complete assessment of sun glint potential. Also, studies should be made of comparable effects on land surfaces.

2
INTRODUCTION AND APPROACH

The atmosphere intervenes between satellite-borne earth resources sensors and the Earth's surface. It both attenuates radiation emanating from the surface and adds extraneous path radiance to that radiance arriving at the sensor from the surface. These attenuation and path radiance effects depend on the sensor's scan geometry in relation to the solar illumination geometry. In addition, surface materials exhibit bidirectional reflection properties which also depend on the view and illumination geometries.

The result of signal variations which depend on scanning geometry can be degraded information extraction, such as less accurate computer recognition processing results, from the remotely sensed data. Processing systems might be designed in the future to remove or minimize such effects, but they still constitute a factor that should not be overlooked in system design and specification.

Two types of scanning geometries have been used thusfar in spaceborne multispectral scanners -- a linear scan in LANDSAT-1 and -2 and a conical scan in the SKYLAB S-192 scanner. Thus, for the future Thematic Mapper, there is a potential for either mode of scan. The objective of the effort reported herein was to characterize any differences between atmospheric effects in Thematic Mapper data that would result from using the two scanning geometries. As a byproduct, insight was gained about the overall effect of the atmosphere on Thematic Mapper signals, together with the effects of time of day. An added analysis was made of the geometric potential for direct specular reflections (sun glint).

A data simulation approach was taken to assess atmospheric effects in Thematic Mapper signals. Computer models existing and implemented at ERIM were used to simulate the major components of spectral radiance at the spacecraft. The simulations included spectral calculations of: direct solar and diffuse sky irradiance, bidirectional surface reflectance characteristics and surface emittance characteristics, atmospheric transmittance and path radiance quantities, and integrated radiance over the currently specified Thematic Mapper spectral bands.

Two distinct analyses were carried out, one for the thermal band and one for the reflective bands. This dichotomy resulted from the distinctly different processes leading to signals in these spectral regions and also the use of different computer models.

Thermal region simulations were performed using the ERIM model referred to in Ref. 1 as the model using the "aggregate method". For the reflective region, a composite multispectral system simulation model was used. Radiative transfer calculations were carried out according to the model developed at ERIM by Dr. Robert Turner [2], while vegetation canopy bidirectional reflectance calculations were performed using a model developed by Dr. Gwynn Suits of ERIM [3]. The atmospheric and reflectance quantities then were combined with sensor response functions to simulate inband radiance for the Thematic Mapper bands.

3
SPECIFICATION OF ANALYSIS PARAMETERS

The first step of the project was to specify the parameters to be used for data simulations.

3.1 SENSOR SYSTEM PARAMETERS

Three characteristics of the sensor system had to be specified in consultation with the Sponsor's Technical Representatives: spectral response functions, scanning geometries, and orbit parameters (e.g., times of pass).

The spectral bands used were those currently defined or under consideration for the Thematic Mapper:

0.45 - 0.52 μm
0.52 - 0.60
0.63 - 0.69
0.74 - 0.80
0.80 - 0.91
0.74 - 0.91
1.55 - 1.75
10.29 - 12.50

A unit-amplitude spectral response function was assumed within these spectral limits.

The scanning geometries were obtained using the following specifications of the Thematic Mapper orbit and swath width:

98.2° Inclination Angle
705 km Altitude
185 km Swath Width
Scan Geometry: (a) Linear
(b) Conical, 17.88° Cone Angle

For the linear scan, the scan angle range is $\pm 7.5^{\circ}$. For purposes of the simulations, five scan angles were used: 0°, $\pm 4^{\circ}$, and $\pm 8^{\circ}$.

The geometry for a conical scanner is somewhat different than that for a line scanner since the zenith scan angle remains fixed while the azimuth position is changed for successive views of the ground. See Fig. 1. Dividing the 48° sector into four equal parts, we have:

$$\psi_{con} = 0^{\circ}, \pm 12^{\circ}, \text{ and } \pm 24^{\circ}$$

These five angles were used for the simulation to correspond with the five angles in the linear scan case.

The final sensor parameters are the time of the satellite overpass and the latitudes of interest. Two times were specified, 9:30 and 11:00 AM, and latitudes of interest were given to be between 70°N and 70°S. Sun positions were read from graphs in Table 170 of Ref. 4 for the two sun times (making no adjustments for orbital deviations in either time or longitude) at 40°N, 0°, and 40°S longitude, for use in the radiance simulations. Positions for three dates, chosen to cover the full range of sun positions throughout the year, were extracted -- i.e., for the summer and winter solstices and the vernal/autumnal equinox.

It should be emphasized, however, that, since the intent of this study was to examine only gross atmosphere-related differences between orbit times for the two scan geometries and since results were needed rapidly, the above expedient method of determining sun positions was employed. These positions do not precisely represent the conditions that would be encountered in actual Thematic Mapper orbits, and the results should be interpreted and used accordingly. Later in the study, more precise calculations were made of the geometries for realistic Thematic Mapper orbital trajectories from 70°N to 70°S latitude, and the two sets of values for 40°N, 0°, and 40°S are compared later in this report (Tables 2 and 3).

3.2 MODEL INPUT GEOMETRIES

The most important single angle for atmospheric effects calculations is the angle χ through which the incident solar radiation vector must be rotated to point toward the sensor, in other words, 180° minus the angle γ subtended by the surface-to-sun and surface-to-sensor vectors (See Fig. 2(a)). The angle χ in radiative transfer theory is called the "scattering angle" and is so referenced hereafter in this report.

The simulation model input angles, however, are in a coordinate system that consists of (a) zenith angles, θ and θ_o, measured from the local vertical to the surface-to-sensor and surface-to-sun vectors, respectively, and (b) the relative azimuth angle, ψ, measured between projections of these vectors onto the horizontal plane of the surface (See Fig. 2(b)). Note that the relative azimuth angle ψ is the projection of the angle γ onto the horizontal plane.

The calculation of the relative azimuth angle involves three factors -- the spacecraft heading relative to the local meridian of longitude, the corresponding sun position, and the scan geometry. The spacecraft heading depends on both the inclination angle of the satellite orbit and the latitude of the satellite (See Fig. 3). The following equation* was used to compute spacecraft heading:

$$\psi_{S/C} = 180^{\circ} + \beta \qquad (1)$$

where

$\psi_{S/C}$ = spacecraft azimuth heading (clockwise from North) relative to local meridian of longitude,

$$\beta = \sin^{-1}\left[\frac{\sin\ (\text{Inclination Angle} - 90^{\circ})}{\cos\ (\text{Latitude})}\right],$$

and

$\sin\ (\text{Inclination Angle} - 90^{\circ}) = 0.142629$ for Thematic Mapper.

*Eq. (1) is the correct equation; however, it was discovered in review that the program actually used to compute the values presented in this report erroneously included a term dependent on the Earth's rotation rate (a term necessary for proper image analysis) which introduces an error of 4° or less in all relative azimuths.

A linear scanner has a different zenith scan angle for every point along either half of the scan line. However, all scan angles on a given side have the same relative azimuth angle, as shown in Fig. 4. Relative azimuth angles for the western side of a scan line were computed using:

$$\psi_{West} = \psi_{Sun} - (\beta + 90^{o}) \tag{2}$$

while, for those on the eastern side, the relationship was:

$$\psi_{East} = 180^{o} - \psi_{West} \tag{3}$$

This latter equation kept the magnitude of the relative azimuth less than 180^{o}, since the sign of the angle is immaterial to the model calculations.

A conical scanner, in contrast, has a constant zenith view angle, but a different relative azimuth angle for each azimuth scan angle, ψ_{Scan}, as defined in Fig. 5. The equation used to compute the relative azimuth angles, ψ_{Con}, for the conical scanner was:

$$\psi_{Con} = \psi_{Sun} - (\psi_{Scan} + \beta) \tag{4}$$

where

ψ_{Sun} is the azimuth of the sun, CW from North,

and

ψ_{Scan} is the conical scanner azimuth angle.

3.3 COMPUTATION OF SCATTERING AND SPECULAR GLINT ANGLES

From the atmospheric scattering point of view, the importance of the radiation scattering angle has been discussed already. The following equation was used to compute the direct scattering angle, χ, for each scan geometry considered:

$$\chi = \arccos[-\cos\theta \cos\theta_o - \sin\theta \sin\theta_o \cos\psi] \quad (5)$$

where

θ = view zenith angle

θ_o = sun zenith angle

and

ψ = relative azimuth angle (from the target location, the horizontal angle between projections of the target-to-sun and target-to-sensor vectors).

Another angle of interest is the slope, δ, that the surface being viewed would have to have in order for there to be a potential for direct specular reflection of sunlight into the sensor field of view. The critical relative azimuth angle for this condition is $\psi = 180^o$, i.e., when the sun and the sensor are in opposite directions from the surface point being viewed. As shown in Fig. 6(a), specular reflection of sunlight by a perfect horizontal mirror would be observed only when the scanner zenith angle equalled the solar zenith angle. Fig. 6(b) indicates the orientation that specular surfaces would have to have in order to produce observable specular reflections for two special cases: $\psi = 180^o$, already identified, and $\psi = 0^o$, the other half of that linear scan line. The surface orientation is defined here by the angle δ, measured from the local zenith to the surface normal.

Since specular surfaces, such as water, are not perfect and not exactly horizontal, there will be a cone of angles, about the idealized geometry, in which specular effects could be expected. To permit an examination of the geometric potential for sun glint, the following general expression was used to compute δ at which specular reflection between the sun and the sensor could occur for the various orbits and modes of scan:

$$\delta = \cos^{-1}\left\{\frac{\cos\theta + \cos\theta_o}{[(\sin\theta_o + \sin\theta \cos\psi)^2 + (\sin\theta \sin\psi)^2 + (\cos\theta + \cos\theta_o)^2]^{1/2}}\right\} \quad (6)$$

3.4 ATMOSPHERE PARAMETERS

For calculations in the thermal spectral region, five standard atmospheres were readily available for use. These were:

Temperate, Summer
Temperate, Winter
Arctic, Summer
Arctic, Winter
Tropic

For the shorter wavelength, reflective region, four standardized atmosphere profiles were chosen. These profiles are labeled by associated horizontal visual ranges, V, although the optical thickness of the atmosphere at each wavelength is the variable used in the calculations. The profiles chosen represent two substantially different conditions (V = 23 km, clear; and 10 km, hazy). In addition, a relatively small displacement from each of these conditions was selected, i.e., V = 20 and 8 km. The V = 20 case represents roughly an 8% increase in optical thickness from V = 23, while the V = 8 case represents roughly a 15% increase in optical thickness from V = 10. As a background albedo, the average reflectance of a large collection of spectra for green leaves was used.

3.5 SURFACE PARAMETERS

For thermal calculations, a 300°K surface target temperature was assumed, along with a 300.5°K target, to allow the calculation of the radiance change, ΔL, for a target temperature change, $\Delta T = 0.5^{\circ}K$, in addition to total radiances.

For surface reflectance properties, two green wheat canopies, with approximately 14% and 79% ground cover, respectively, were simulated. The underlying soil was assigned Condit's mean soil reflectance spectrum [6]. Spectral parameters were readily available only from 0.4 to 1.1 μm for these canopies.

3.6 OVERALL EQUATION FOR REFLECTIVE-BAND RADIANCE SIMULATION

The basic equation used for computing reflective spectral radiances, $L(\lambda)$, at the satellite is:

$$L(\lambda) = \frac{1}{\pi}\left(E^{\lambda}_{Sun} \cdot \rho^{\lambda}_{Bidirect} + \tilde{E}^{\lambda}_{Sky} \cdot \rho^{\lambda}_{Diffuse} \right) T^{\lambda} + L^{\lambda}_{Path} \qquad (7)$$

where E^{λ}_{Sun} is the direct solar spectral irradiance,

E^{λ}_{Sky} is the diffuse sky spectral irradiance,

$\rho^{\lambda}_{Bidirect}$ is the bidirectional spectral reflectance of the surface, relative to that of a perfect Lambertian surface,

$\rho^{\lambda}_{Diffuse}$ is the Lambertian (i.e., diffuse) spectral reflectance of the surface,

T^{λ} is the spectral transmittance of the atmosphere,

and L^{λ}_{Path} is the spectral path radiance.

These individual quantities also have varying degrees of dependence on the geometry of the situation, with the radiance itself depending on both the sun and view geometries. Of the spectral quantities in Eq. (7), all were computed with the Turner model, except $\rho^{\lambda}_{Bidirect}$ and $\rho^{\lambda}_{Diffuse}$ which were computed with the Suits' model.

The effective inband radiance for Thematic Mapper Band i was obtained by integration, i.e.,

$$L_i = \int R_i(\lambda) L(\lambda) d\lambda \qquad (8)$$

where $R_i(\lambda)$ is the relative spectral response function for Band i. The calculations were carried out with a spectral interval of 0.01 μm and a summation of products to replace the continuous integration indicated in Eq. (8).

4
RESULTS AND ANALYSIS FOR THERMAL BAND

Because there is insignificant reflection of solar radiation in the thermal spectral region, one need consider only the influence of viewing geometry on atmospheric effects, omitting the bistatic solar geometry necessary for the reflective channels.

When scanning through a constant atmosphere, a conical scanner will induce no variation in atmospheric effects but a linear scanner will. To explore the extent of this variation, calculations were made with the ERIM thermal radiative transfer model, using the five standard atmospheres previously described. Path transmittance, path radiance, and total radiance in the 10.29-to-12.50-μm spectral passband at the sensor were calculated. The results are presented in Table 1. As a point of interest, the change in radiance for a $0.5^{\circ}K$ change in target temperature also was calculated and included in Table 1.

The results show very little change in total target radiance in going from a 0° to an 8° scan angle. This is due in part to the opposite effects of increased path length on transmittance and path radiance. Fig. 7 illustrates the miniscule changes that occur in total inband radiance in the presence of the drastic differences in path transmittance that exist for the five atmospheres considered.

The other potential source of atmosphere-related signal variation lies in the atmospheric conditions throughout the scene. Because of the slightly longer path length with the conical scanner, the effect of atmosphere inhomogeneities would be slightly greater for it than for the linear scanner. Using a simplified expression for the thermal radiance at the spacecraft, one can derive an expression for the variance in received radiance from both linear and conical scanners, and determine the conditions under which the two variances would be equal. Such an analysis follows.*

*This analysis was suggested by Mr. Jerry L. Beard of ERIM.

Assume, for deviations about a reference condition, that

$$L = L_o\tau + L_p'(1 - \tau) \tag{9}$$

where L = total radiance

L_o = target radiance at surface

L_p' = scaled path radiance for the reference condition, i.e., $L_p' = L_{p_{ref}} \cdot (1 - \tau_{ref})^{-1}$

and τ = transmittance.

Letting $\tau = e^{-kx}$

where k = absorption coefficient

and x = slant path length through the atmosphere

leads to:

$$L = L_o e^{-kx} + L_p'(1 - e^{-kx}) \tag{10}$$

Taking partial derivatives, one obtains:

$$\partial L = -kxe^{-kx}\,(L_o - L_p')\left(\frac{\partial x}{x} + \frac{\partial k}{k}\right) \tag{11}$$

or

$$\partial L = C\left(\frac{\partial x}{x} + \frac{\partial k}{k}\right) \tag{12}$$

where $C = -kxe^{-kx}(L_o - L_p')$

Assuming x and k to be independent, the variance $(\partial L)^2$ in L is approximately

$$(\partial L)^2 \simeq C^2 \left[\left(\frac{\partial x}{x}\right)^2 + \left(\frac{\partial k}{k}\right)^2\right] \tag{13}$$

For the conical scanner, $\partial x = 0$ and $k_c = (\sec 18^o)k_o = 1.05\ k_o$, while for the linear scanner, $\partial x = (\sec 8^o - 1)x = 0.01x$ and $k_l = k_o$. Letting $(\partial L)^2_{conical} = (\partial L)^2_{linear}$ and solving for $\frac{\partial k}{k}$, one obtains

$$\frac{\partial k}{k} \simeq \frac{\left(\frac{\partial x}{x}\right)}{\sqrt{1.1e^{-0.1k_o x} - 1}} \tag{14}$$

Some sample values for the condition where the conical variance would reach the linear variance are:

$\tau = e^{-k_o x}$	$\left(\frac{\partial k}{k}\right)$	Approx. C	For T = 300°K Approx. $(C/L)^2$
0.4	0.165	-0.367	0.036
0.6	0.047	-0.398	0.044
0.8	0.036	-0.286	0.023
0.9	0.034	-0.175	0.008

The approximate values for C and $(C/L)^2$ were computed using interpolated values from Table 1. The right-hand column in the above table shows that roughly 1 to 4% of the variance from the atmosphere and/or path length would be reflected in the variance of the received radiance, i.e.,

$$\left(\frac{\partial L}{L}\right)^2 \simeq \left(\frac{C}{L}\right)^2 \left[\left(\frac{\partial x}{x}\right)^2 + \left(\frac{\partial k}{k}\right)^2\right] \tag{15}$$

Furthermore, in cases where the $(\partial k/k)^2$ term dominates, the conical variance would not be expected to exceed 1.1 times the linear variance. The atmosphere profiles in Table 1 represent large changes in the absorption coefficient, k. If one were to move from a condition corresponding to the Arctic Summer profile at one end of a scan to one corresponding to the Temperate Summer profile at the other end, a nearly 40% change in absorption coefficient would occur. Yet, as can be seen in Table 1 and Fig. 8, the change in radiance from a 300°K target would be less than that caused by a 0.5°K change in target temperature. Normally, the changes encountered in atmospheric parameters throughout a frame would be expected to be smaller than those illustrated here.

In summary, there would be very little difference between atmospheric effects in signals generated in the thermal region by a Thematic Mapper with a conical scan and by one with a linear scan.

5
RESULTS AND ANALYSIS FOR REFLECTIVE BANDS

The geometry of the sun relative to scanning directions is very important to signals in the reflective region of the spectrum. Consequently, results of our geometrical calculations are presented and discussed before the simulations of total radiance, atmospheric effects, and surface reflectances are presented and discussed.

5.1 GEOMETRICAL FACTORS

Two special cases of scanner-sun geometry are of interest -- (a) when the scattering angle approaches 180°, i.e., when the scanner view direction approaches the spacecraft shadow point (this also corresponds to the so-called "hot spot" for surface reflectances, as defined by photointerpreters) and (b) when conditions exist that are favorable for specular reflection from the Earth's surface into the scanner field of view, i.e., the so-called "sun glint" condition. Both depend on the sun's position relative to the direction of view.

5.1.1 SUN POSITIONS

Tables 2 and 3 present the approximate values for solar zenith and solar azimuth angles which were used in the radiance simulations. These angles were extracted from Ref. 4 for solar times of 9:30 AM and 11:00 AM; latitudes of 40°N, 0°, and 40°S; and dates of Jun 21, Mar/Sep 21, and December 21. For comparison, Tables 2 and 3 also present the more precise sun positions computed for Thematic Mapper orbits having 9:30 AM and 11:00 AM (GMT) equator crossings at 0° longitude. The agreement is good at 0°, as would be expected, but the approximate values at $\pm 40^{\circ}$N differ by up to 5° in solar zenith and up to 12° in solar azimuth. These differences are not believed to be great enough to adversely affect the general analysis of simulated radiances and the conclusions drawn from it; however, use of specific magnitudes should be made with caution.

Graphs of the more accurate solar zenith and solar azimuth angles are plotted in Figs. 9-12 as a function of latitude from 70°N to 70°S for the two orbits. The minimum solar zenith angle occurs on June 21 in mid-northern latitudes and is approximately 30° for the 9:30 orbit and 12° for the 11:00 orbit. In December, when the minimum solar zenith angles occur at southern latitudes, the westward motion along the orbit track causes the minimum to be larger than for northern latitudes in June. Tabulations of the angles plotted may be found in Tables 4-21 which present geometry synopses for the various orbits, dates, and scan modes. (Note that sunlight disappears for $\theta_o \geq 90°$, neglecting refraction.)

5.1.2 SCATTERING ANGLES AND THE BACKSCATTER CASE

As will be shown later, in the simulated radiances, atmospheric path radiance is the major component of signals in the shorter-wavelength spectral bands. The atmosphere is a very non-isotropic scattering medium. In other words, the amount of radiation scattered into a given direction from an incoming beam of sunlight depends strongly on that direction, i.e., on the scattering angle. Figs. 13 and 14 (from Ref. 5) illustrate the orders of magnitude differences that exist in the amount of radiation scattered in different directions by atmospheric aerosols. Note how the amount of scattered radiation decreases drastically and rapidly from 0° scattering angle until it reaches a minimum at about 115° and then rises again as one approaches the pure backscattering case at 180° scattering angle. Fig. 14 is an enlargement of the 90°-to-180° portion of the λ = 0.45-μm curve of Fig. 13. This region is of particular interest since it encompasses nearly all the direct scattering angles computed for the Thematic Mapper and presented next in Figs. 15-20.

Several facts should be kept in mind when Figs. 13-20 are examined and compared. First, the maximum change in scattering angle that can occur during one linear scan sweep is 16°; for purposes of discussion, let us consider a 10° change. If this change were to occur from 110° to 120°, very little change in path radiance would be expected, based on Fig. 14. On the other hand, if it were to occur anywhere in the interval between 130° and 160°, a substantial scan angle effect might be expected. Also, one might expect the average magnitude of path radiance to be greater

for angles from 150° to 160° than for those from 110° to 120°. While essentially accurate, the expectations based on the single-scattering phase functions of Figs. 13 and 14 and the direct (or single-scattering) scattering angle, δ, of Figs. 15-20 should be tempered by the fact that multiple scattering takes place in the atmosphere. The radiance simulations in this report incorporate multiple scattering effects (See Figs 62-63)

Scattering angles computed for the 9:30 and 11:00 orbits are presented in Figs. 15 and 16 for the linear scan mode, while the forward-looking conical scan mode is portrayed in Figs. 17 and 18. All scattering angles for a June pass, for example, would lie on or between the curves plotted with the symbols "1" and "2". An "X" denotes the intersection of two or more curves. For any given time of year, the scattering angles exhibit a pattern which is low for the extreme latitudes considered and higher for an intermediate latitude. A change in month of year causes a latitude shift of the pattern.

A comparison of curves for the two scan modes at either time shows that, although different scattering angles occur at a given latitude, nearly identical ranges of angles occur for the two scan modes throughout the entirety of the latitude range. In fact, the two plots overlay almost exactly if the conical scanner plot is shifted by 18° toward Northern latitudes. Then, one finds the only difference to be a very slightly smaller range of scattering angles on a given date for the conical scanner at any fixed latitude; also, the mean range over all latitudes is slightly smaller for the conical scanner (See Table 22).

There are four differences between scattering angles computed for the 11:00 and 9:30 orbits. First, a change in season of the year causes a greater shift for 9:30 than for 11:00 in the latitude at which the maximum scattering angle occurs. Second, there is a substantial reduction ($\sim$20°) in maximum scattering angle for 9:30 from that for the 11:00 orbit and, third, average values for 9:30 are 10° less than for 11:00. Further, the average spread of scattering angles induced by differing scan angles during one scan for 11:00 is roughly 2/3 that for 9:30. Specific values leading to the last three observations are present in the statistics of Table 22.

The forward-looking mode for the conical scanner is not the only possible configuration. For example, it could just as well look rearward. Another set of calculations was made, therefore, to explore the range of scattering angles that would result from a rearward-looking Thematic Mapper. These results are presented in Figs. 19 and 20. Here again, the pattern is very similar to that of Figs. 15-16 (and 17-18); this time they match best if the rearward-looking conical curves are shifted toward Southern latitudes. Table 22 shows the rearward-looking scanner to have slightly lower maximum, average, and range of scattering angles than the other two scan modes.

From an examination of Figs. 15-20, one cannot find an obvious basis for choosing between the linear and conical scan modes, without restricting the latitudes considered (e.g., scattering angles for the mid-northern latitudes on the average are lowest for the forward-looking conical scanner). As far as choosing between the two orbit times, the 9:30 orbit clearly has smaller scattering angles which should reduce some of the atmospheric path radiance effects; this relationship will be explored more fully in later sections.

5.1.3 RELATIVE AZIMUTH ANGLES AND THE SPECULAR CASE

The critical relative azimuth angle for the specular reflection case is 180°, i.e., when the sun and the sensor are in opposite directions from the surface point being observed, as discussed earlier. Relative azimuth angles were computed using the relationships described earlier in Sec. 3.2. Tables 4-21 contain values for each of the three scan modes. In addition, the values are plotted for the two orbits in Figs. 21 and 22 for the linear scan, Figs. 23 and 24 for the (forward-looking) conical scan, and Figs. 25 and 26 for the rearward-looking conical scan. All scan angles in the western half of the linear scan pattern have relative azimuth angles plotted with odd-number symbols in Figs. 21 and 22, while those on the eastern half are plotted with corresponding even-number symbols. For the conical scanners, on the other hand, relative azimuths range continuously between the extreme values plotted, e.g., between curves 1 and 2

for June. Relative azimuth values were restricted to the range 0° to 180° for plotting purposes by reflection about axes at 0° and 180°, where necessary, because the sign of the relative azimuth is immaterial to the calculations.

From Figs. 21 and 22, it is clear that the relative azimuth angle will equal 180° once each Thematic Mapper pass with a linear scan mode. The latitude at which this will occur depends on both the month of year and time of day, ranging at 11:00 AM from roughly 25°N latitude in June to 20°S in December and at 9:30 AM from 35°N in June to 20°S latitude in December. A comparison of these figures with the solar zenith angles plotted on Figs. 9 and 10 shows that when $\psi = 180^{\circ}$, the sun is near its minimum zenith (maximum elevation) angle. Since the maximum linear scan zenith is 8°, the smaller the solar zenith, the greater the chance of specular reflections. The likelihood is much greater at 11:00 than at 9:30 because their solar zenith angles corresponding to $\psi = 180^{\circ}$ are approximately 14° and 34°, respectively.

For the conical scanner, on the other hand, Figs. 23 and 24 show that the relative azimuth angles never reach 180° for the 9:30 orbit, but do so on the eastern side of the swath in winter months for the 11:00 AM orbit.

A more thorough evaluation of the potential for solar glint, such as from water surfaces which may not be horizontal, involves computation of the surface slope angle, δ, at which specular reflection could occur (See Sec. 3.3). Calculations were made of δ at latitude increments of 5° from 70°N to 70°S for nine scan angles (e.g., -8°, -6°, -4°, -2°, 0°, 2°, 4°, 6°, and 8° for the linear scanner) that span the entire 100-km-wide surface coverage swath of the Thematic Mapper. This permitted a mapping of the zone of potential glint problems for each orbit time, time of year, and scan mode.

Fig. 25 presents six such maps for the linear scan mode. Consider yourself to be looking down on a strip map of a Thematic Mapper orbital pass; East, the general direction of the sun, is up and North is to the left.

Each spatial cell in this map is represented by a symbol which indicates the severity of the glint potential in it. A "5" indicates that a specular surface with a slope of as little as 5^{o} could produce sun glints. Similarly a "4" indicates that a slope of 10^{o} or more would be required, and so forth to a "1" for slopes of 30^{o} or more and a blank for required slopes greater than 30^{o}.

A comparison of the maps in Fig. 25 shows that the glint potential is substantially greater for the 11:00 orbit than for the 9:30 orbit. For the most part, slopes of 20^{o} or more are required for glint at 9:30, while substantial areas having 10^{o} slopes at 11:00 could produce glints. The reason for this is the higher sun elevation angles (smaller sun zenith angles) at 11:00. The latitude region for high glint potential shifts from predominantly northern latitudes in June to predominantly southern latitudes in December. The glint potential is most severe in June.

To interpret these maps for the case of sun glint off water, the higher the slope required, the rougher is the sea state required to produce glint conditions. For complete interpretation, the correspondence between surface slope distribution and sea state is needed. The calculations here assume a random azimuthal orientation of the wave surfaces which produce specular reflections. If there were a non-random preferred azimuthal alignment of the waves, glint would not be found in as large a region as is indicated on these maps for any given surface slope.

Maps of potential glint zones for the conical scanner, presented in Fig. 26, are very similar to those for the linear scanner. Again, the glint potential is substantially greater for the 11:00 AM orbit.

The 9:30 maps from Figs. 25 and 26 are duplicated and presented together in Fig. 27 to facilitate comparison of the glint zones for the two types of scan. The conical scanner zones of glint for severity levels 2 and 3 appear to be a little smaller than those for the linear scanner, and are shifted toward northern latitudes.

Similar maps also were generated for the rearward-looking conical scanner and are presented for both orbits in Fig. 28. The sizes of the severity 2 and 3 zones for the rearward case are a little larger than those for the forward case, being nearly identical to those for the linear scanner. The southward shift of the glint zone for the rearward-looking case is evident in Fig. 29 which presents maps for the two conical scanners for 9:30 orbits.

5.2 RADIANCE SIMULATIONS

Calculations were made employing the realistic simulation models to determine the dependence of key radiation quantities on the particular levels of the sensor, atmospheric, and surface factors of interest, which have been discussed previously and are summarized in Table 23. Figs. 30-61 display these quantities as a function of particular subsets of these factors and levels. A brief presentation and explanation of these figures will be given before they are discussed and conclusions are drawn from them.

5.2.1 RESULTS

Figs. 30-32 display total inband radiances in Bands 0.45-0.52, 0.63-0.69, and 0.74-0.91 μm, respectively, calculated for one vegetation canopy (dense green wheat). At each point along the ordinate, ten data values are plotted, representing five levels of scan geometry and two levels of atmospheric visibility. The headings and dashed lines indicate the order in which factors and the levels within each factor vary along the ordinate. These factors, from most slowly varying to most rapidly varying, are: time of day (9:30, 11:00 AM), scanner configuration (conical, linear); latitude (40°N, 0°, 40°S); time of year (June, March, December); and atmospheric condition (hazy, clear). The symbols indicate the number of values within each display cell -- "*" for one, "2-9" for two through nine, and "X" for ten or more. The "hazy" atmosphere denotes calculations for five scan angles for each of two visibilities, 8 and 10 KM, while the "clear" atmosphere denotes those for visibilities of 20 and 23 KM.

Figs. 33 and 34 display the scan angle dependence of total inband radiances in Band 0.45-0.52 μm for the same vegetation canopy but each for one time of day, 9:30 and 11:00 AM, respectively. At each point along the ordinate, two data values are plotted, corresponding to visibilities of 23 and 8 KM. The factors varying along the ordinate from slowest to fastest are: scanner configuration (conical, linear); latitude (40^{o}N, 0^{o}, 40^{o}S); time of year (June, March, December); and scan geometry. There are five scan geometry levels for each scanner configuration: scan angles of -8^{o}, -4^{o}, 0^{o}, $+4^{o}$ and $+8^{o}$ ranging from East to West for the linear scanner and azimuth scan angles of -24^{o}, -12^{o}, 0^{o}, $+12^{o}$ and $+24^{o}$, also ranging from East to West for the conical scanner with a cone angle of 18^{o}. Figs. 35-36 and Figs. 37-38 represent the same displays of total inband radiance but in Bands 0.63-0.69 μm and 0.74-0.91 μm, respectively.

To permit an assessment of the relative contributions of the ground and the atmospheric path to total radiance, Figs. 39-42, 43-46 and 47-50 display both total inband radiances and ground inband radiances in three four-plot groups, corresponding to Bands 0.47-0.52, 0.63-0.69, 0.74-0.91 μm, respectively. Equation (7) expresses total radiance as the sum of two components, the path radiance and a term dependent on the ground reflectances; this latter term will be referred to hereafter as ground radiance. Within each group, each plot displays these two quantities for the same vegetation canopy as previous plots and for a fixed time of day and atmospheric visibility. The times of day are 9:30 and 11:00 AM and the visibilities are 8 and 23 KM. The particular combination of time of day and visibility for each plot is indicated in its title. The factors and levels included in these plots are the same as those in Figs. 33-38.

Figs. 51-52 and 53-54 also are plots of total inband and ground inband radiances for Bands 0.45-0.52 and 0.74-0.91 μm, respectively, but they are calculated for a different vegetation canopy (sparse green wheat). The time of day is fixed at 9:30 AM and the visibility is fixed in each plot as either 8 or 23 KM, as indicated in the title.

Figs. 55-58 display inband path radiance in Bands 0.45-0.52, 0.63-0.69, 0.74-0.91, and 1.55-1.75 μm, respectively. At each point along the ordinate two data values are plotted for visibilities of 23 and 8 KM. The time of day is held fixed at 9:30 AM. The factors and levels included in these plots are also the same as in Figs. 32-38.

Finally, Figs. 59-61 display total surface irradiances (direct solar plus diffuse sky) for Bands 0.45-0.52, 0.63-0.69, 0.74-0.91 μm, respectively, for the two times of day on each plot.

5.2.2 DISCUSSION

The simulations of inband Thematic Mapper radiances and atmospheric effects within them have demonstrated the relative importance of a number of key factors which affect these radiances.

Time of day is a major factor, as is evident in Figs. 30-32 where total radiances are presented for the bands 0.45-0.52, 0.63-0.69, and 0.74-0.91 μm at 9:30 and 11:00 AM Solar Time. The consistently larger magnitudes at 11:00 AM are due in large part to the smaller sun zenith angles (higher sun elevation angles) that exist at 11:00. As illustrated in Figs. 59-61, the total irradiance decreases markedly as sun-zenith angle increases. Another observation made from the data, but not illustrated in this report, is that the ratio of diffuse to direct irradiance increases as sun zenith angle increases; this effect keeps the falloff rate lower than it would be if only direct irradiance were present.

Another feature of Figs. 30-32 is that the variances, as well as the magnitudes, present in the radiances are greater at 11:00 AM than at 9:30 AM. These variances are shown to depend on two other factors, latitude and time of year, which affect the levels of inband radiance in substantial ways, again in large part due to related changes in sun geometry. Another important relationship is the effect of these factors on the scattering angles present, as will be discussed later in more detail.

There are two remaining factors identified in Figs. 30-32, i.e., scan mode and atmosphere condition. Discussion of scan mode will be deferred until later. Average radiances for hazy conditions are consistently higher than those for clear conditions in the 0.45-0.52- and 0.63-0.69-μm bands, but the opposite is true for 0.74-0.91 μm. Also, the amount of variability decreases as the wavelength increases. Two reasons for these effects (e.g., see Ref. 7) are: (a) both the amount of scattering in the atmosphere and the overall effect of the atmosphere on radiance signals is greater at shorter wavelengths and (b) the relative effects of path transmittance and path radiance on the total radiance depend on the background albedo as well as on the amount of atmospheric haze present. Relative to (b), Fig. 3 of Ref. 7 shows that total radiance (at 0.95 μm) could either increase or decrease with increased amounts of haze, depending on the value of background albedo (which has a strong effect on path radiance). Table 24 lists the background albedos used in the current simulations.

The scatter of points under the hazy and clear conditions represents largely the scan angle dependence of total radiance, combined with small changes in atmospheric condition (e.g., visual ranges of 8 and 10 km for hazy and 20 and 23 km for clear). Figs. 33-38 display the scan angle dependence explicitly on an expanded scale for the 8- and 23-km visual ranges. Where scan angle variations are large, there is an equal or greater change in total radiance over the range of scan angles for one visibility than there is in changing from V=8 to V=23 km for a given angle. In Figs. 33-36, for the 0.45-0.52- and 0.63-0.69-μm bands, there is generally an increase in total radiance as one scans from the eastern to the western side of the ground swath. On the other hand, in Figs. 37 and 38 for the 0.74-0.91-μm band, there is a V-shaped pattern for the linear scanner and a predominantly constant or slightly rising E-to-W pattern for the conical scanner. As will be shown next, these scan angle dependencies originate predominantly in path radiance for the 0.45-0.52- and 0.63-0.69-μm bands and in ground radiance for the 0.74-0.91-μm band. The magnitude of the scan-angle-dependent variations is greatest at 11:00 AM and for the shortest wavelength band.

An examination of Figs. 39-42, shows first that ground radiance is a relatively small fraction of total radiance for both visual ranges. Thus, path radiance is the dominant term in the 0.45-0.52-μm band. Second, ground radiance exhibits almost no scan angle dependence, so the major source of scan angle variations in this band is the path radiance. Ratios of ground radiance to path radiance are roughly the same for the two orbit times for comparable conditions.

A lack of scan angle dependence in ground radiance is similarly found in Figs. 43-46 for the 0.63-0.69-μm band. Also, path radiance is still the major component of total radiance, but not by as large a factor as for the shorter wavelength band.

Figs. 47-50, for the 0.74-0.91-μm band, exhibit ground radiances with scan-angle dependent patterns that are very similar to those for total radiance. Therefore, it is a combination of surface bidirectional reflectance and path transmittance that produces these angle effects. Also, it is evident that, at these longer wavelengths, path radiance comprises only a small fraction of the total radiance. For the linear scanner, the longer path length for off-nadir angles would result in more attenuation, giving rise to an inverted-V shape in radiance vs scan angle, as opposed to the V shape observed. Thus, it must be surface bidirectional effects which predominate. The main reason for the observed pattern is that, in the band of interest, the soil's reflectance is lower than the vegetation's reflectance so the overall reflectance is lowest at the nadir when most soil is being viewed and is highest at the scan angle extremes when least soil is being viewed. The converse is true in some of the other spectral bands. Another interesting point is that bidirectional reflectances of wheat for the conical scanner tend to be less variable than for the linear scanner, due to the constant zenith angle of view.

All total and ground radiances discussed to this point have been for the denser of the two wheat canopies simulated. Figs. 51-54, for the sparser canopy, display the total and ground radiances for two spectral

bands at 9:30 AM. For the 0.45-0.52-μm band, they are higher for the sparse canopy than for the dense, whereas the opposite is true for the 0.74-0.91-μm band. This pattern is consistent with the average reflectance values listed in Table 24 for these two vegetation canopies. Angle effects are similar for the two canopies, but appear to be of lesser magnitude in total radiance for the sparse canopy at the longer wavelengths.

Path radiances alone can be examined in Figs. 55-58 at 9:30 AM as a function of the various factors for four spectral bands, including 1.55-1.75-μm which was not simulated in total radiances. The scan-angle and time-of-year dependencies are clear in these figures, with scan angle effects becoming progressively smaller as the wavelength increases and/or as the haze content decreases (visual range increases). Path radiance magnitudes at 1.55-1.75-μm are very small.

The path radiance effects which were simulated can better be interpreted in light of other analyses that were carried out. Figs. 62 and 63 are scatter diagrams of 0.45-0.52-μm band, path and total radiance, respectively, vs. the direct radiation scattering angle previously defined. Values for all four visual ranges, all scan angles, both scan modes, and both times are included, with each plot symbol indicating the number of cases in the particular display cell. Both radiances have a clear dependence on scattering angle.

A coarse measure of the degree of this dependence is the correlation coefficient between the two variables. Table 25 presents three correlation matrices computed for the total radiance values, one lumping all visual ranges together and the others stratifying them according to hazy (V=8 and 10 km) and clear (V=20 and 23 km). The bottom line of each matrix gives the correlation coefficient between the scattering angle and radiances in each of the six wavelength bands analyzed. The correlation is highest (∿0.85) for the shortest wavelength band and decreases

as the wavelength increases. This relationship is consistent with the preponderance of path radiance in the short wavelength bands and its diminishing fraction of total radiance at the longer wavelengths. The correlation is greater for the hazy condition than for the clear one in every band except the first where they are approximately equal. This again is consistent with the fact that path radiance comprises a greater fraction of the total radiance for hazy conditions.

The upper parts of the correlation matrices of Table 25 also are of interest for the Thematic Mapper. These contain the between-spectral-band correlation coefficients. At an early stage of sensor specification, the 0.74-0.91-μm band was present as two separate bands, 0.74-0.80 μm and 0.80-0.91 μm. These two were then combined into the single band because of studies which showed them to be highly correlated with little or no independent information present in one, given the other. While by no means being a definitive measure, since only two surface covers were included and separations in spectral space were not computed, the very high correlations present between the simulated radiances in these bands (i.e., $\geq$0.9993) serve as an independent source of information which tends to support the prior decision to combine the two bands.

5.3 JOINT INTERPRETATION OF GEOMETRIC AND RADIANCE SIMULATIONS FOR COMPARISON OF SCAN MODES

The primary objective of this study was to determine the differences, if any, between atmospheric effects that would be present in linear and conical scanning geometries for the Thematic Mapper. The three latitudes chosen early in the study for radiance simulations (40^{o}N, 0^{o}, and 40^{o}S) did permit a demonstration of the influence of atmospheric variables and other factors on Thematic Mapper radiances, but by themselves do not permit a definitive comparison between the linear and conical modes of

scanning. The reason for this deficiency lies in the patterns of scattering angles that apply throughout entire orbital passes from 70°N to 70°S latitude.

As was shown in Figs. 15-20 and Table 22, the range of scattering angles encountered by the different scan modes for each orbit are quite similar. However, the latitudes at which the peak scattering angles occur for any given date are shifted relative to each other for the scan modes considered. Since it also has been shown that path radiance magnitudes and scan-angle variations depend on both the mean scattering angle and the deviation from it during one scan, a definitive radiance simulation should include latitudes and times which represent the extreme conditions that would be encountered with each scan mode.

The three latitudes selected do not give such a representation of the scattering angles, so one should not base a comparison of the two scan modes on the absolute magnitudes simulated and presented side by side in Figs. 30-58. A fairer comparison using data generated in this study would be based on scattering angles calculated for the entire orbits, in view of the strong relationship that has been demonstrated between scattering angle and both path and total radiance (especially in the 0.45-0.52-μm band for which atmospheric effects are greatest).

From the statistics summarized in Table 22, one would expect very little difference between atmospheric effects with the linear and the conical scan modes over the full range of latitudes. The conical mode perhaps would have slightly smaller effects on the average, with a rearward-looking scanner having a slight advantage over a forward-looking scanner. Another fact, for which it is more difficult to estimate an effect without added radiance simulation, is that the minimum sun zenith angles occur with the maximum scattering angles for the linear scanner, but are displaced in latitude for the conical scanners. If one were to restrict the latitudes of consideration, e.g., to the mid-northern latitudes, substantial differences might exist between scan modes.

Given: $\phi_{Con} = 17.88^{\circ}$

$H = 705$ Km

W = Swath Width = 185 Km

Then: $R = H \tan \phi_{Con} = 227$ Km

$$\alpha = 2 \sin^{-1}\left(\frac{W}{2R}\right) = 48^{\circ}$$

since $W = 2R \sin \frac{\alpha}{2}$

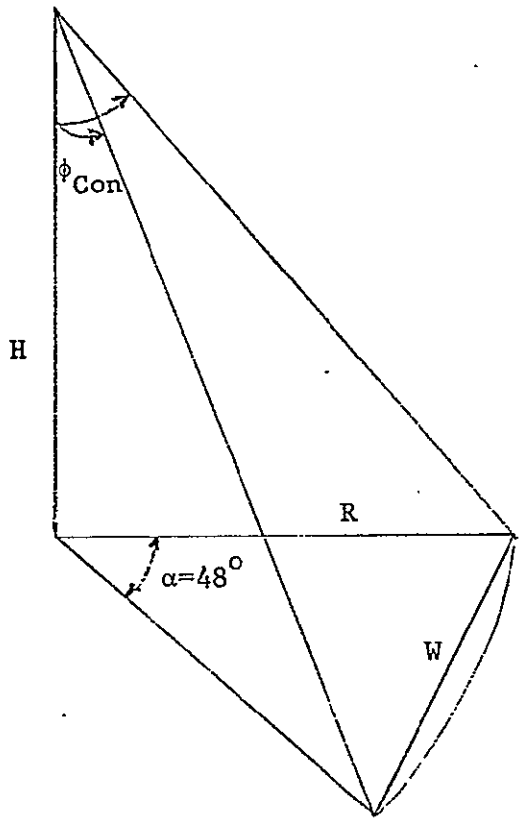

FIGURE 1. CONICAL SCAN COVERAGE PATTERN

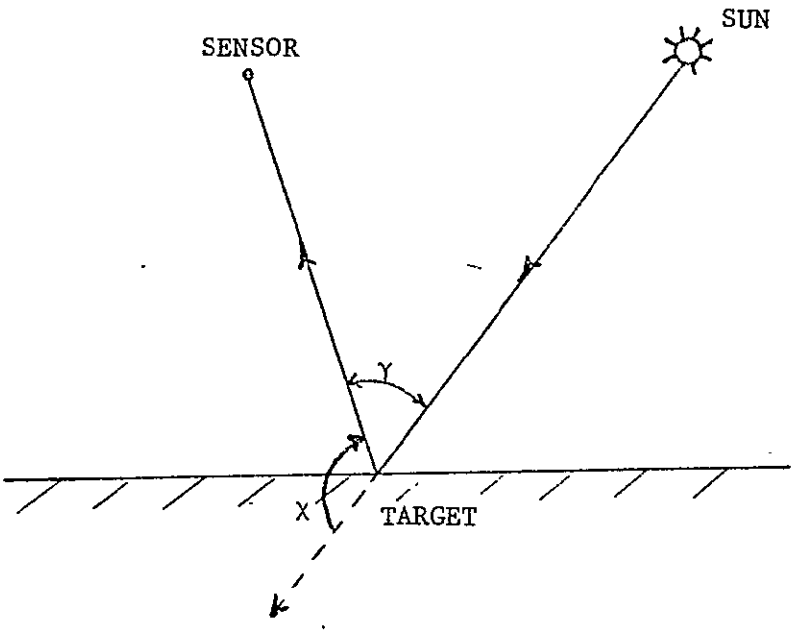

Part (a) In Plane of Sun, Target, and Sensor

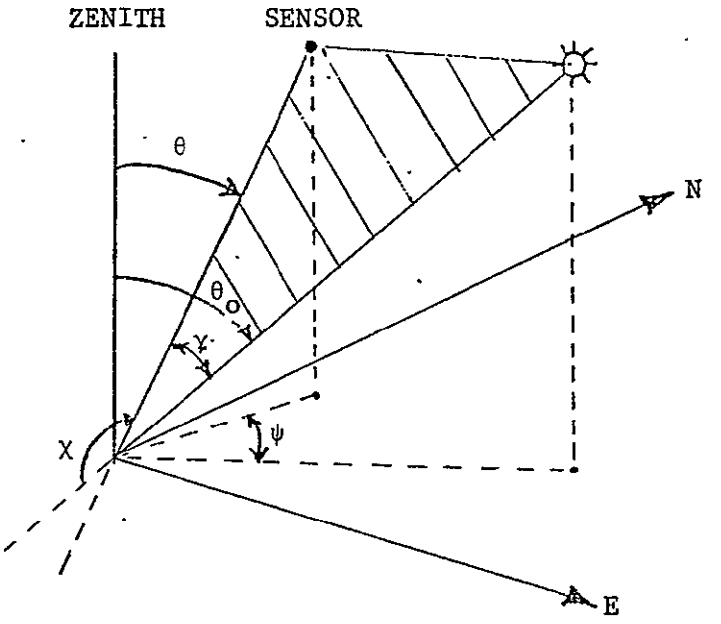

Part (b) General Case

FIGURE 2. DEFINITION OF SCATTERING ANGLE, χ; SUN-TARGET-SENSOR ANGLE, γ; AND RELATIVE AZIMUTH ANGLE, ψ.

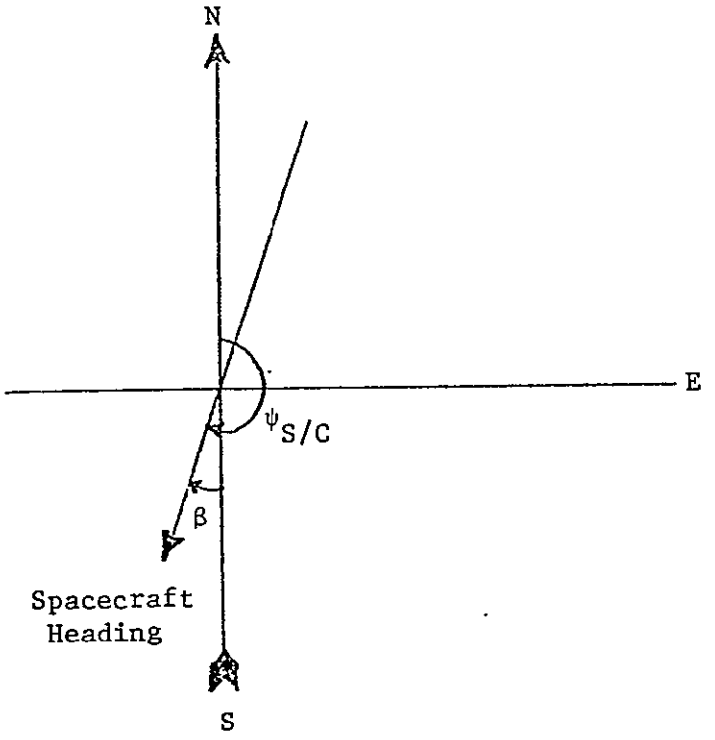

FIGURE 3. GEOMETRY FOR SPACECRAFT HEADING

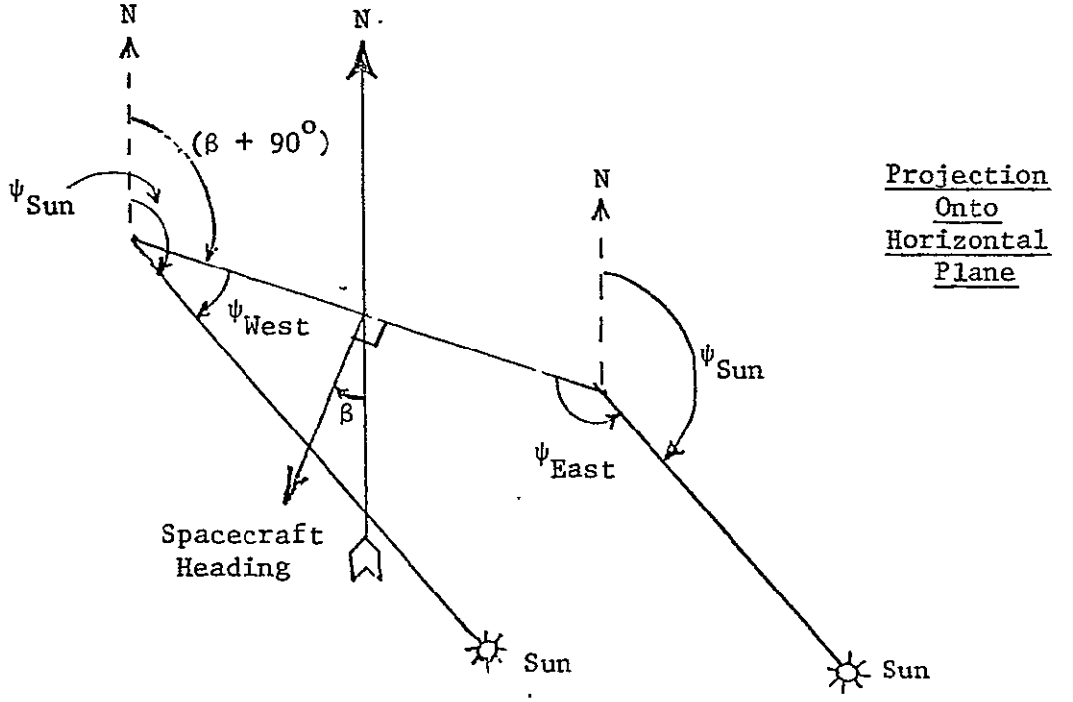

FIGURE 4. GEOMETRY FOR RELATIVE AZIMUTH ANGLES, LINEAR SCAN MODE

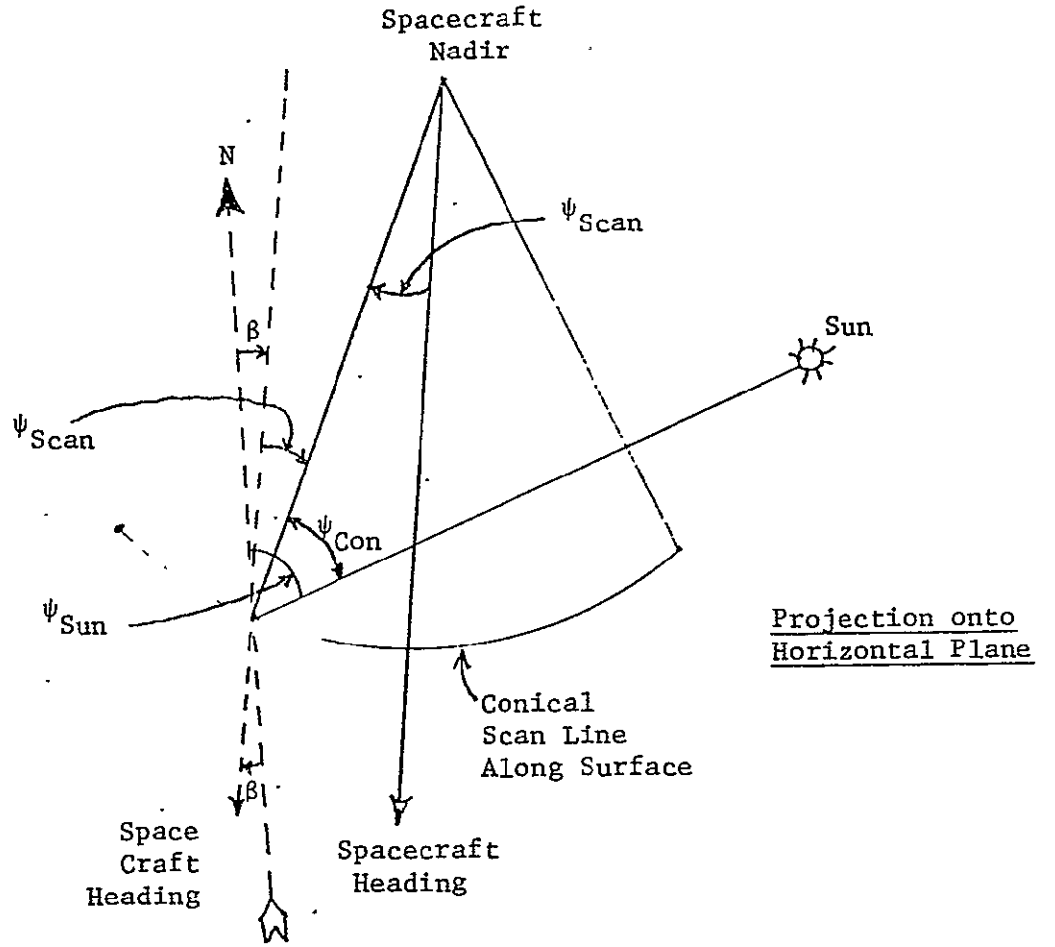

FIGURE 5. GEOMETRY FOR RELATIVE AZIMUTH ANGLES, CONICAL SCAN MODE

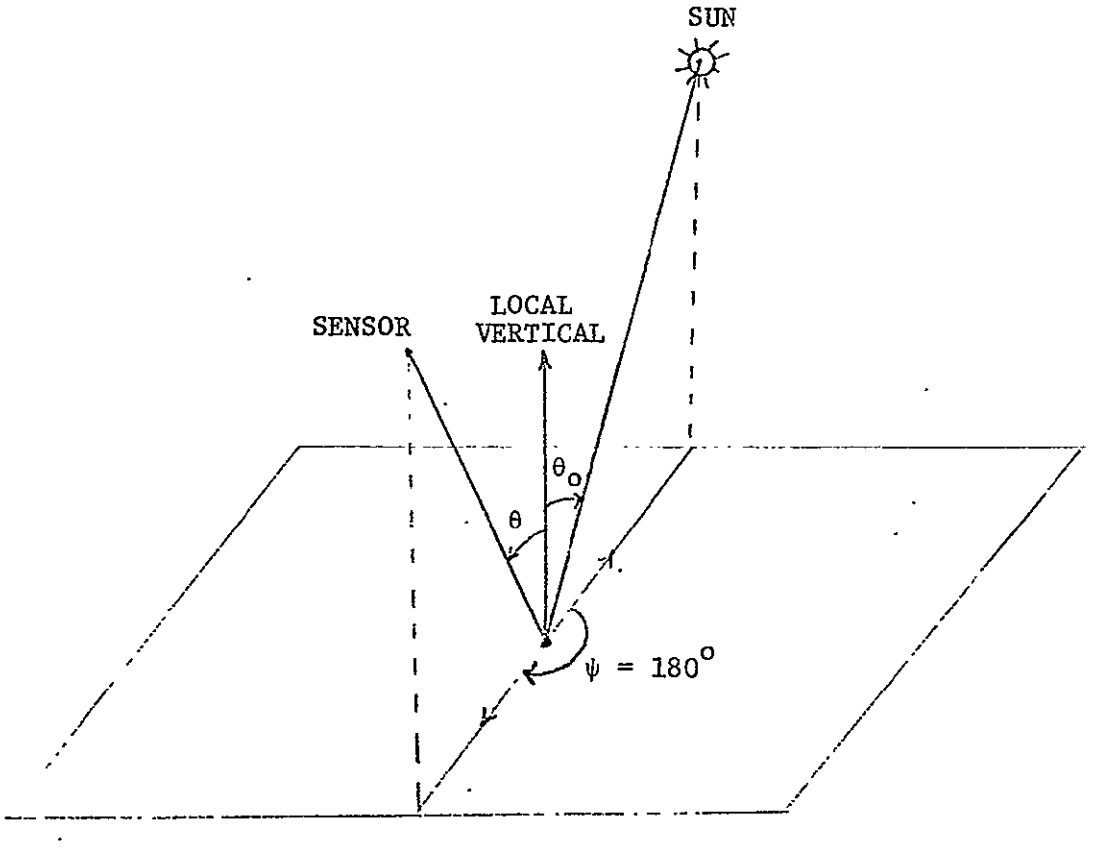

For perfect horizontal mirror, specular reflection observed only for $\theta = \theta_o$; non-perfect non-horizontal reflectors will produce a cone of angles in which specular reflections will be observed.

Part (a) Horizontal Surfaces

FIGURE 6. GEOMETRY FOR SPECULAR REFLECTIONS

For $\psi = 0^{o}$

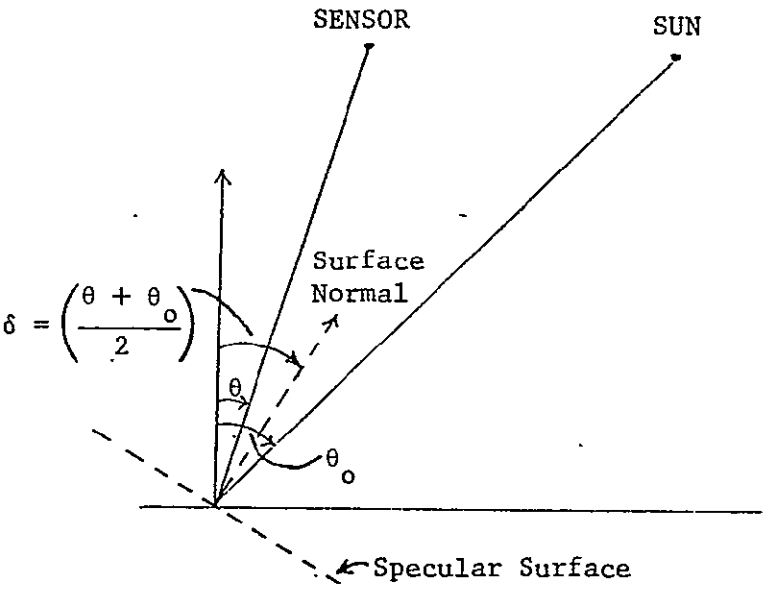

For $\psi = 180^{o}$

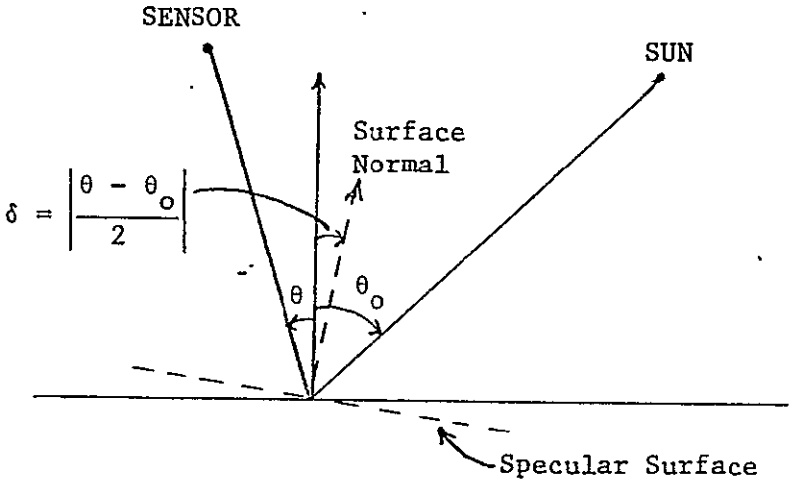

Part (b) Non-Horizontal Surfaces

FIGURE 6. GEOMETRY FOR SPECULAR REFLECTIONS

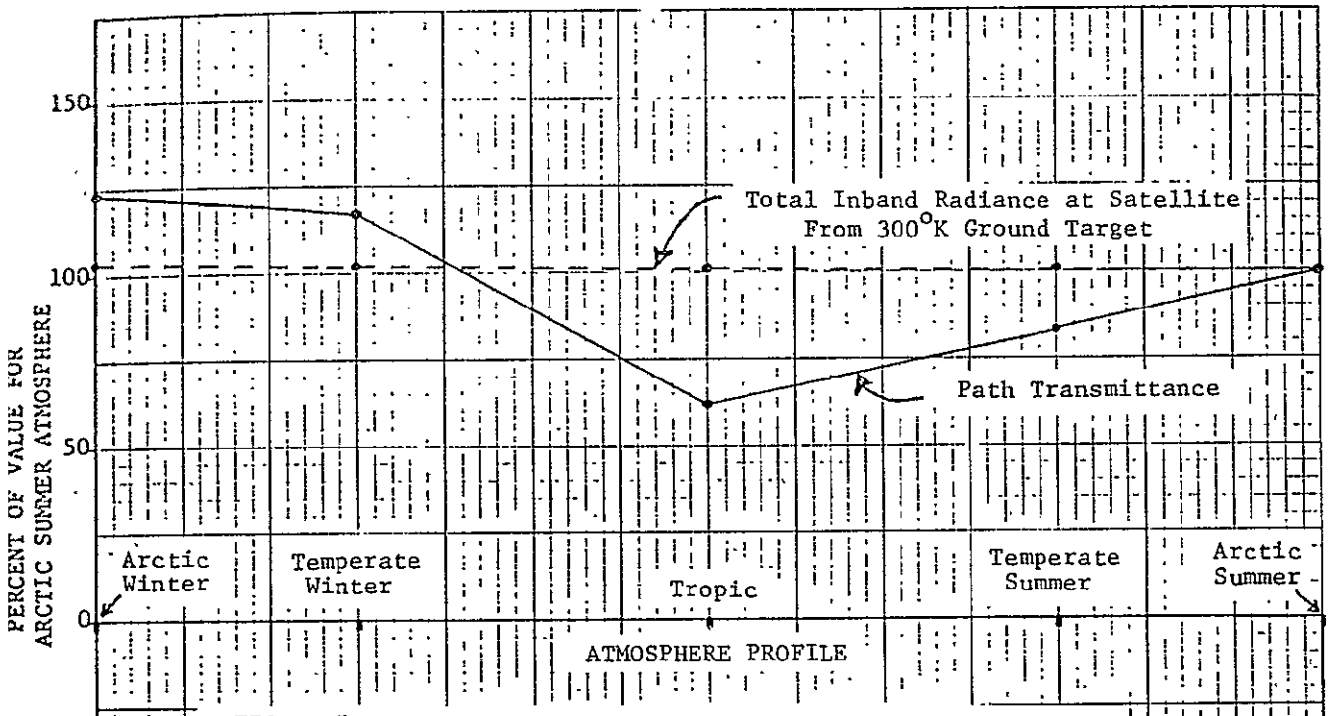

FIGURE 7. ILLUSTRATION OF THE MINISCULE CHANGES IN TOTAL INBAND TARGET RADIANCE (10.29-12.50-μm Band) DESPITE DRASTIC CHANGES IN PATH TRANSMITTANCE FOR A WIDE RANGE OF ATMOSPHERE PROFILES.

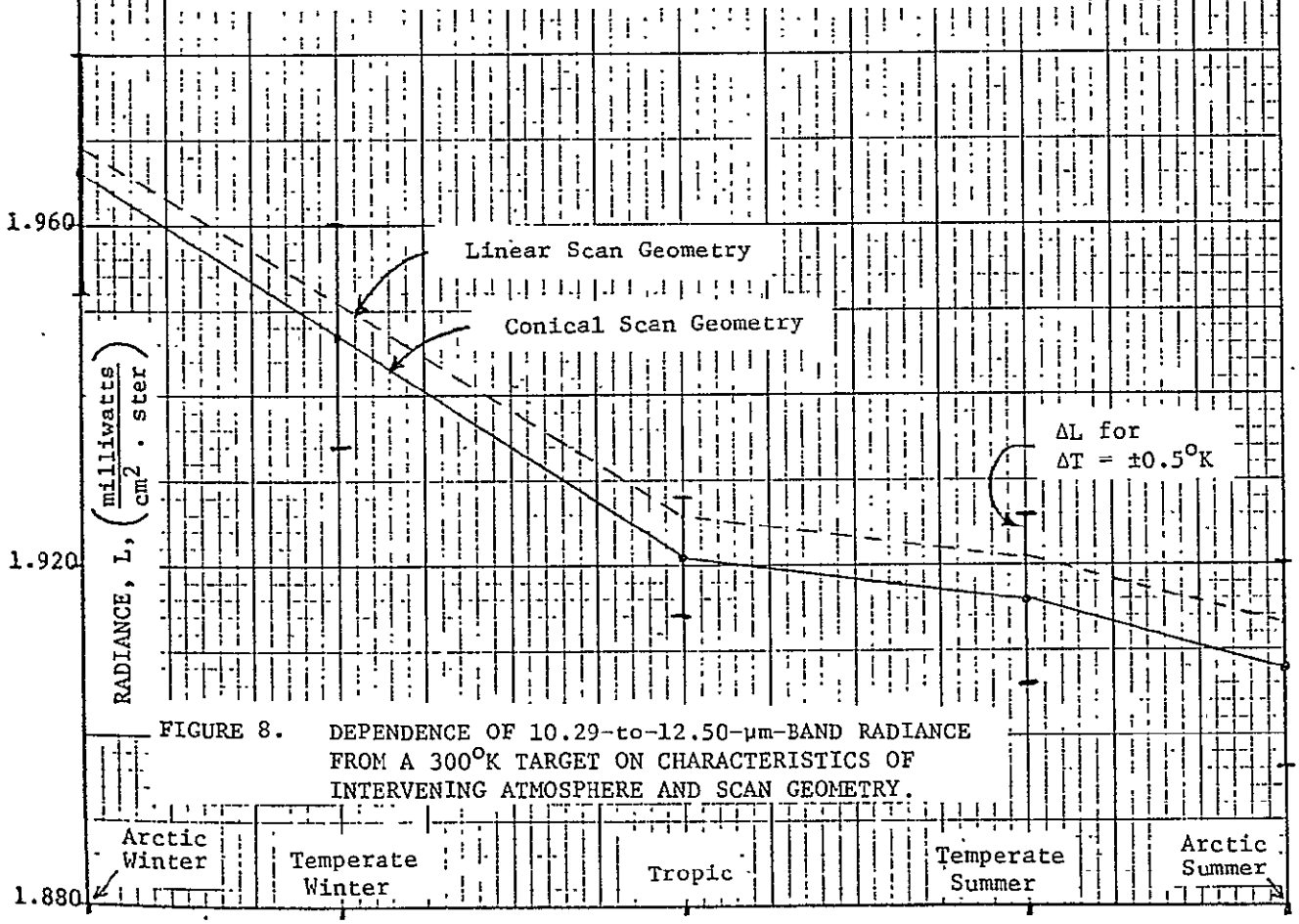

FIGURE 8. DEPENDENCE OF 10.29-to-12.50-μm-BAND RADIANCE FROM A 300°K TARGET ON CHARACTERISTICS OF INTERVENING ATMOSPHERE AND SCAN GEOMETRY.

FIGURE 9 SUN ZENITH FOR 9.30 AM EQUATOR CROSSING

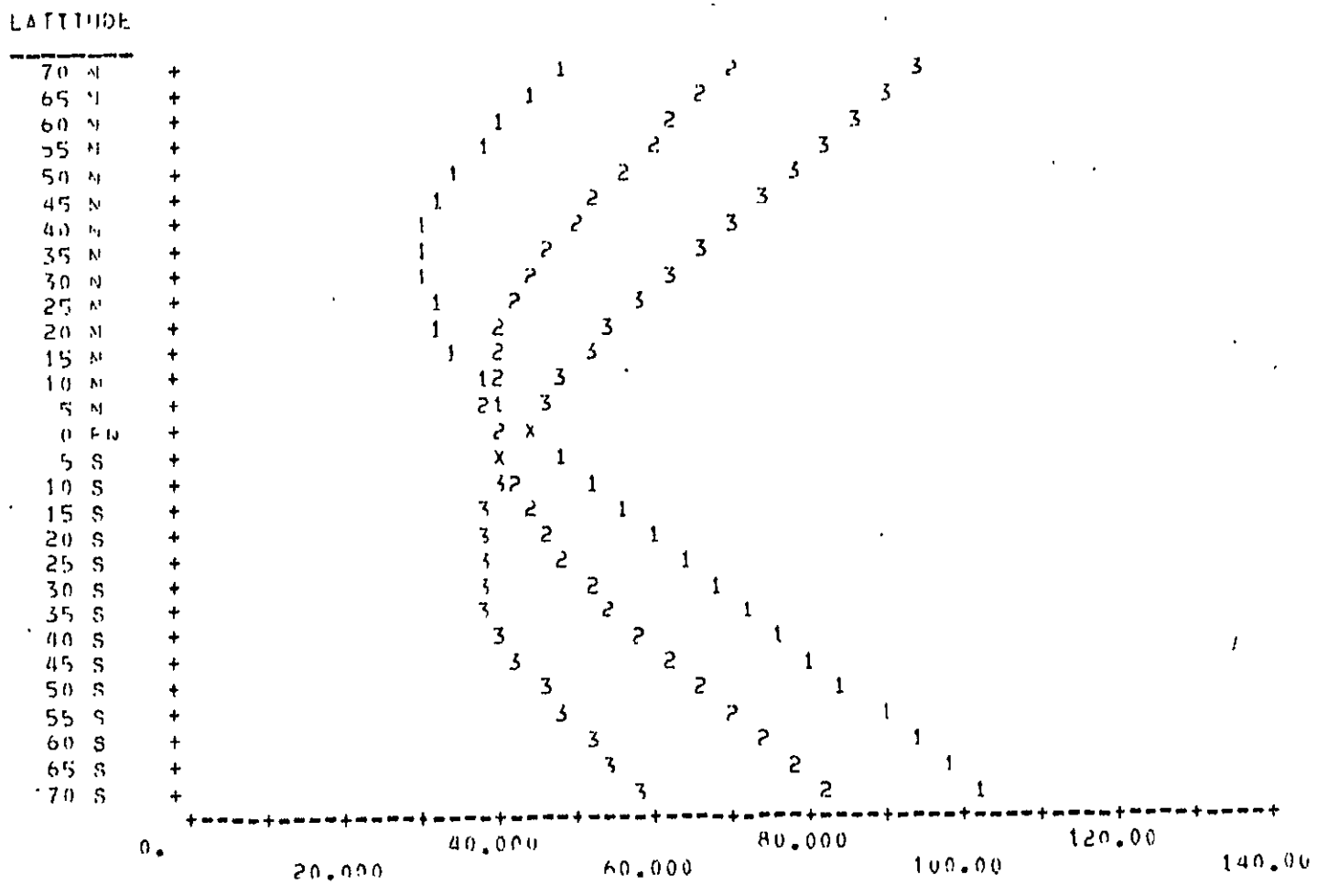

(1) SUNZEN 6 (2) SUNZEN 3 (3) SUNZEN12

KEY:

SYMBOL	DATE
1	JUN 21, 1978
2	MAR/SEP 21, 1978
3	DEC 21, 1977

ERIM

FIGURE 10 SUN ZENITH FOR 11.00 AM EQUATOR CROSSING

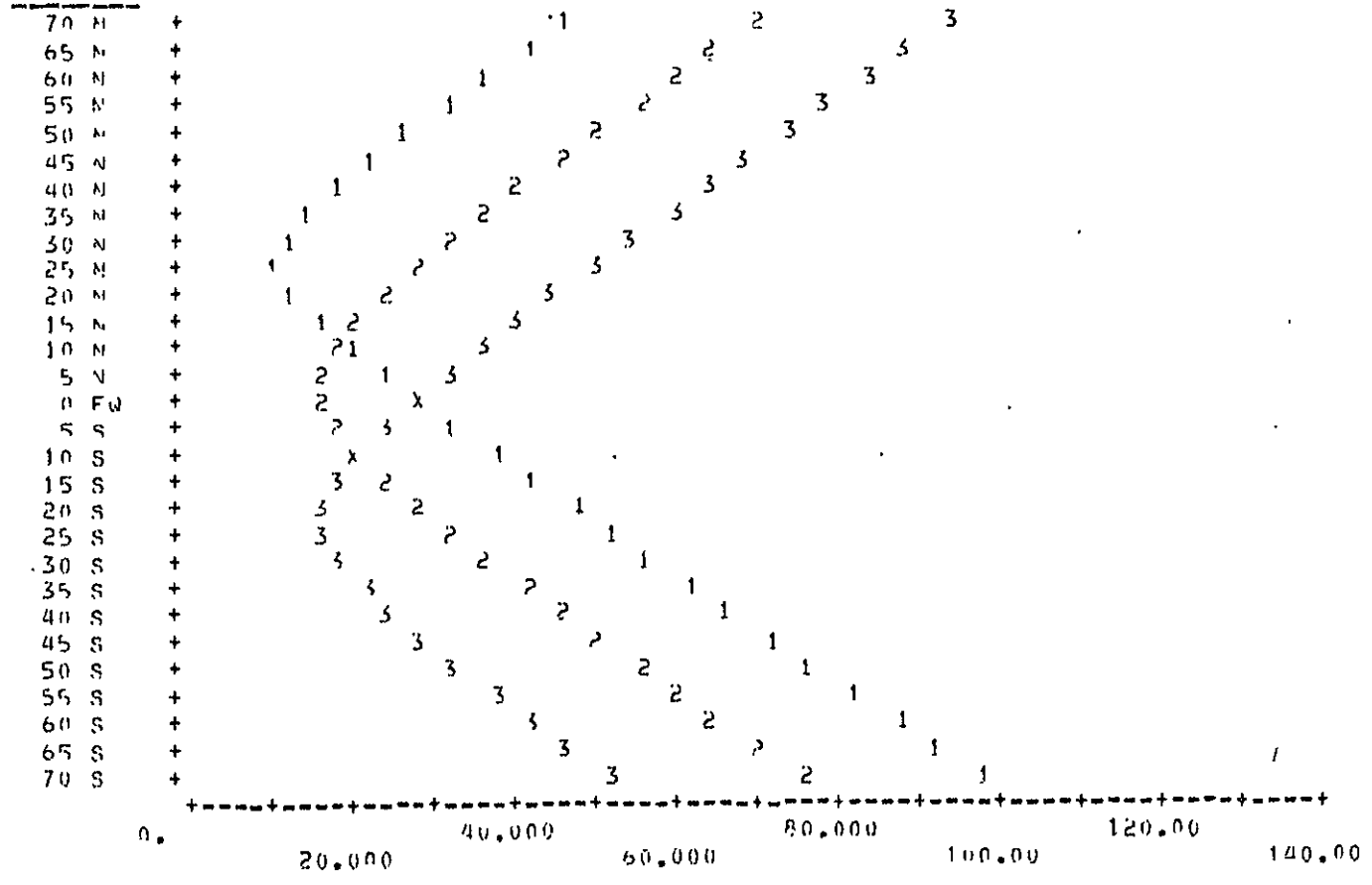

KEY:

SYMBOL	DATE
1	JUN 21, 1978
2	MAR/SEP 21, 1978
3	DEC 21, 1977

ERIM

FIGURE 11 SUN AZIMUTH FOR 9.30 AM EQUATOR CROSSING

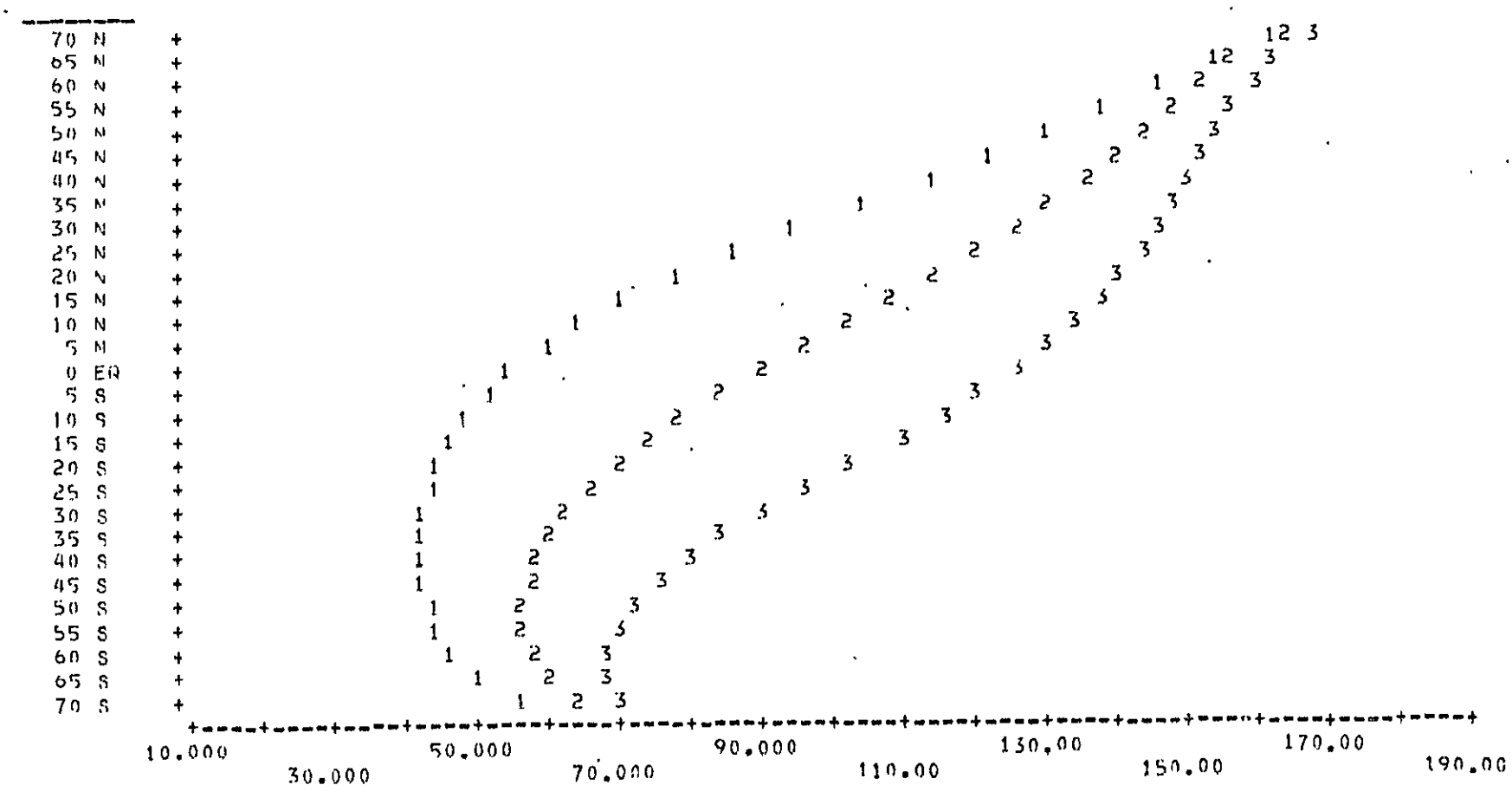

(1) SUN AZ 6 (2) SUN AZ 3 (3) SUN AZ12

KEY:

SYMBOL	DATE
1	JUN 21, 1978
2	MAR/SEP 21, 1978
3	DEC 21, 1977

ERIM

FIGURE 12 SUN AZIMUTH FOR 11.00 AM EQUATOR CROSSING

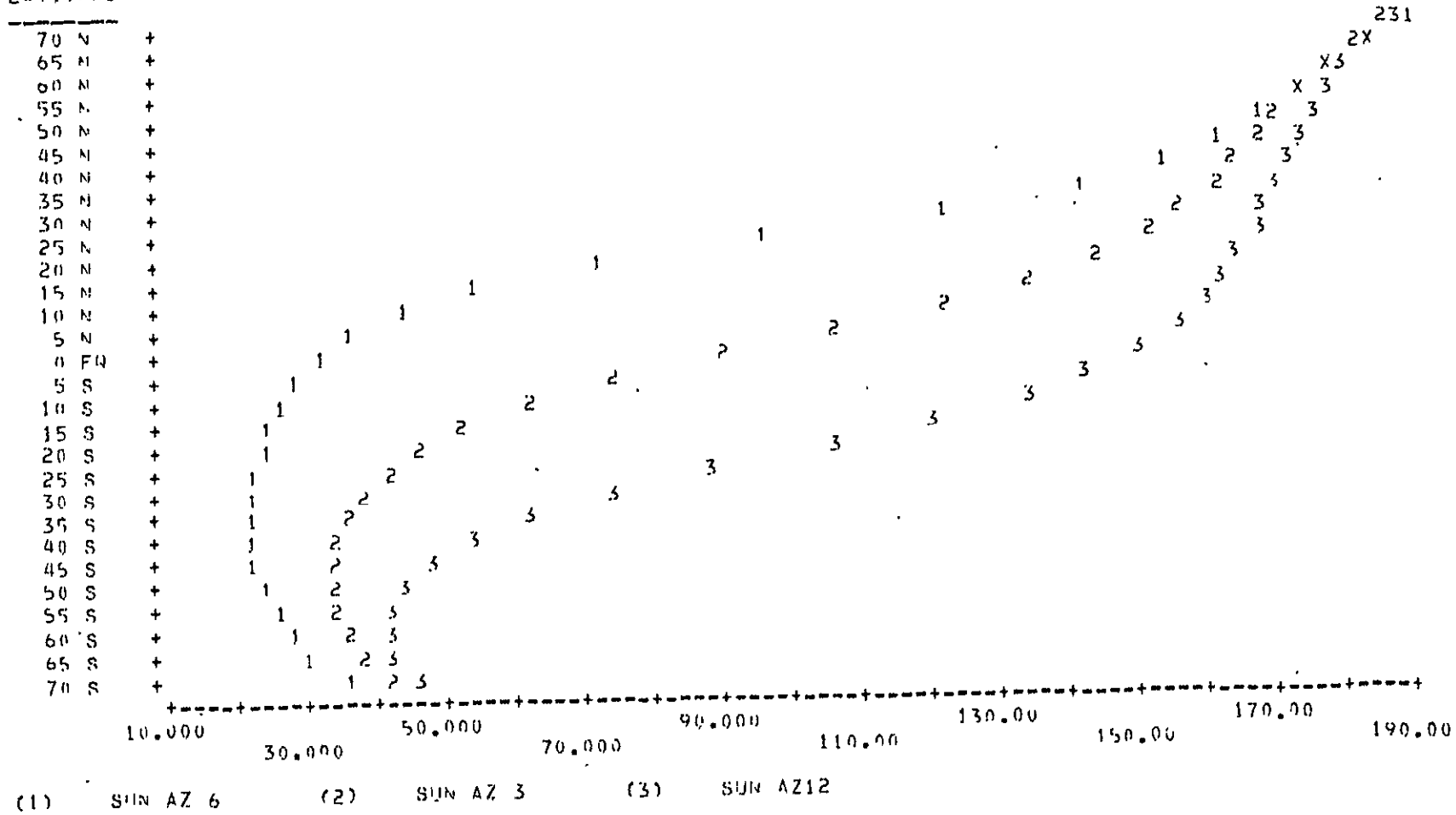

(1) SUN AZ 6 (2) SUN AZ 3 (3) SUN AZ12

KEY:

SYMBOL	DATE
1	JUN 21, 1978
2	MAR/SEP 21, 1978
3	DEC 21, 1977

ERIM

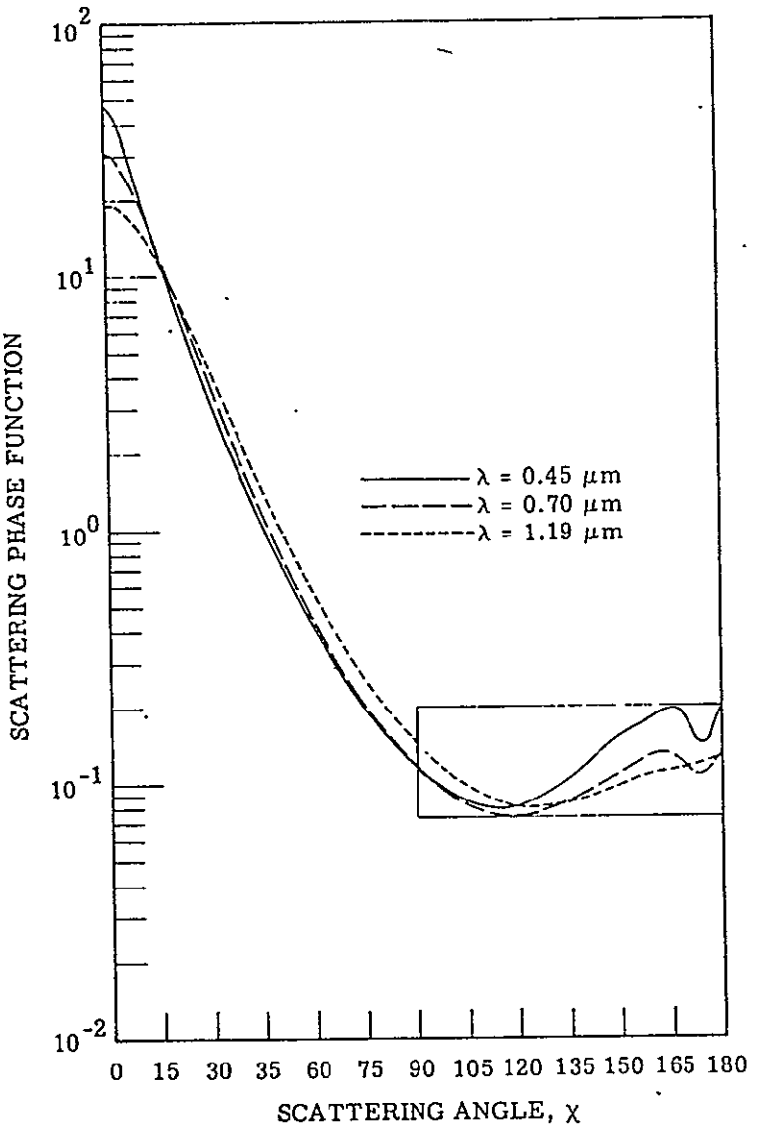

FIGURE 13. SINGLE SCATTERING PHASE FUNCTION FOR DEIRMENDJIAN'S CONTINENTAL TYPE AEROSOL [From Ref. 5]

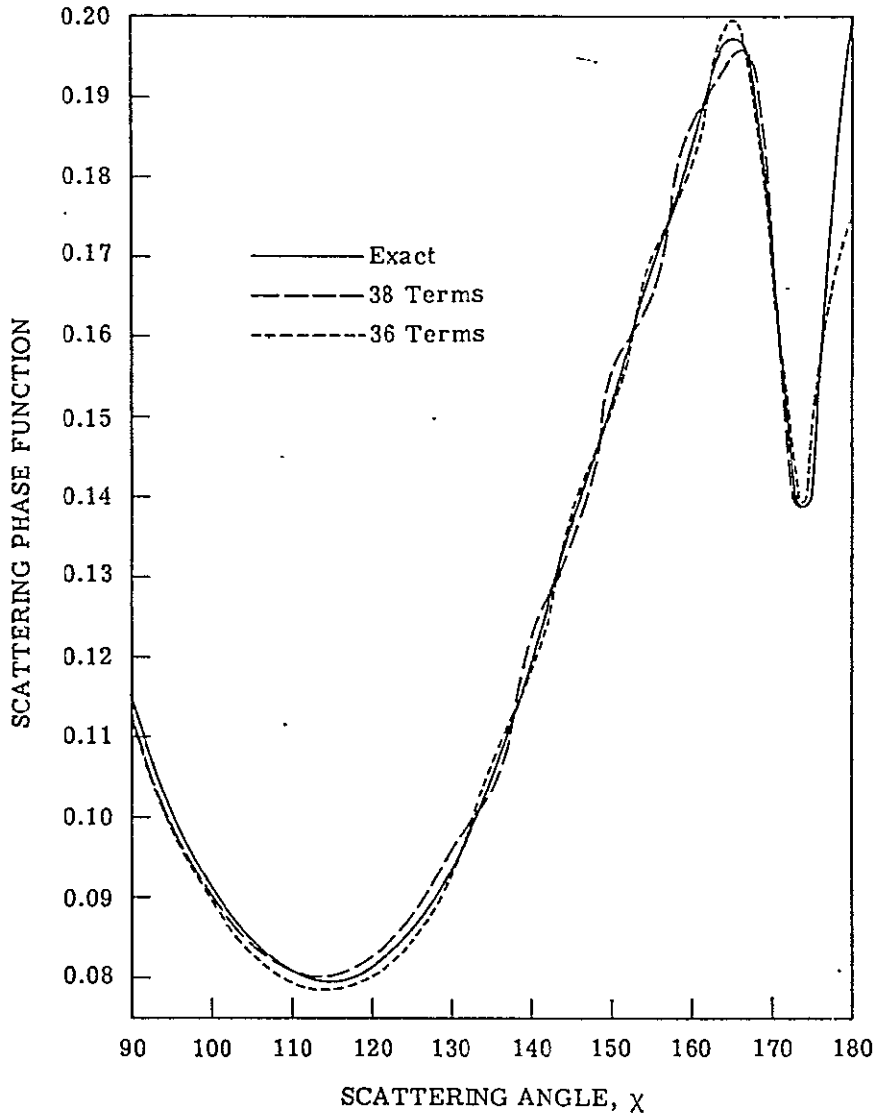

FIGURE 14. COMPARISON BETWEEN EXACT SINGLE SCATTERING PHASE FUNCTION AND APPROXIMATE LEGENDRE SERIES EXPANSION IN THE BACKWARD HEMISPHERE FOR DEIRMENDJIAN'S CONTINENTAL TYPE AEROSOL. $\lambda = 0.45\ \mu m$.
[From Ref. 5]

FIGURE 15 SCATTERING ANGLE FOR 9.30 AM EQUATOR CROSSING. LINEAR SCAN MODE

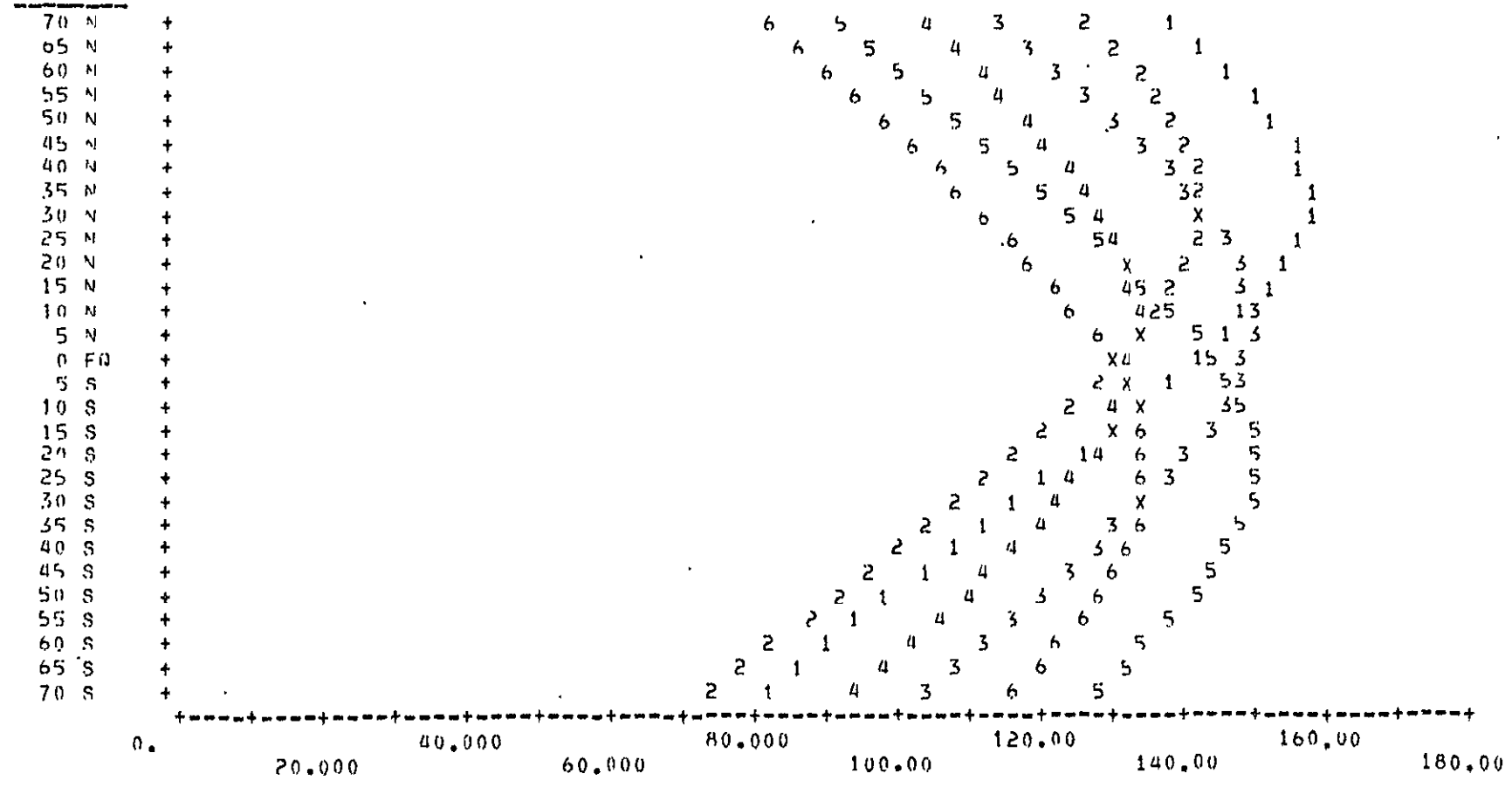

(1) SCA W 6 (2) SCA E 6 (3) SCA W 3 (4) SCA E 3 (5) SCA W 12

(6) SCA E 12

KEY:	SYMBOL	DATE
	1,2	JUN 21, 1978
	3,4	MAR/SEP 21, 1978
	5,6	DEC 21, 1977

ERIM

FIGURE 16 SCATTERING ANGLE FOR 11.00 AM EQUATOR CROSSING. LINEAR SCAN MODE

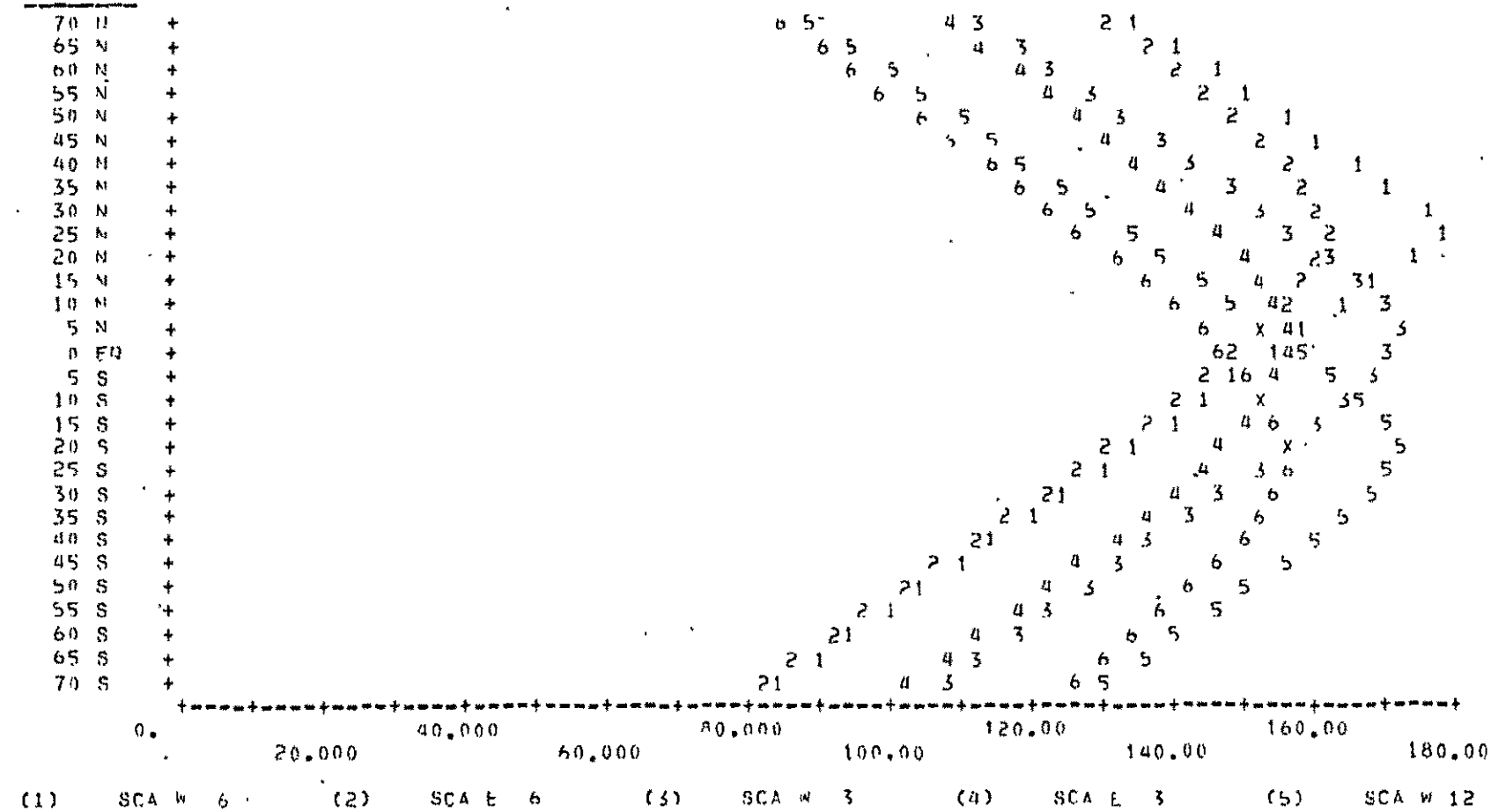

(1) SCA W 6 (2) SCA E 6 (3) SCA W 3 (4) SCA E 3 (5) SCA W 12

(6) SCA E 12

KEY:

SYMBOL	DATE
1,2	JUN 21, 1978
3,4	MAR/SEP 21, 1978
5,6	DEC 21, 1977

ERIM

FIGURE 17 SCATTERING ANGLE FOR 9.30 AM EQUATOR CROSSING, CONICAL SCAN MODE

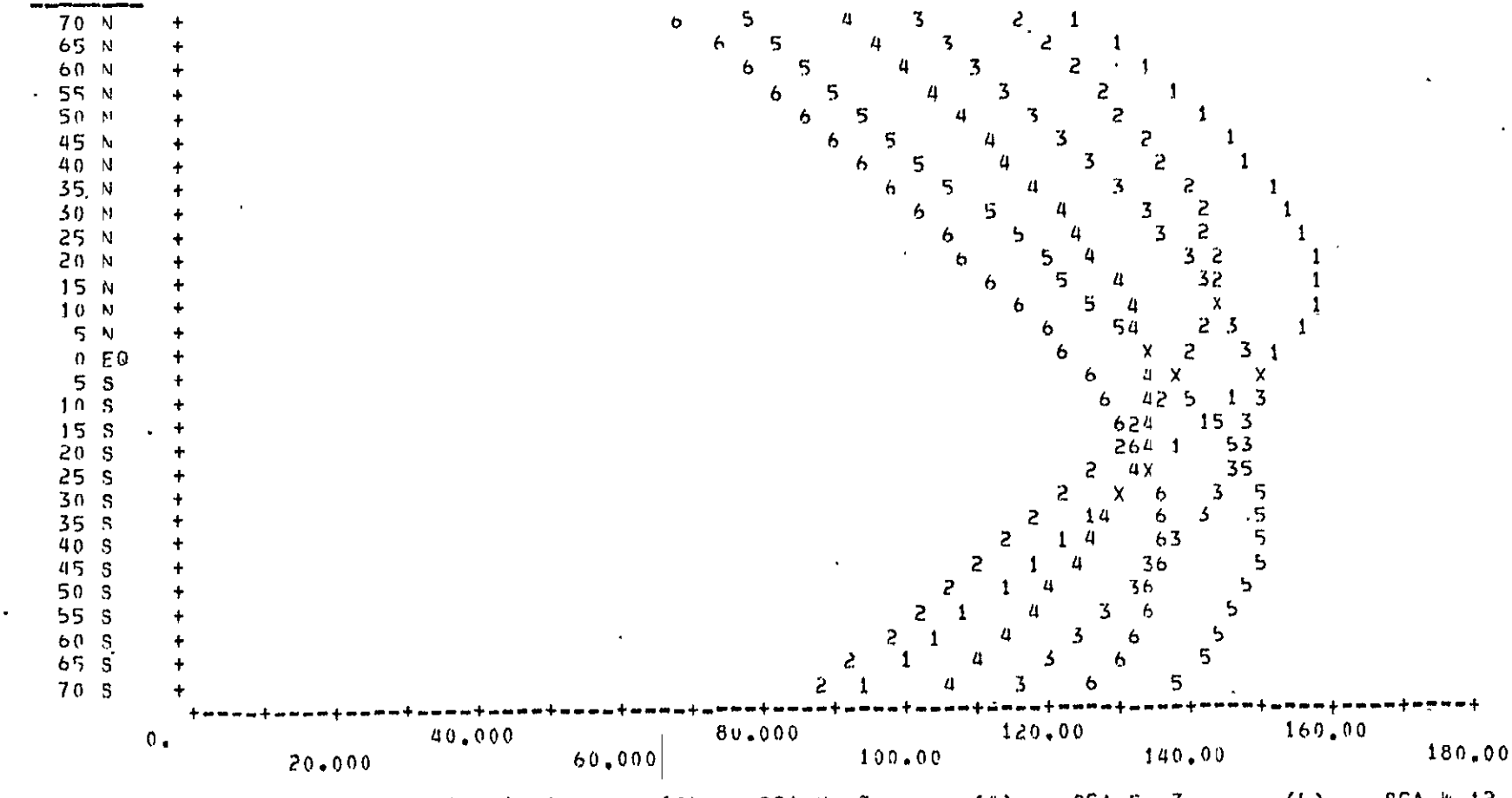

(1) SCA W 6 (2) SCA E 6 (3) SCA W 3 (4) SCA E 3 (5) SCA W 12

(6) SCA E 12

KEY:

SYMBOL	DATE
1,2	JUN 21, 1978
3,4	MAR/SEP 21, 1978
5,6	DEC 21, 1977

ERIM

FIGURE 18 SCATTERING ANGLE FOR 11.00 AM EQUATOR CROSSING. CONICAL SCAN MODE

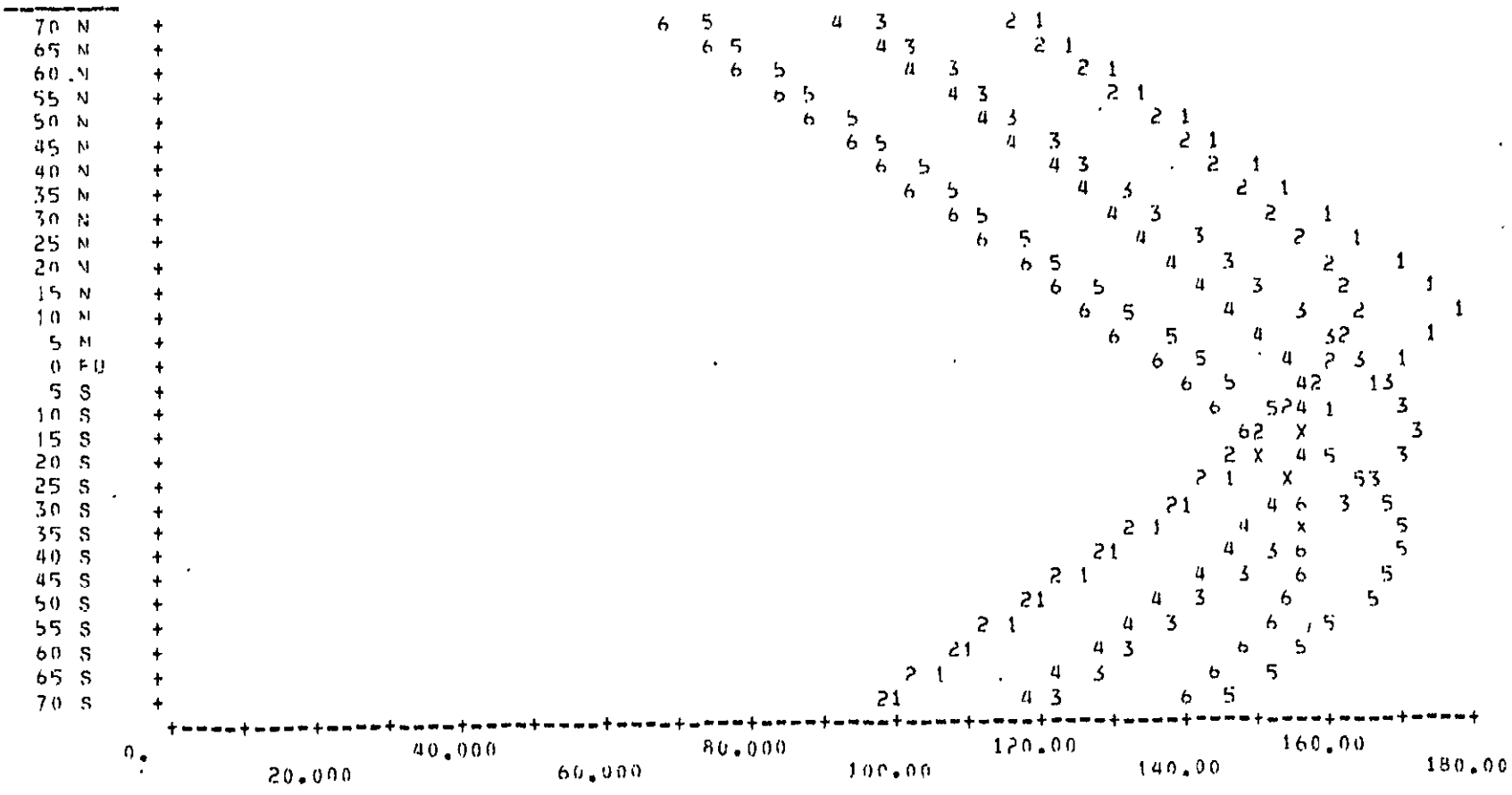

(1) SCA W 4 (2) SCA E 6 (3) SCA W 3 (4) SCA E 3 (5) SCA W 12

(6) SCA E 12

KEY:	SYMBOL	DATE
	1,2	JUN 21, 1978
	3,4	MAR/SEP 21, 1978
	5,6	DEC 21, 1977

ERIM

FIGURE 19 SCATTERING ANGLE FOR 9.30 AM EQUATOR CROSSING. CONICAL SCAN, REARWARD LOOKING

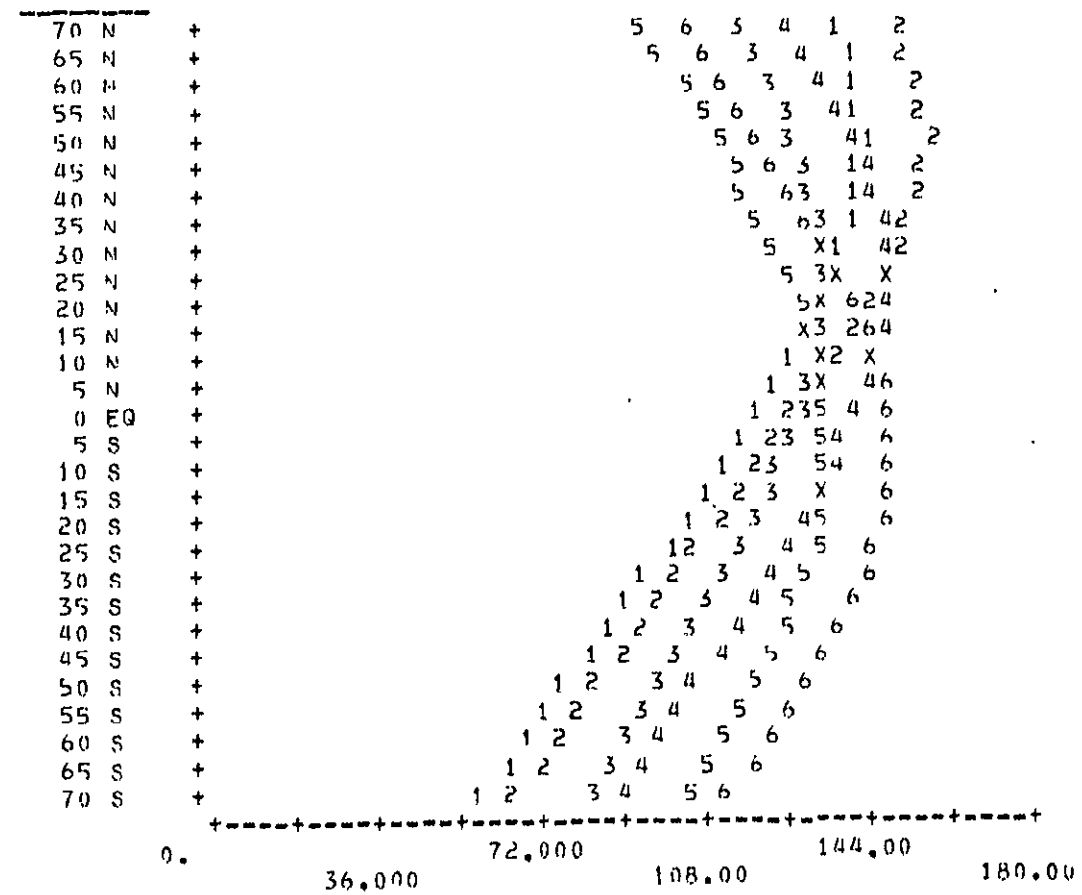

(1) SCA W 6 (2) SCA E 6 (3) SCA W 3

(4) SCA E 3 (5) SCA W 12 (6) SCA E 12

KEY: SYMBOL	DATE
1,2	JUN 21, 1978
3,4	MAR/SEP 21, 1978
5,6	DEC 21, 1977

ERIM

FIGURE 20 SCATTERING ANGLE FOR 11.00 AM EQUATOR CROSSING.
CONICAL SCAN, REARWARD LOOKING

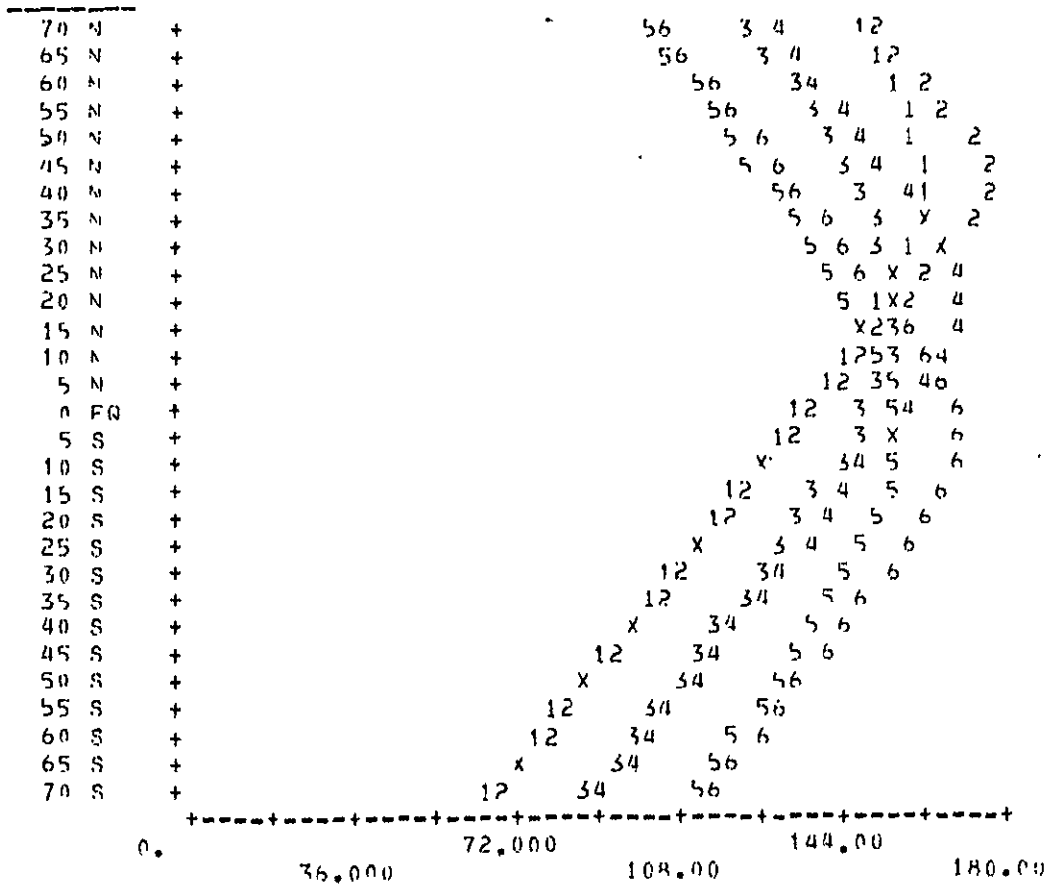

(1) SCA W 6 (2) SCA E 6 (3) SCA W 3

(4) SCA E 3 (5) SCA W 12 (6) SCA E 12

KEY:	SYMBOL	DATE
	1,2	JUN 21, 1978
	3,4	MAR/SEP 21, 1978
	5,6	DEC 21, 1977

ERIM

FIGURE 21 RELATIVE AZIMUTH FOR 9.30 AM EQUATOR CROSSING. LINEAR SCAN MODE

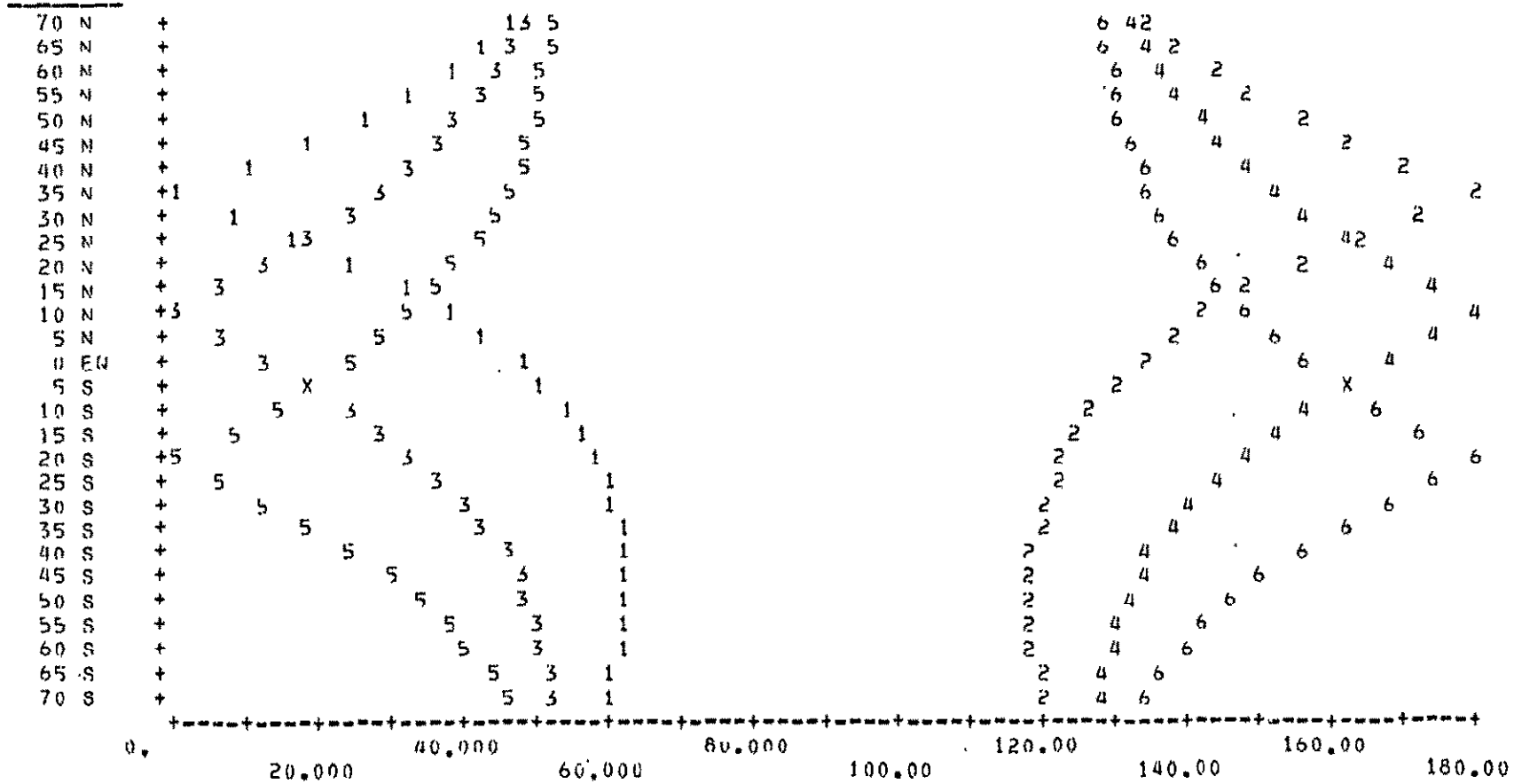

(1) RAZ W 6 (2) RAZ E 6 (3) RAZ W 3 (4) RAZ E 3 (5) RAZ W 12

(6) RAZ E 12

KEY:

SYMBOL	DATE
1,2	JUN 21, 1978
3,4	MAR/SEP 21, 1978
5,6	DEC 21, 1977

ERIM

FIGURE 22 RELATIVE AZIMUTH FOR 11.00 AM EQUATOR CROSSING. LINEAR SCAN MODE

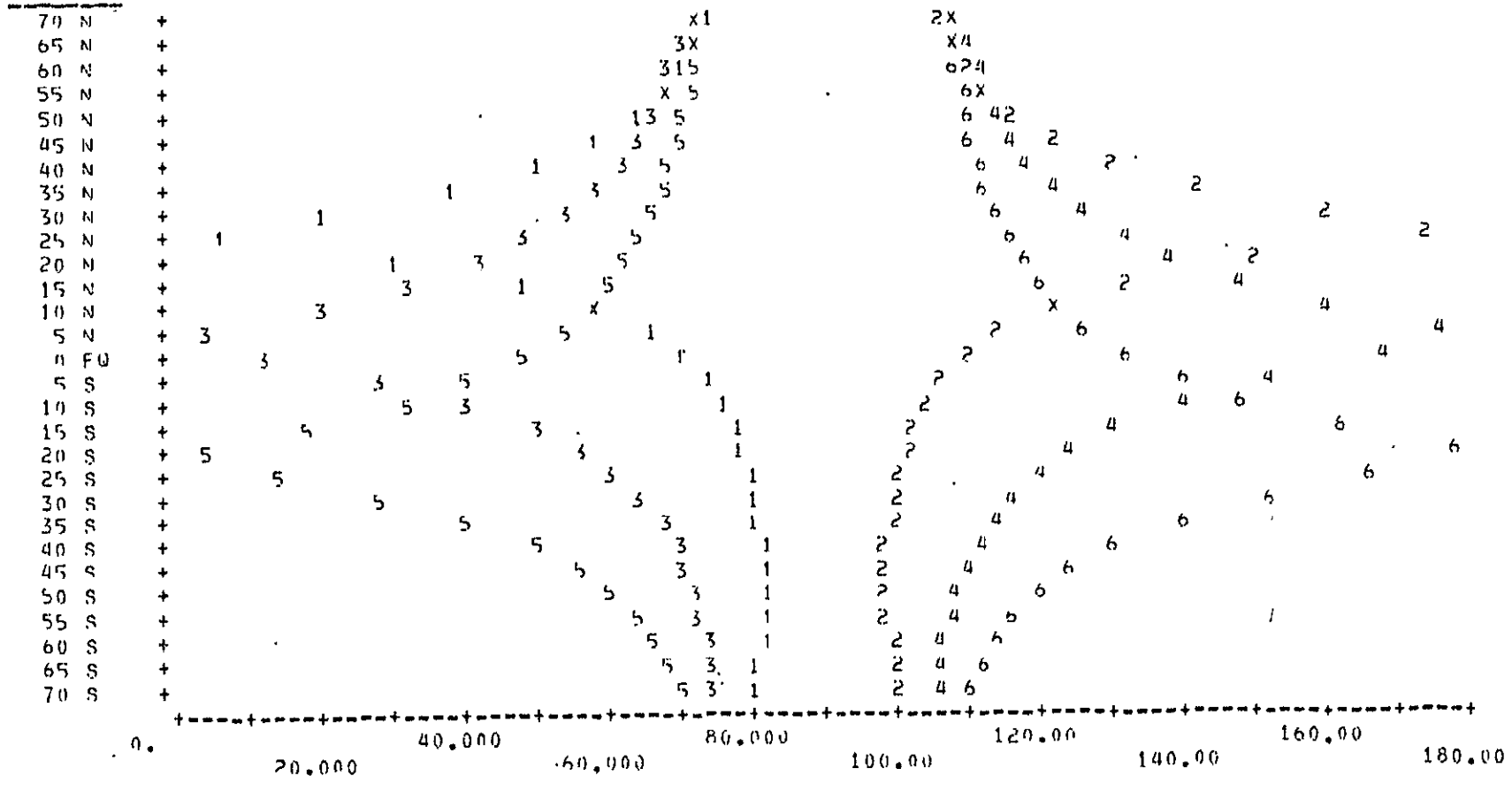

(1) RAZ W 6 (2) RAZ E 6 (3) RAZ W 3 (4) RAZ E 3 (5) RAZ W 12

(6) RAZ E 12

KEY:	SYMBOL	DATE
	1,2	JUN 21, 1978
	3,4	MAR/SEP 21, 1978
	5,6	DEC 21, 1977

ERIM

FIGURE 23 RELATIVE AZIMUTH FOR 9.30 AM EQUATOR CROSSING, CONICAL SCAN MODE

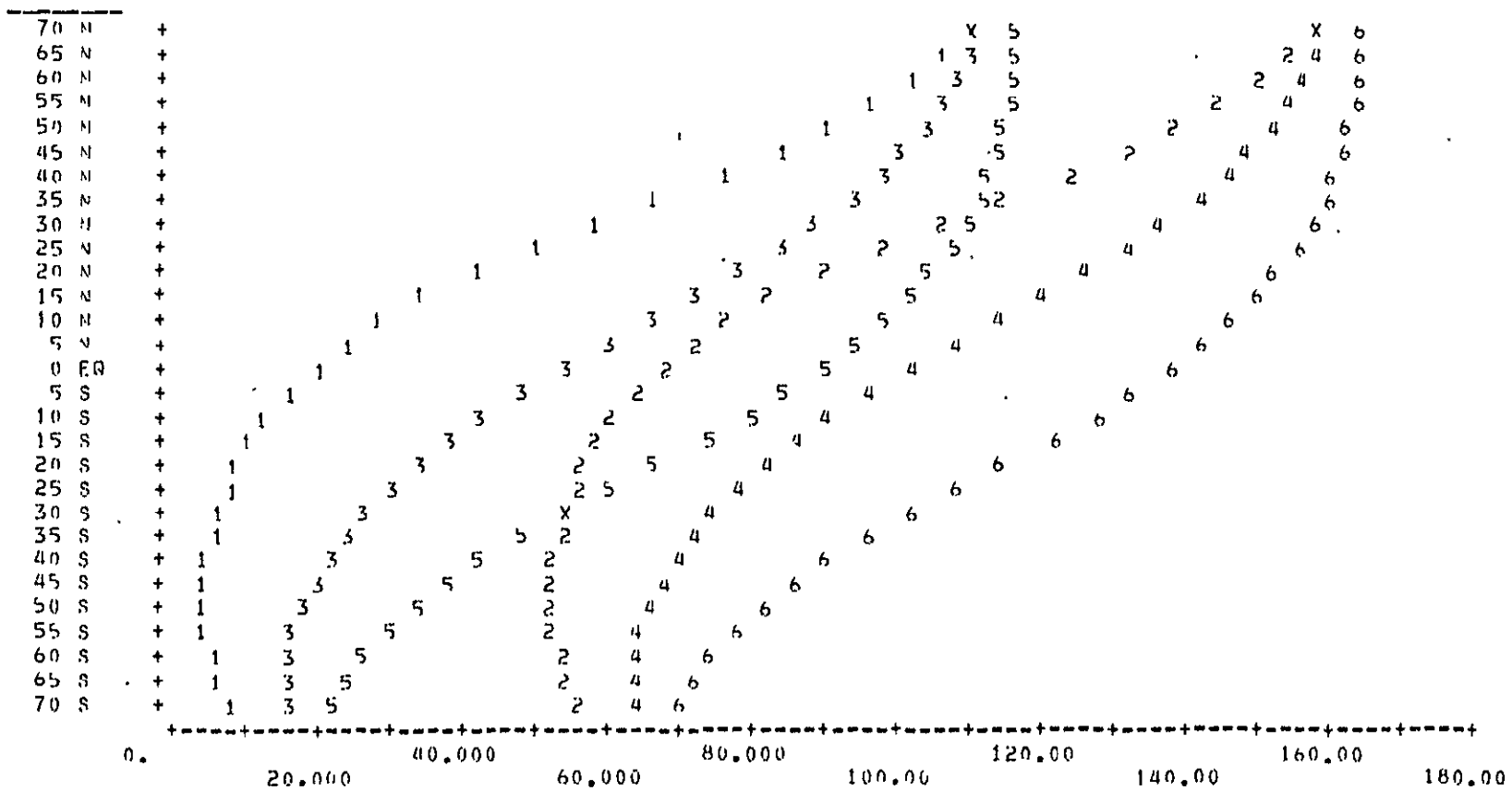

(1) RAZ W 6 (2) RAZ E 6 (3) RAZ W 3 (4) RAZ E 3 (5) RAZ W 12

(6) RAZ E 12

KEY:	SYMBOL	DATE
	1,2	JUN 21, 1978
	3,4	MAR/SEP 21, 1978
	5,6	DEC 21, 1977

ERIM

FIGURE 24 RELATIVE AZIMUTH FOR 11.00 AM EQUATOR CROSSING. CONICAL SCAN MODE

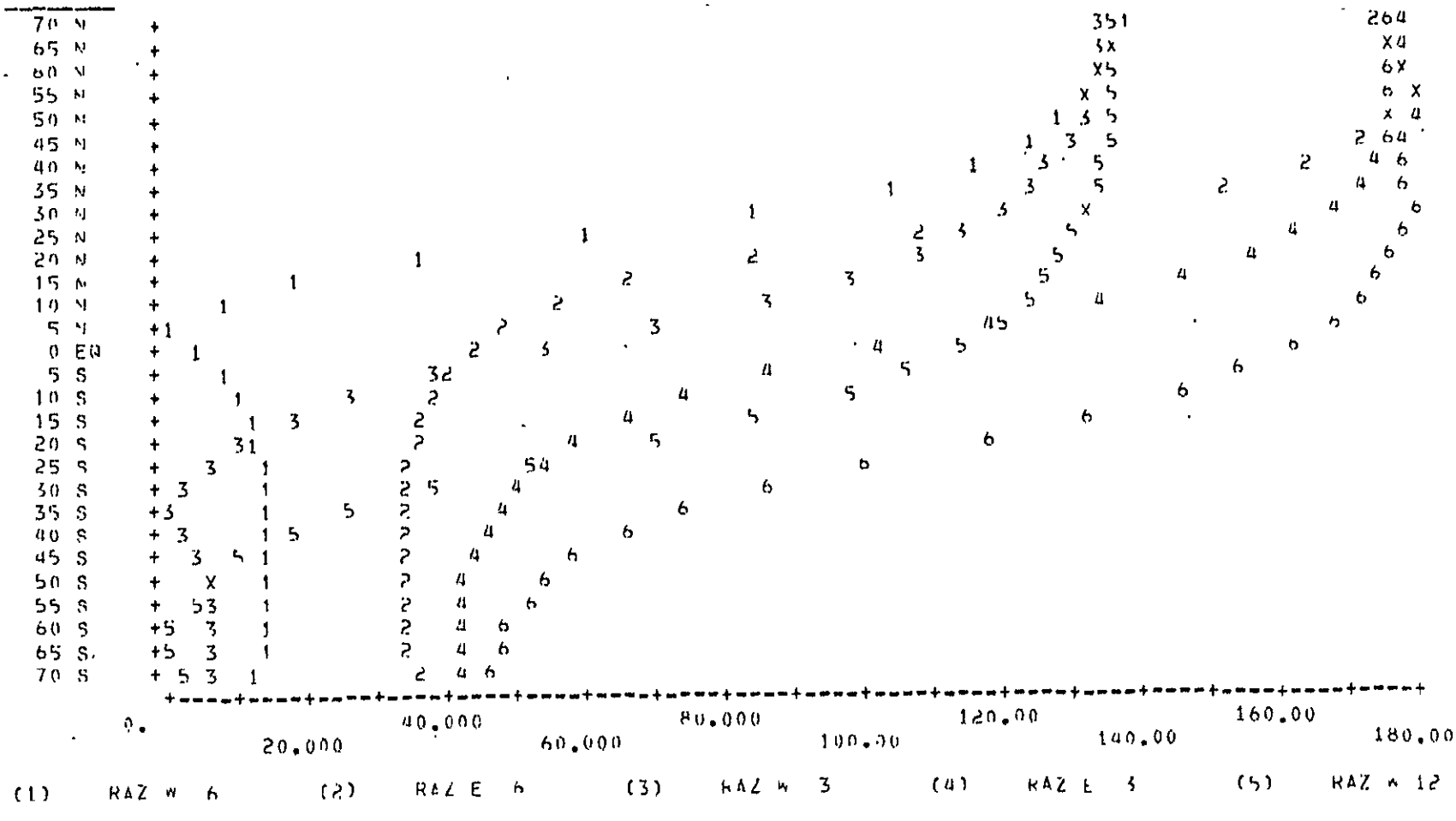

(1) RAZ W 6 (2) RAZ E 6 (3) RAZ W 3 (4) RAZ E 3 (5) RAZ W 12

(6) RAZ E 12

KEY:

SYMBOL	DATE
1,2	JUN 21, 1978
3,4	MAR/SEP 21, 1978
5,6	DEC 21, 1977

ERIM

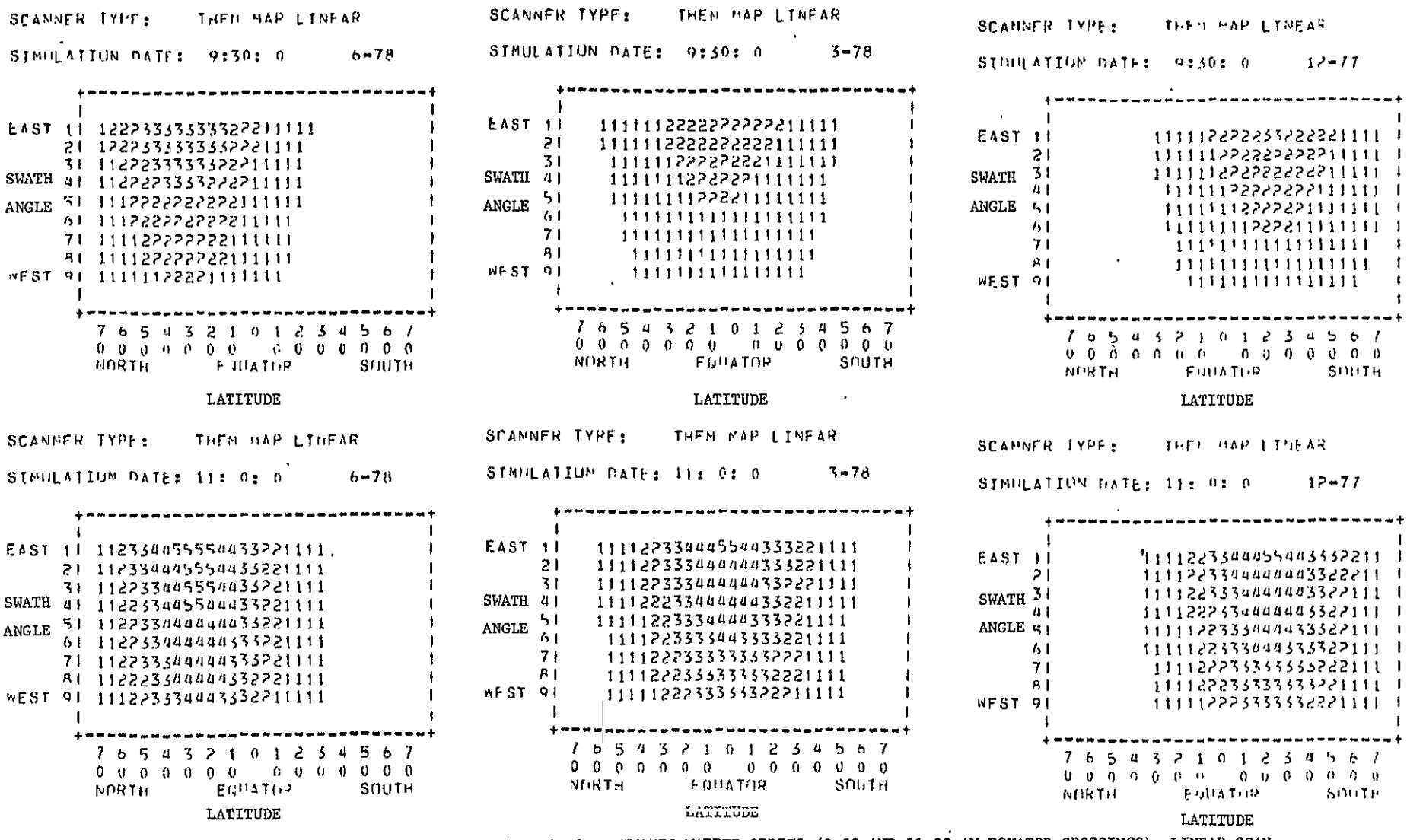

FIGURE 25. MAPS OF POTENTIAL SUN GLINT ZONES, THEMATIC MAPPER ORBITS (9:30 AND 11:00 AM EQUATOR CROSSINGS); LINEAR SCAN.

Key: Numbers indicate surface slopes (0° = horizontal) for which glint conditions could exist:

1 = $\geq 30^{\circ}$
2 = $\geq 20^{\circ}$
3 = $\geq 15^{\circ}$
4 = $\geq 10^{\circ}$
5 = $\geq 5^{\circ}$

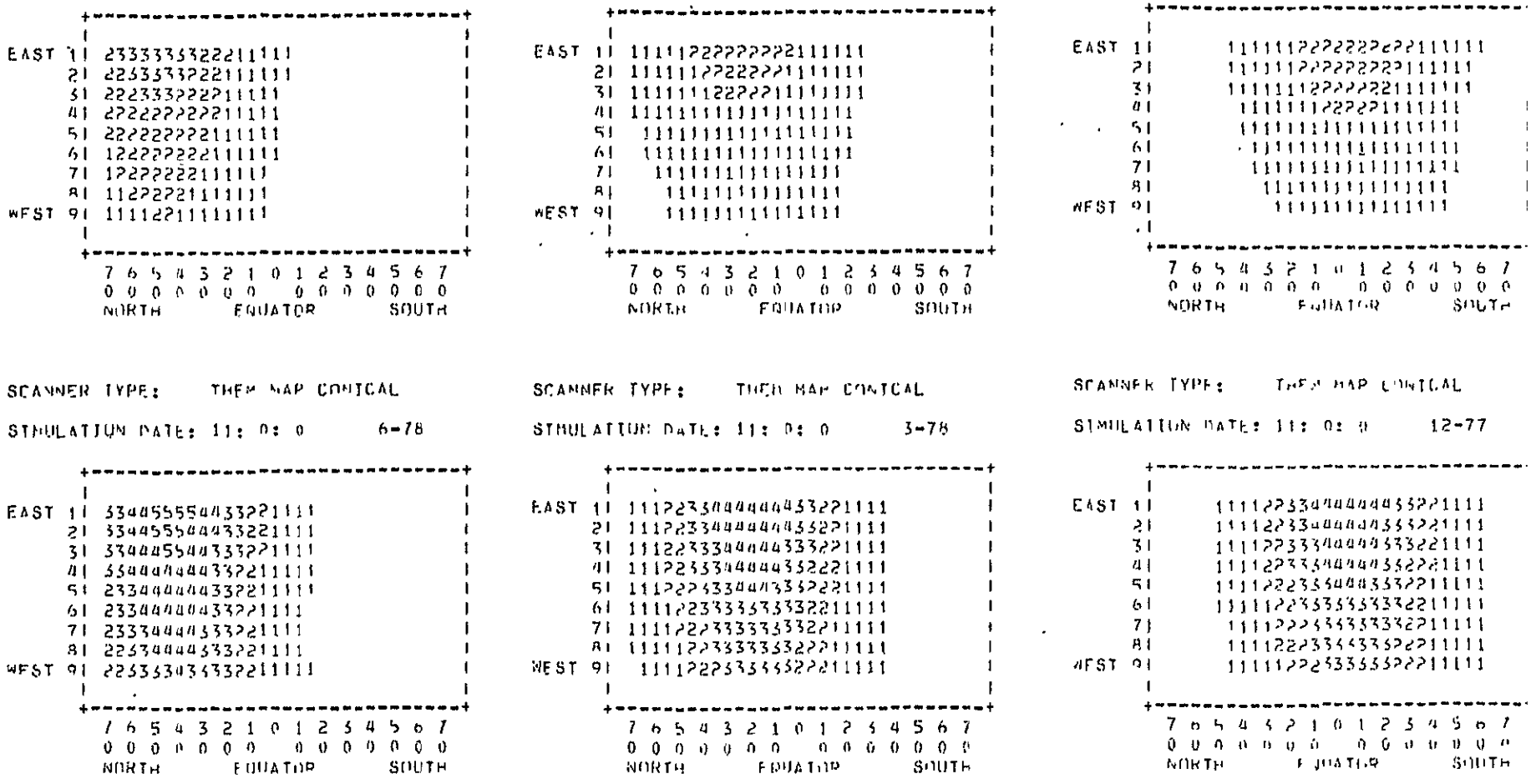

FIGURE 26. MAPS OF POTENTIAL SUN GLINT ZONES, THEMATIC MAPPER ORBITS (9:30 AND 11:00 AM EQUATOR CROSSINGS); CONICAL SCAN.

Key: Numbers indicate surface slopes (0^o = horizontal) for which glint conditions could exist:

1 = $\geq 30^o$ 4 = $\geq 10^o$
2 = $\geq 20^o$ 5 = $\geq 5^o$
3 = $\geq 15^o$

SCANNER TYPE: THEM MAP LINEAR

STMULATION DATE: 9:30: 0 6-78

```
EAST 1| 12223333333322211111
     2| 1222333333332221111
     3| 112223333332222111111
     4| 1122223333222211111
     5| 111222222222211111
     6| 11122222222221111
     7| 1111222222222111111
     8| 111112222222111111
WEST 9| 11111122222111111
```

7 6 5 4 3 2 1 0 1 2 3 4 5 6 7
0 0 0 0 0 0 0 0 0 0 0 0 0 0 0
NORTH EQUATOR SOUTH

SCANNER TYPE: THEM MAP LINEAR

STMULATION DATE: 9:30: 0 3-78

```
EAST 1|   1111112222222222211111
     2|   1111112222222222211111
     3|    111111222222222111111
     4|    111111122222221111111
     5|   1111111122222111111111
     6|    111111111111111111111
     7|   1111111111111111111
     8|    111111111111111111
WEST 9|    11111111111111
```

7 6 5 4 3 2 1 0 1 2 3 4 5 6 7
0 0 0 0 0 0 0 0 0 0 0 0 0 0 0
NORTH EQUATOR SOUTH

SCANNER TYPE: THEM MAP LINEAR

STMULATION DATE: 9:30: 0 12-77

```
EAST 1|          1111122222232222221111
     2|          1111112222222222211111
     3|          1111112222222222211111
     4|           111111222222222111111
     5|           111111122222221111111
     6|           111111112222211111111
     7|            1111111111111111111
     8|            1111111111111111111
WEST 9|             11111111111111
```

7 6 5 4 3 2 1 0 1 2 3 4 5 6 7
0 0 0 0 0 0 0 0 0 0 0 0 0 0 0
NORTH EQUATOR SOUTH

SCANNER TYPE: THEM MAP CONICAL

STMULATION DATE: 9:30: 0 6-78

```
EAST 1| 2333333322211111
     2| 223333322211111
     3| 22233322221111
     4| 2222222222111111
     5| 222222222111111
     6| 12222222111111
     7| 1122222211111
     8| 111122211111111
WEST 9| 11112211111111
```

7 6 5 4 3 2 1 0 1 2 3 4 5 6 7
0 0 0 0 0 0 0 0 0 0 0 0 0 0 0
NORTH EQUATOR SOUTH

SCANNER TYPE: THEM MAP CONICAL

STMULATION DATE: 9:30: 0 3-78

```
EAST 1|  1111122222222211111
     2|  1111112222222211111111
     3|  1111111222222111111111
     4|  1111111111111111111
     5|   111111111111111111
     6|  1111111111111111111
     7|   11111111111111
     8|    1111111111111
WEST 9|    111111111111
```

7 6 5 4 3 2 1 0 1 2 3 4 5 6 7
0 0 0 0 0 0 0 0 0 0 0 0 0 0 0
NORTH EQUATOR SOUTH

SCANNER TYPE: THEM MAP CONICAL

STMULATION DATE: 9:30: 0 12-77

```
EAST 1|      1111112222222222211111
     2|      1111112222222222111111
     3|      1111111222222222111111
     4|       111111122222221111111
     5|       111111111111111111111
     6|       111111111111111111111
     7|       111111111111111111
     8|        1111111111111111
WEST 9|         11111111111111
```

7 6 5 4 3 2 1 0 1 2 3 4 5 6 7
0 0 0 0 0 0 0 0 0 0 0 0 0 0 0
NORTH EQUATOR SOUTH

FIGURE 27. COMPARISON OF LINEAR AND CONICAL POTENTIAL GLINT ZONES, THEMATIC MAPPER ORBIT, 9:30 AM EQUATOR CROSSING.

Key: Numbers indicate surface slopes (0° = horizontal)
for which glint conditions could exist:

1 = ≥ 30° 4 = ≥ 10°
2 = ≥ 20° 5 = ≥ 5°
3 = ≥ 15°

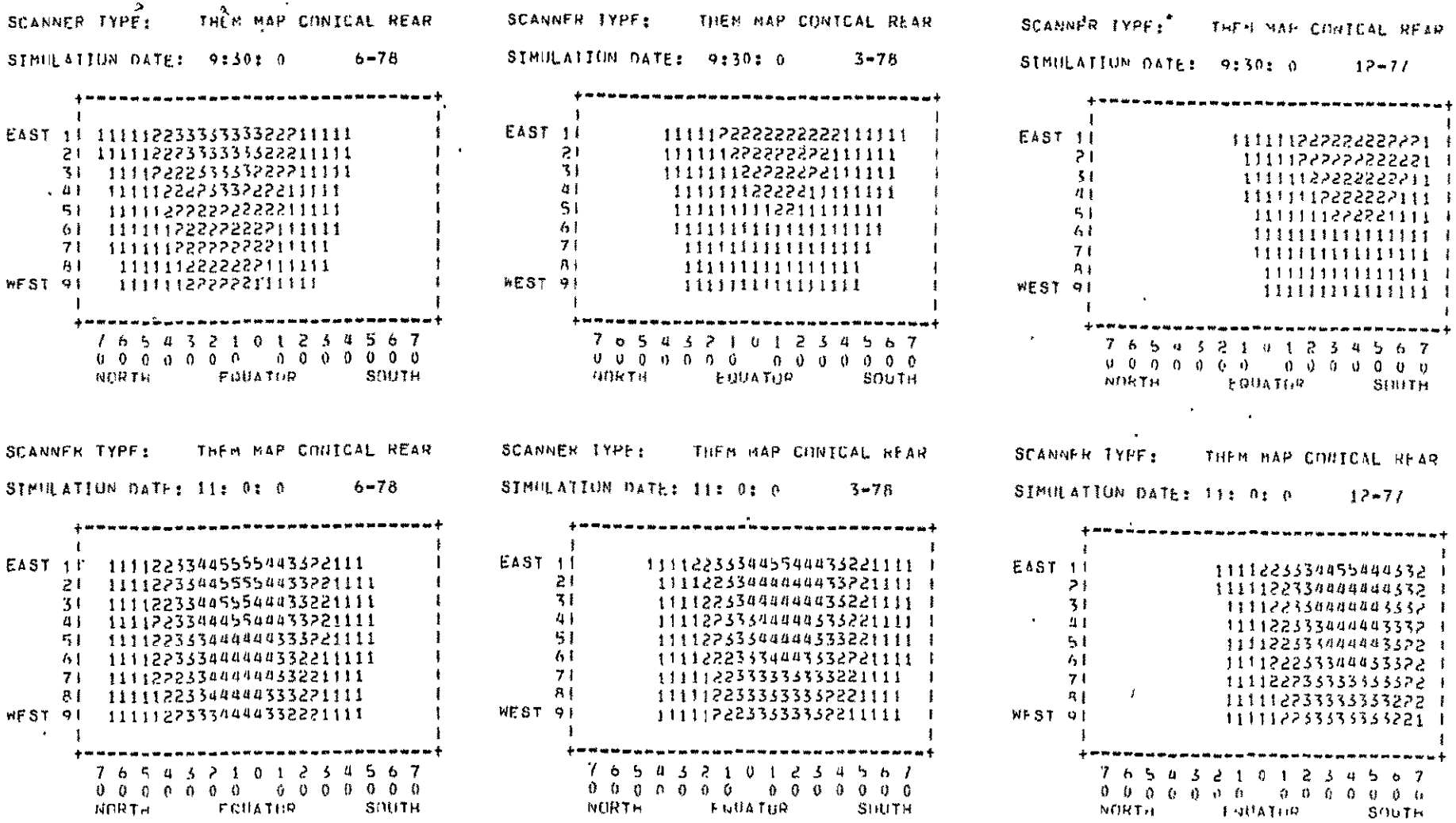

FIGURE 28. MAPS OF POTENTIAL SUN GLINT ZONES, THEMATIC MAPPER ORBITS (9:30 AND 11:00 AM EQUATOR CROSSINGS); CONICAL SCAN, REARWARD LOOKING.

Key: Numbers indicate surface slopes (0° = horizontal) for which glint conditions could exist:

1 = $\geq 30^\circ$ 4 = $\geq 10^\circ$

2 = $\geq 20^\circ$ 5 = $\geq 5^\circ$

3 = $\geq 15^\circ$

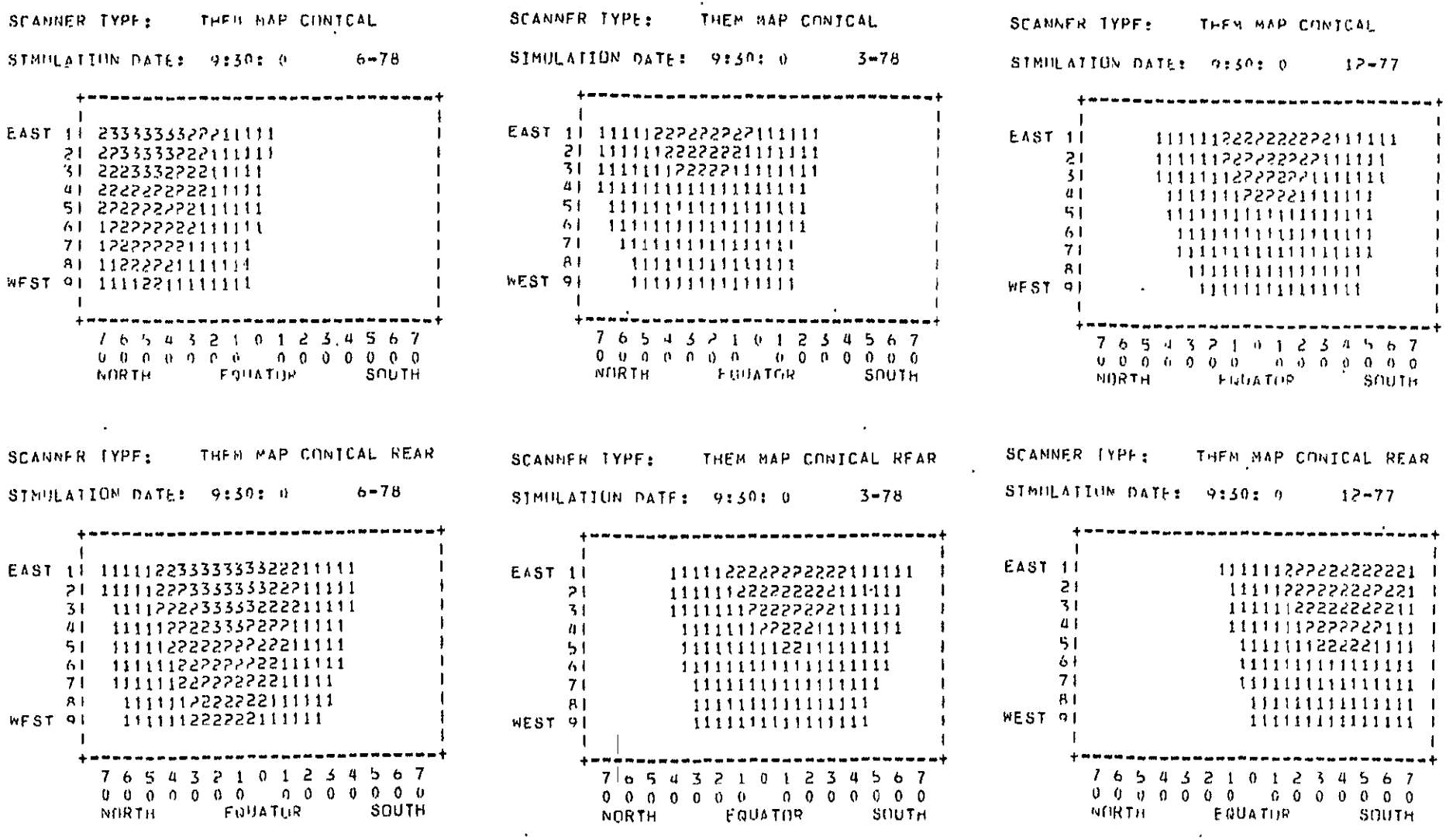

FIGURE 29. COMPARISON OF POTENTIAL GLINT ZONES, FOR FORWARD- AND REARWARD-LOOKING CONICAL SCANNERS, THEMATIC MAPPER ORBIT, 9:30 AM EQUATOR CROSSING.

Key: Numbers indicate surface slopes (0^{o} = horizontal) for which glint conditions could exist:

1 = $\geq 30^{o}$ 4 = $\geq 10^{o}$

2 = $\geq 20^{o}$ 5 = $\geq 5^{o}$

3 = $\geq 15^{o}$

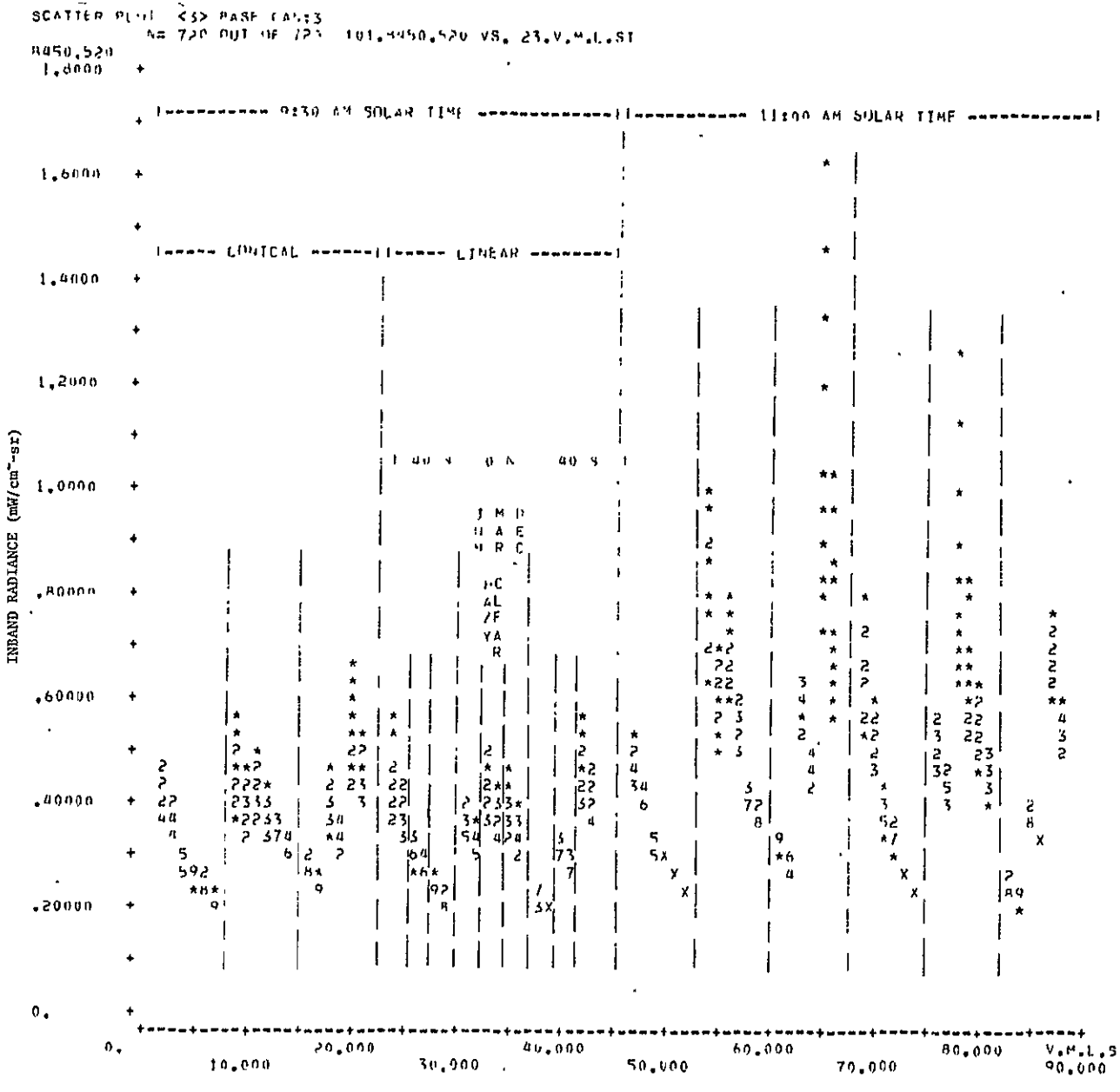

FIGURE 30. FACTORS AFFECTING TOTAL RADIANCE, 0.45-0.52-μm BAND

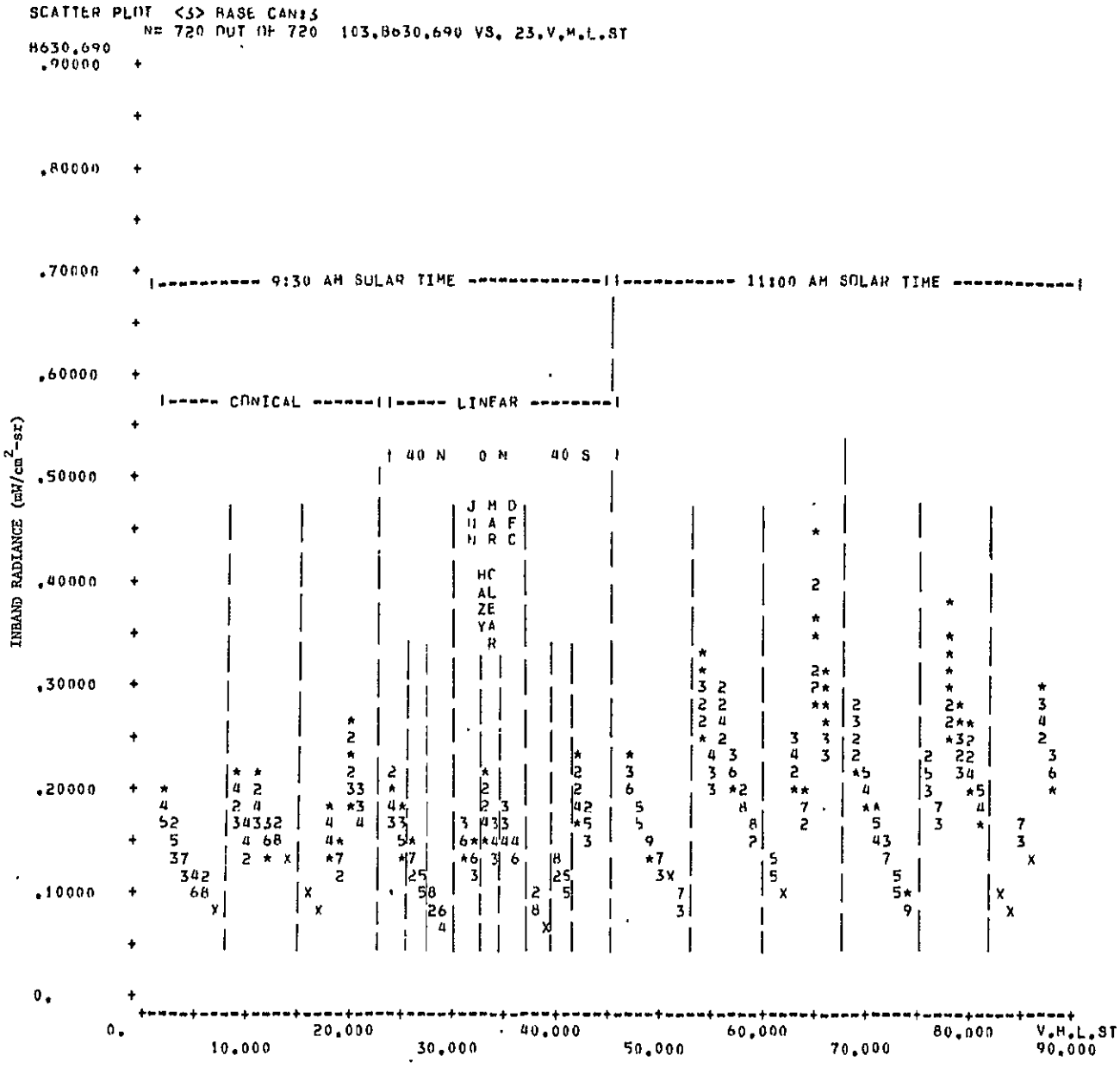

FIGURE 31. FACTORS AFFECTING TOTAL RADIANCE, 0.63-0.69-um BAND

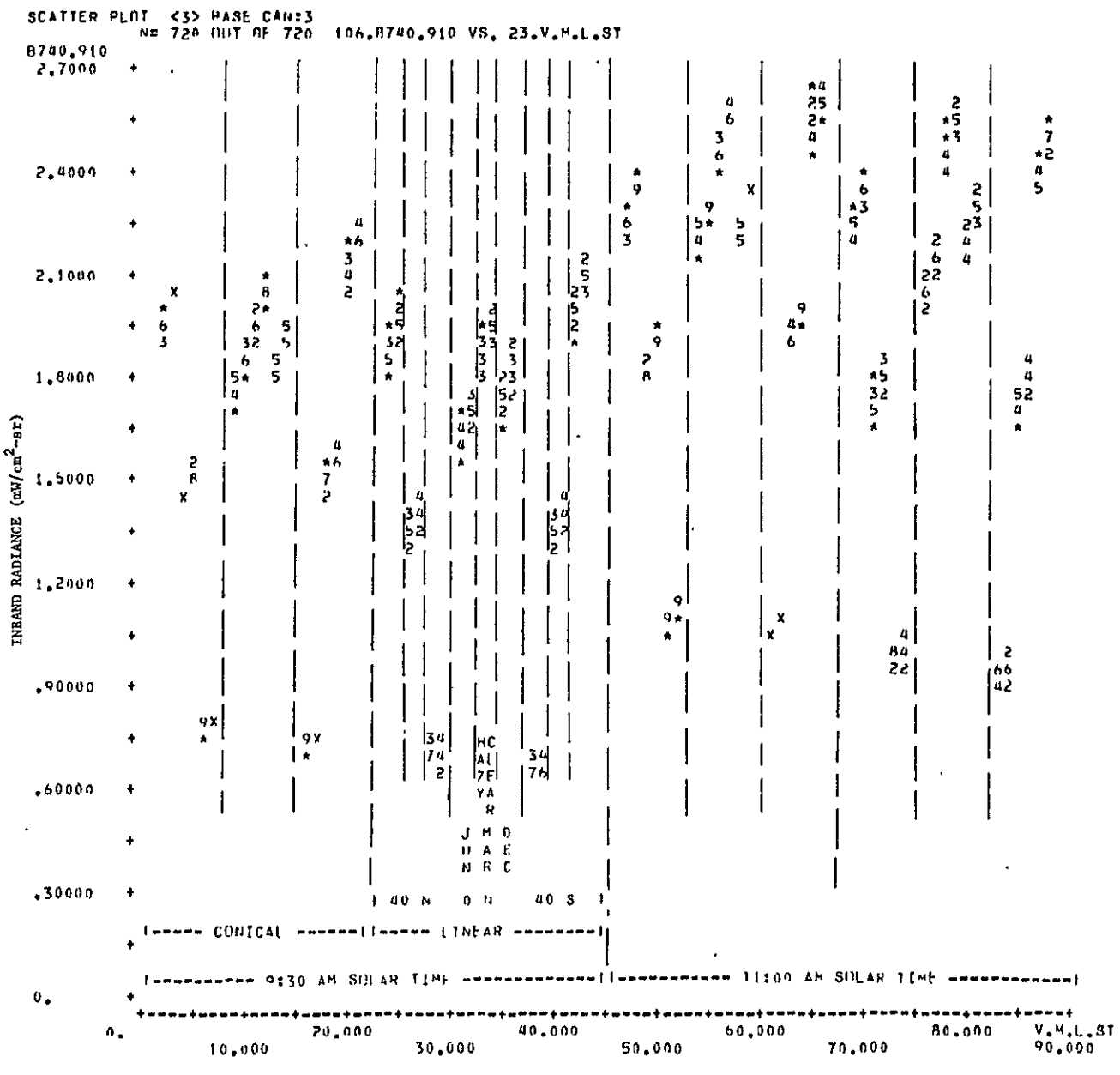

FIGURE 32. FACTORS AFFECTING TOTAL RADIANCE, 0.74-0.91-μm BAND

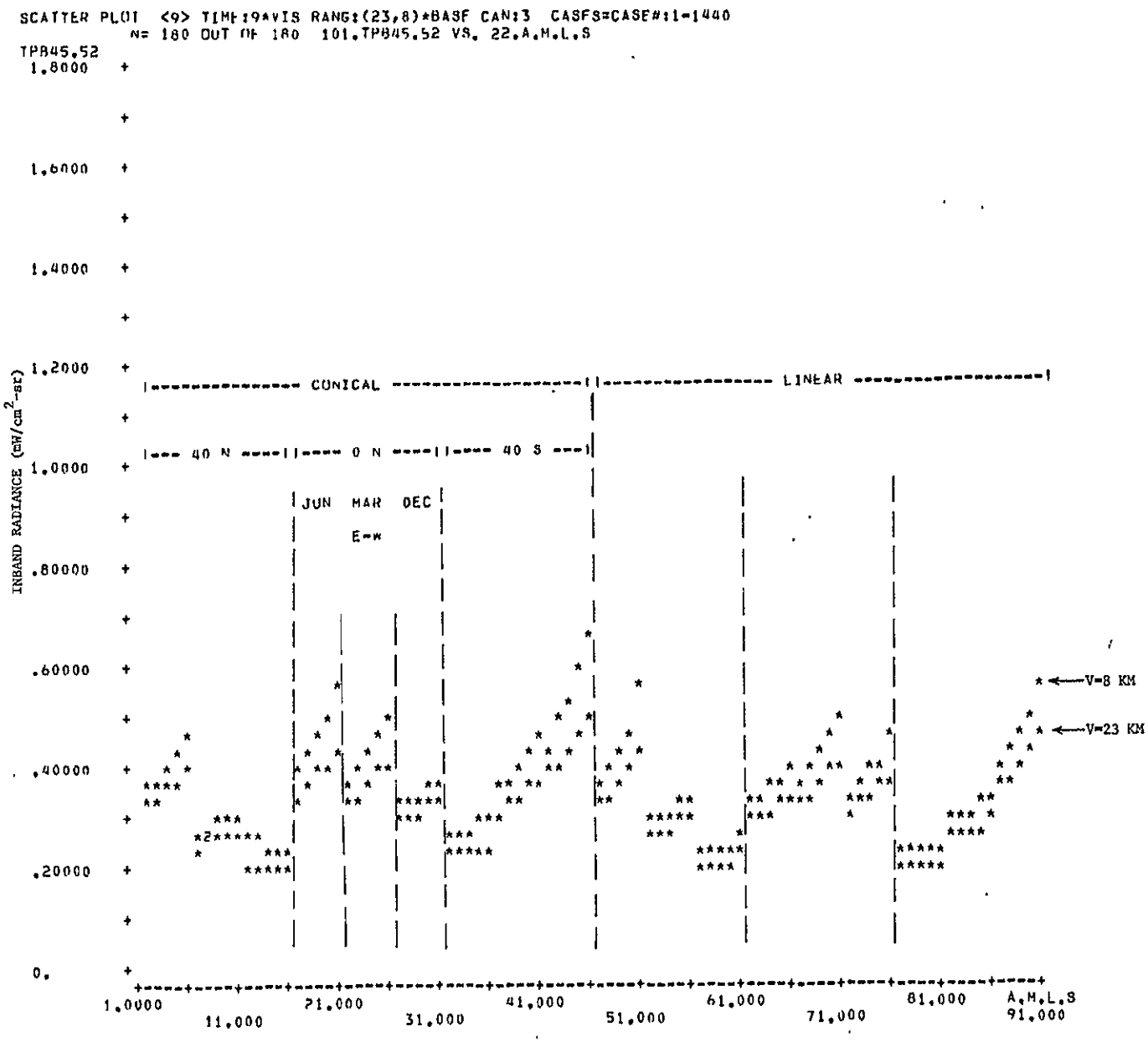

FIGURE 33. SCAN ANGLE DEPENDENCE OF TOTAL RADIANCE FOR V=8 AND 23 KM, 0.45-0.52-μm BAND, 9:30 AM

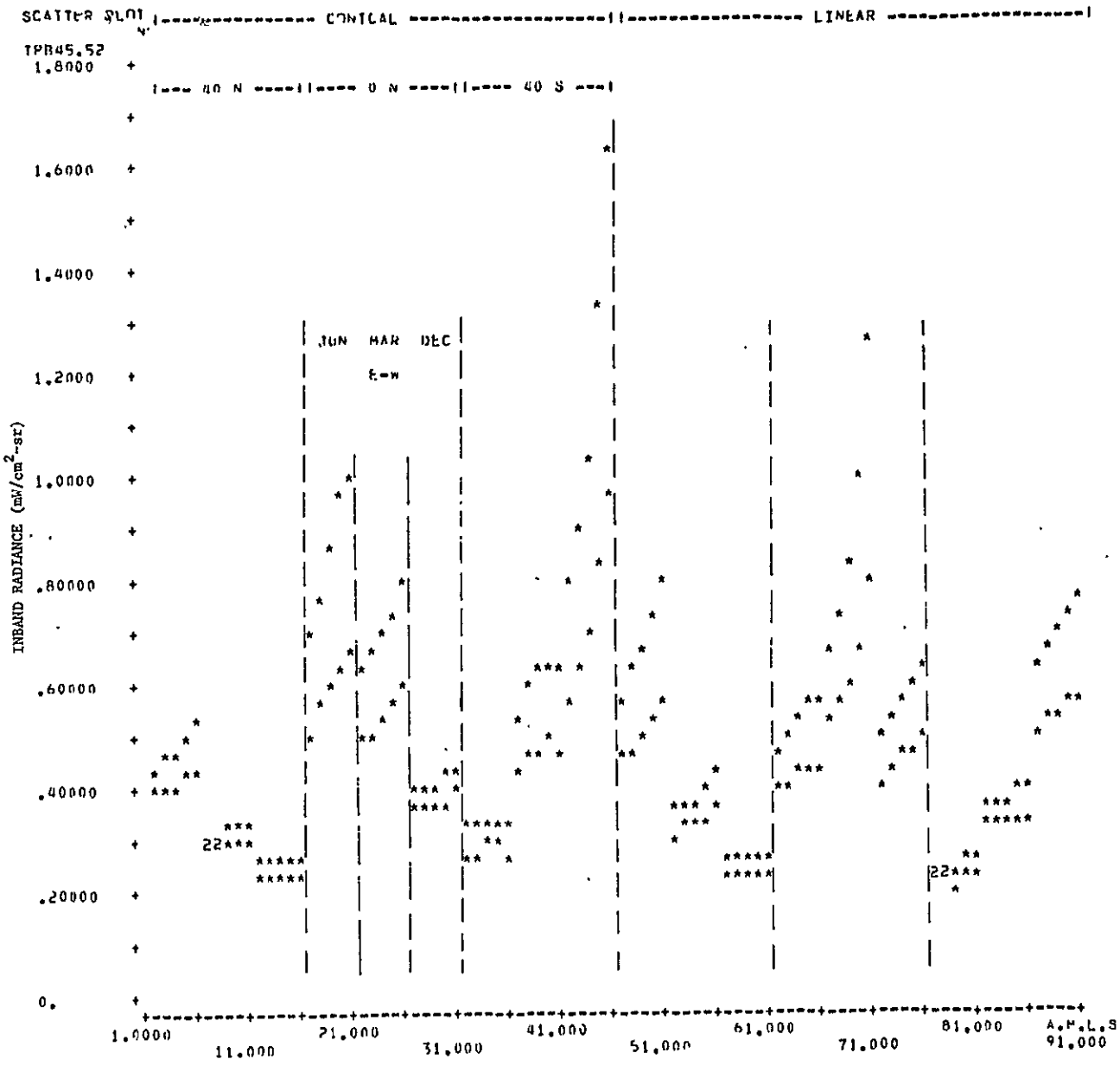

FIGURE 34. SCAN ANGLE DEPENDENCE OF TOTAL RADIANCE FOR V=8 AND 23 KM, 0.45-0.52-μm BAND, 11:00 AM

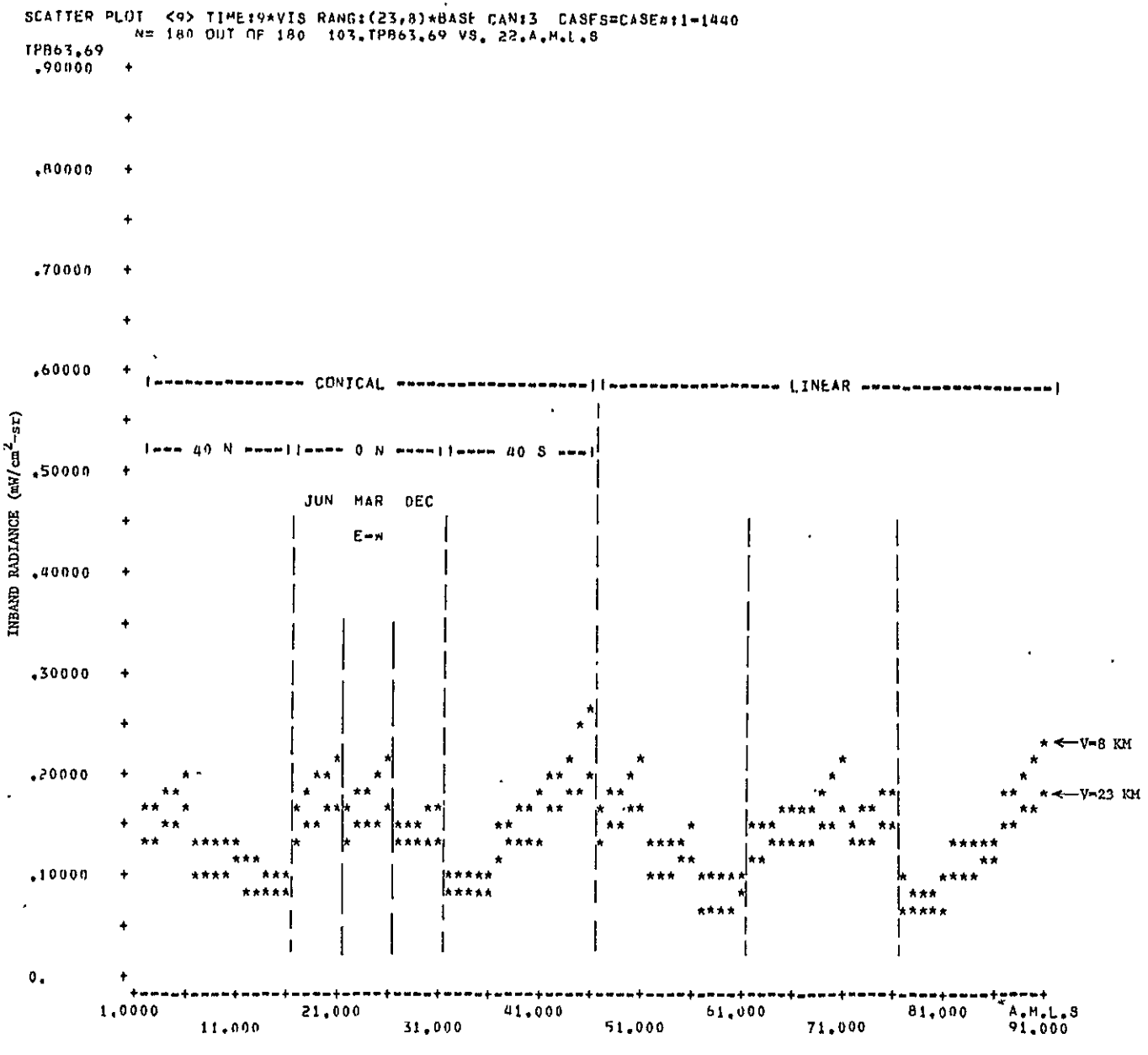

FIGURE 35. SCAN ANGLE DEPENDENCE OF TOTAL RADIANCE FOR V=8 AND 23 KM, 0.63-0.69-μm BAND, 9:30 AM

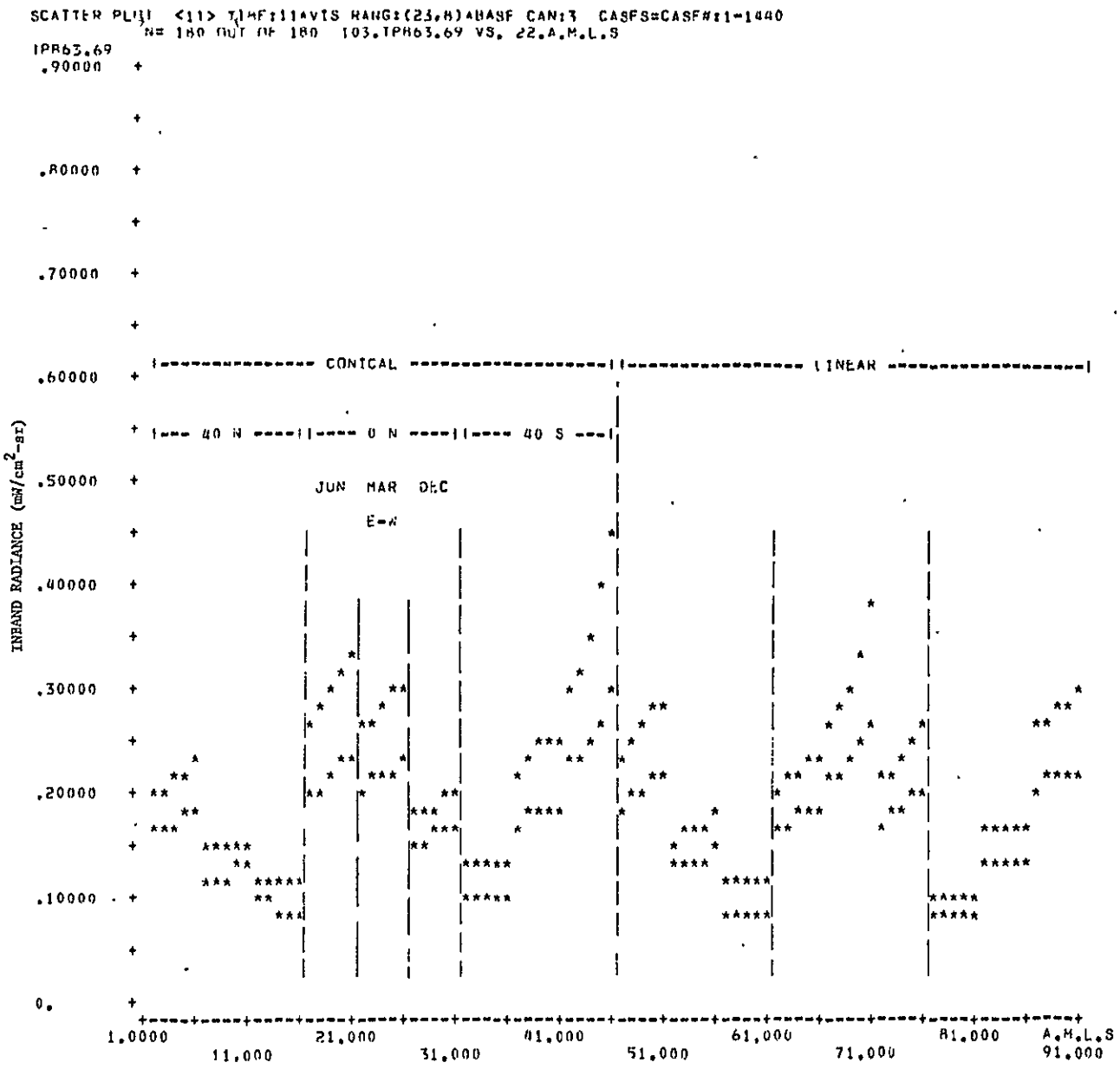

FIGURE 36. SCAN ANGLE DEPENDENCE OF TOTAL RADIANCE FOR V=8 AND 23 KM, 0.63-0.69-μm BAND, 11:00 AM

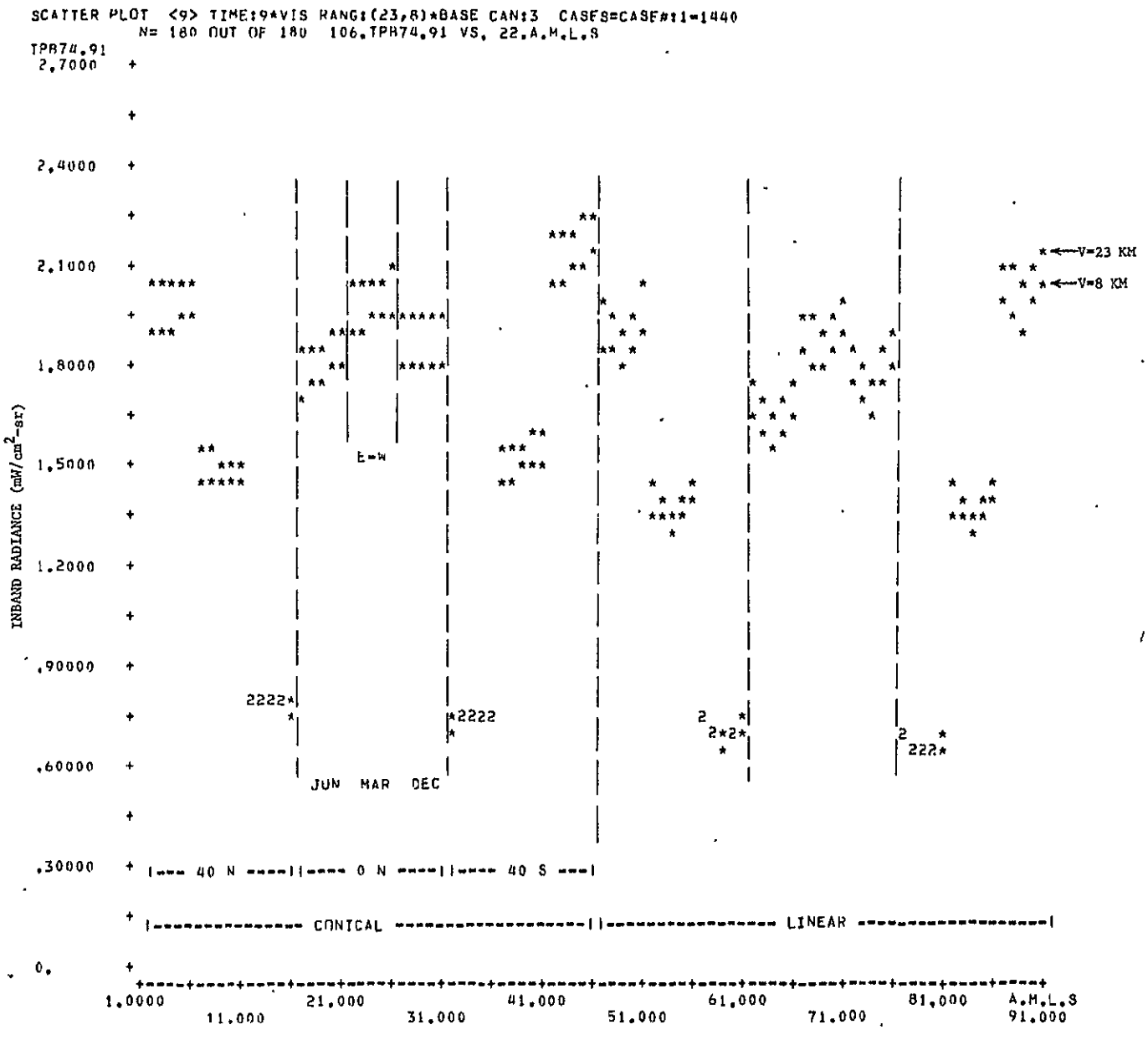

FIGURE 37. SCAN ANGLE DEPENDENCE OF TOTAL RADIANCE FOR V=8 AND 23 KM, 0.74-0.91-μm BAND, 9:30 AM

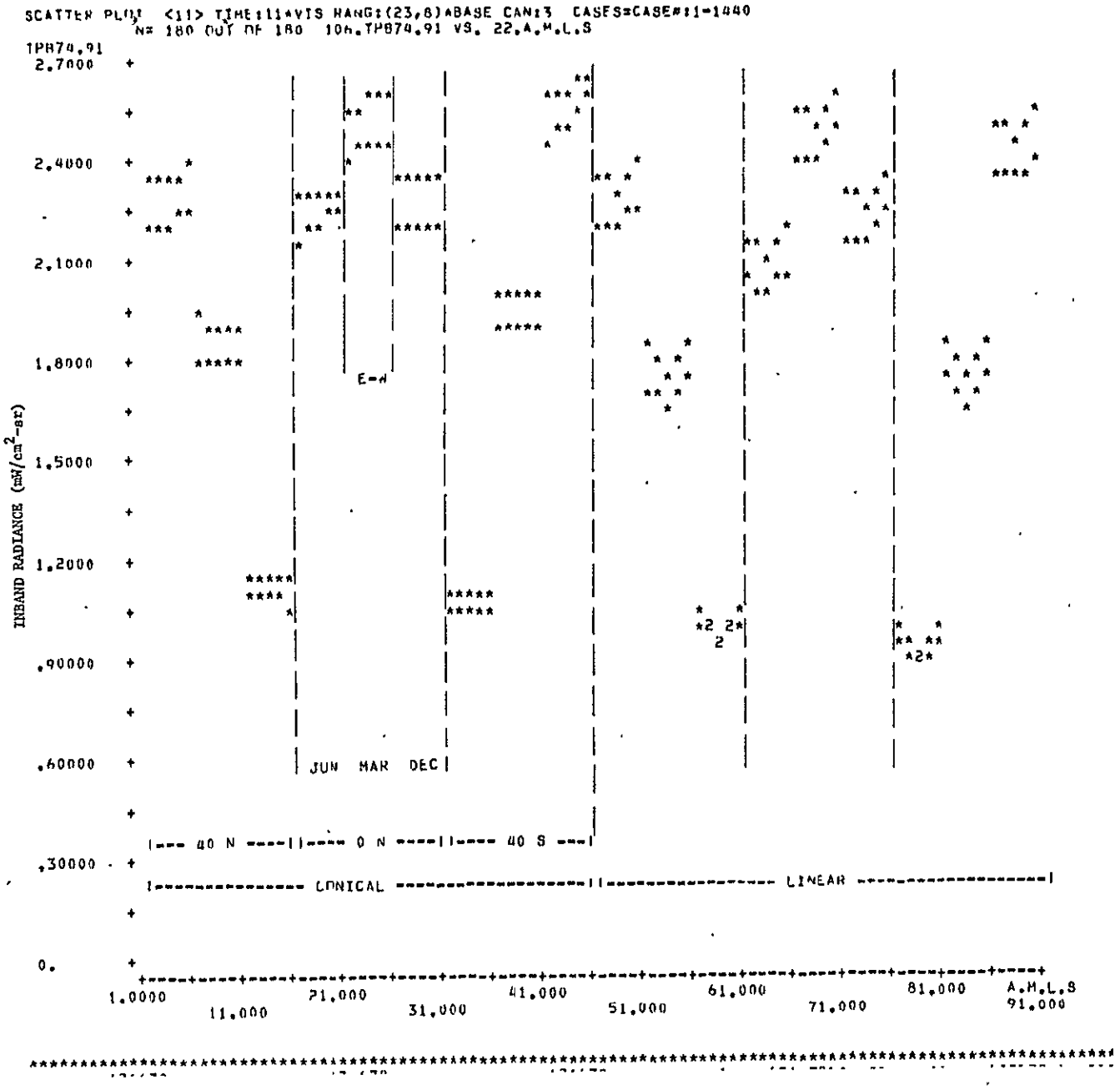

FIGURE 38. SCAN ANGLE DEPENDENCE OF TOTAL RADIANCE FOR V=8 AND 23 KM, 0.74-0.91-μm BAND, 11:00 AM

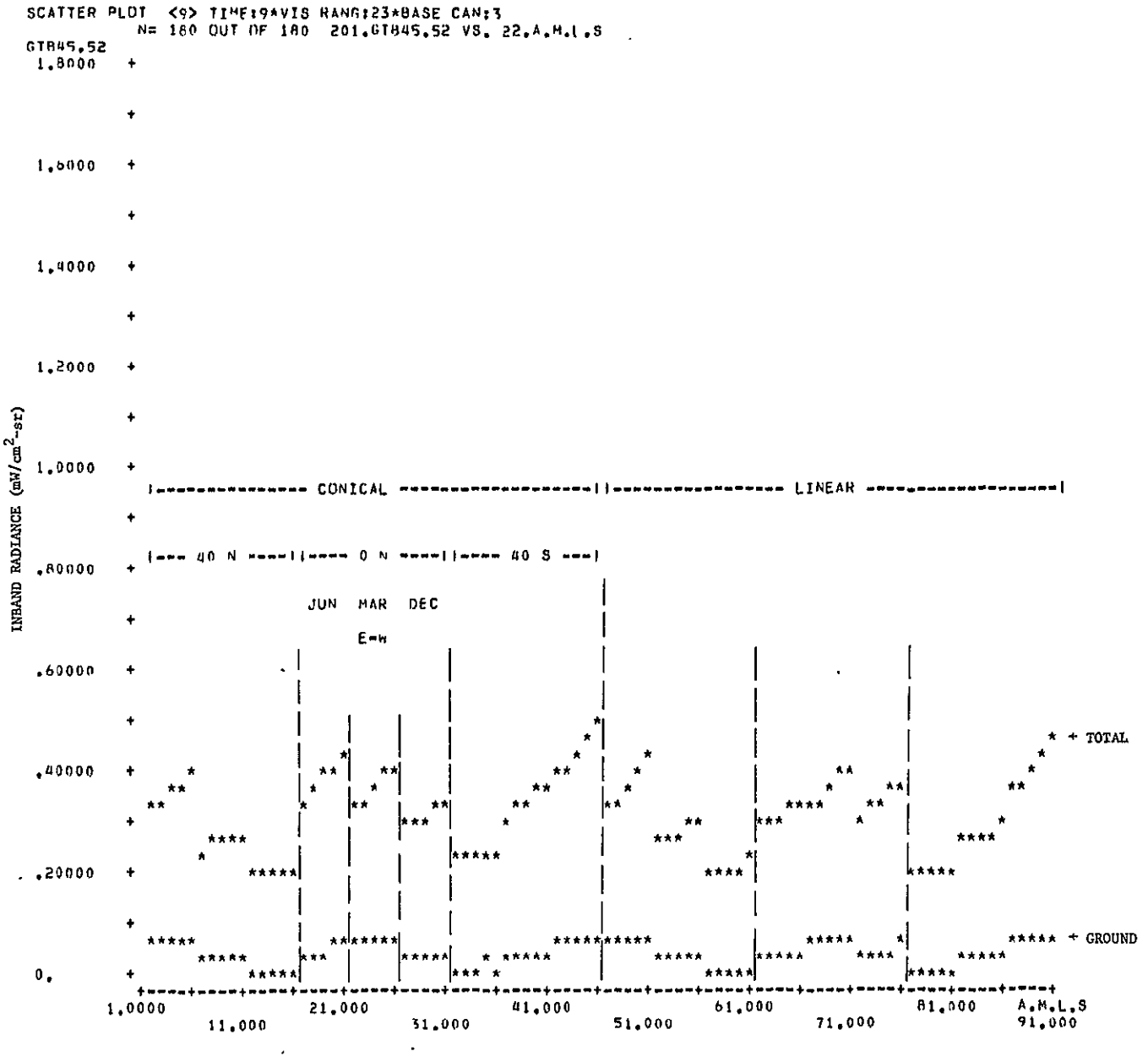

FIGURE 39. COMPARISON OF TOTAL AND GROUND RADIANCES; 0.45-0.52-μm BAND, V=23 KM, 9:30 AM

ERIM

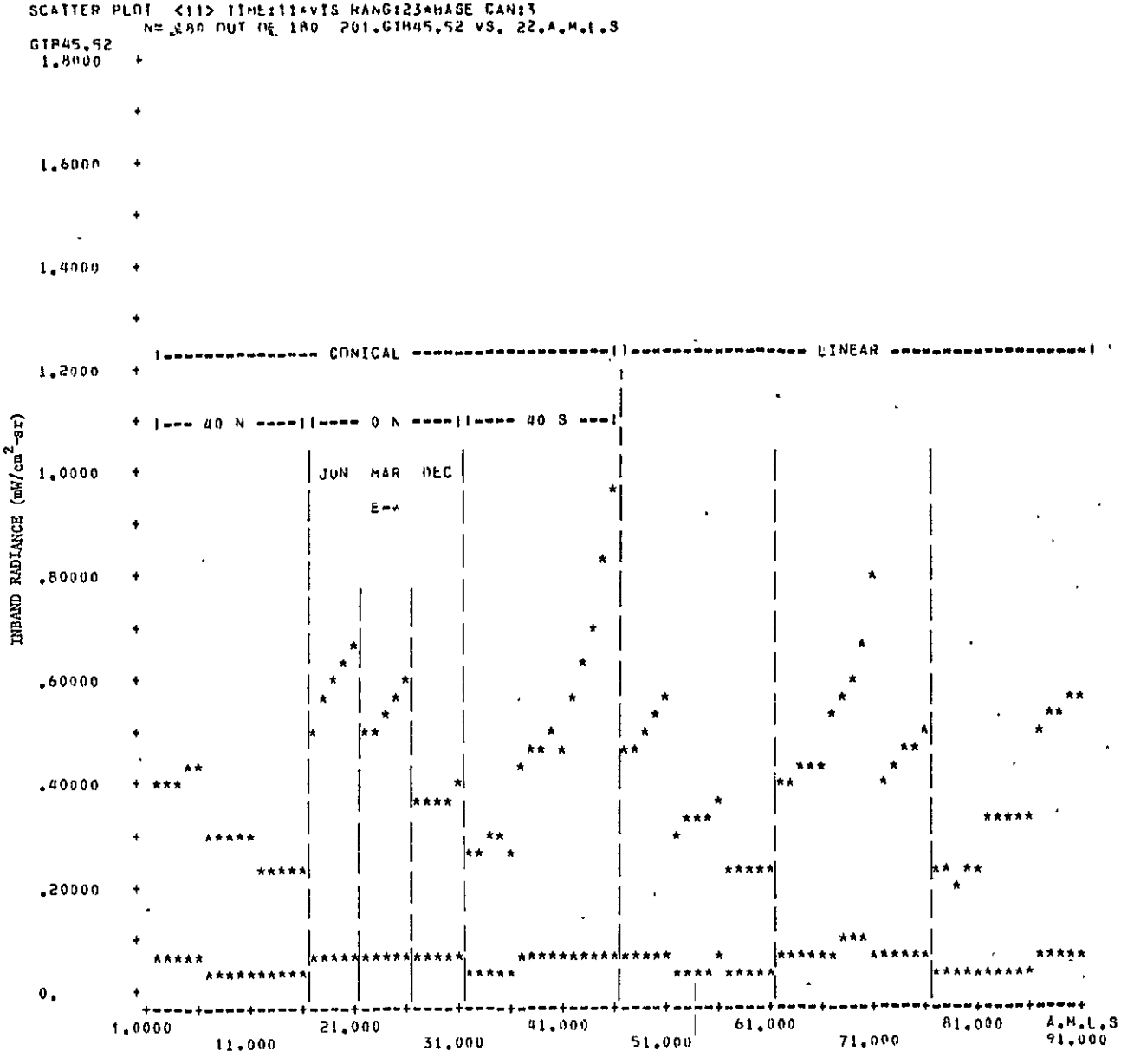

FIGURE 40. COMPARISON OF TOTAL AND GROUND RADIANCES; 0.45-0.52-μm BAND, V=23 KM, 11:00 AM

ERIM

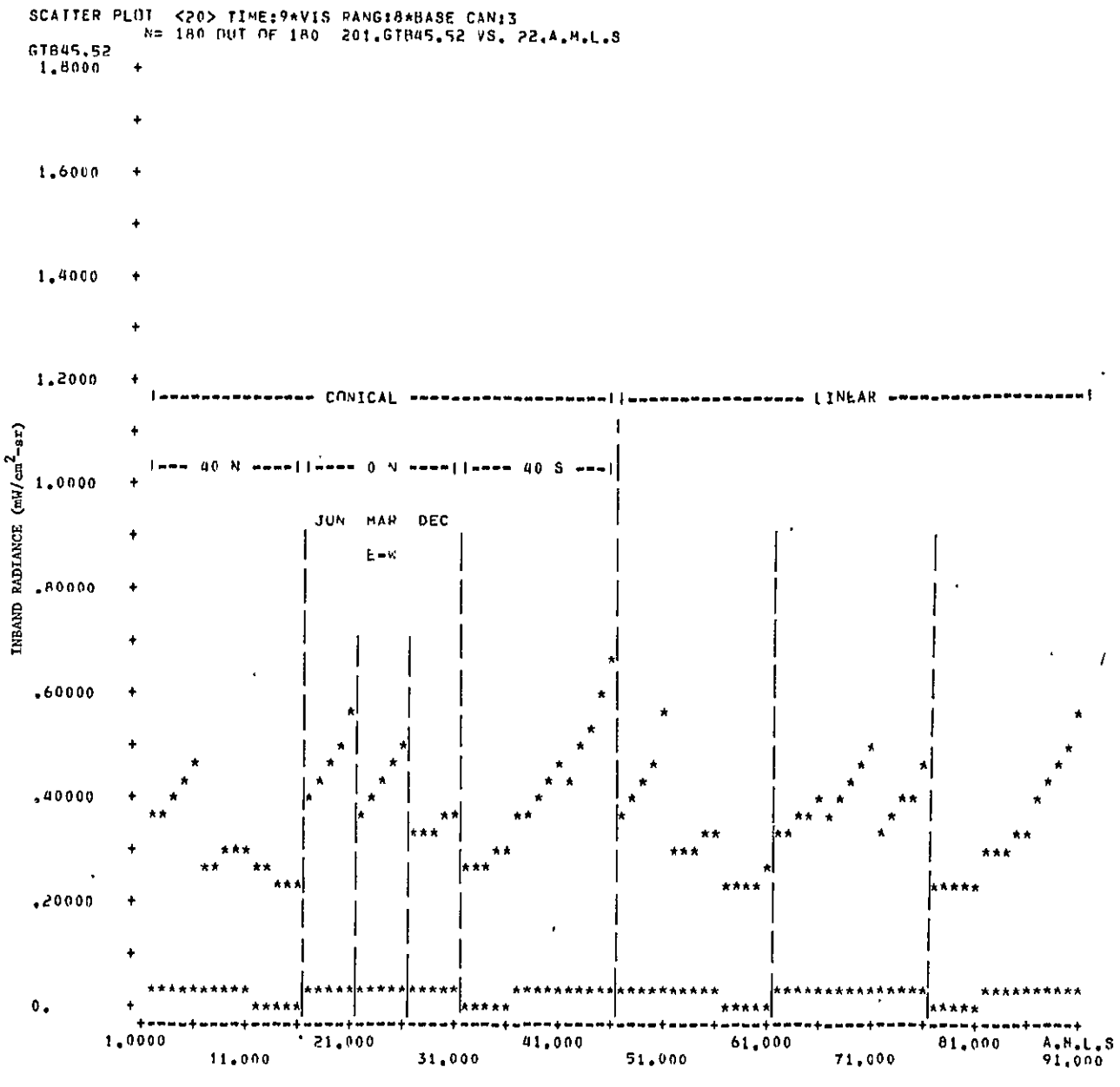

FIGURE 41. COMPARISON OF TOTAL AND GROUND RADIANCES; 0.45-0.52-μm BAND, V=8 KM, 9:30 AM

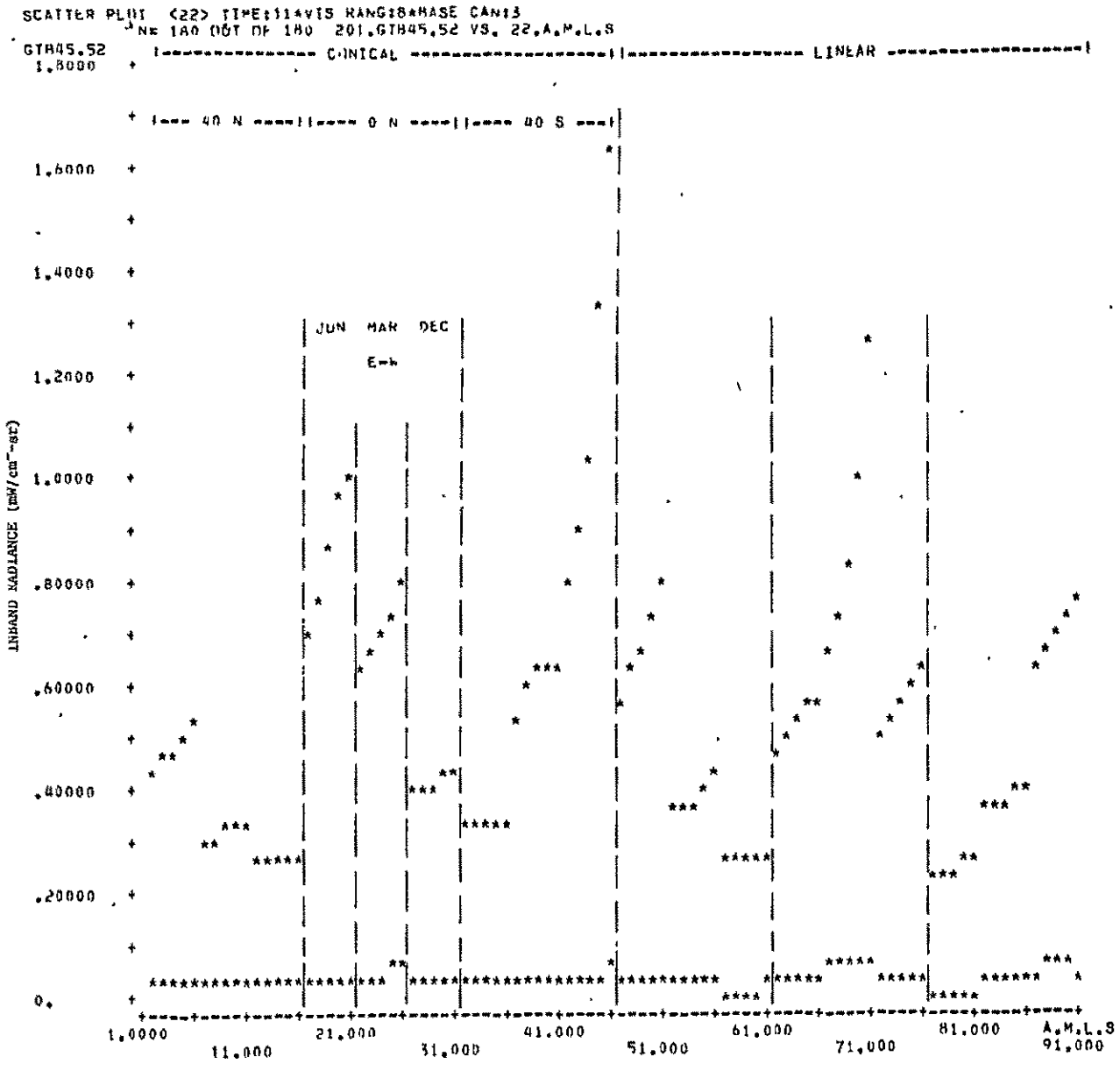

FIGURE 42. COMPARISON OF TOTAL AND GROUND RADIANCES; 0.45-0.52-μm BAND, V=8 KM, 11:00AM

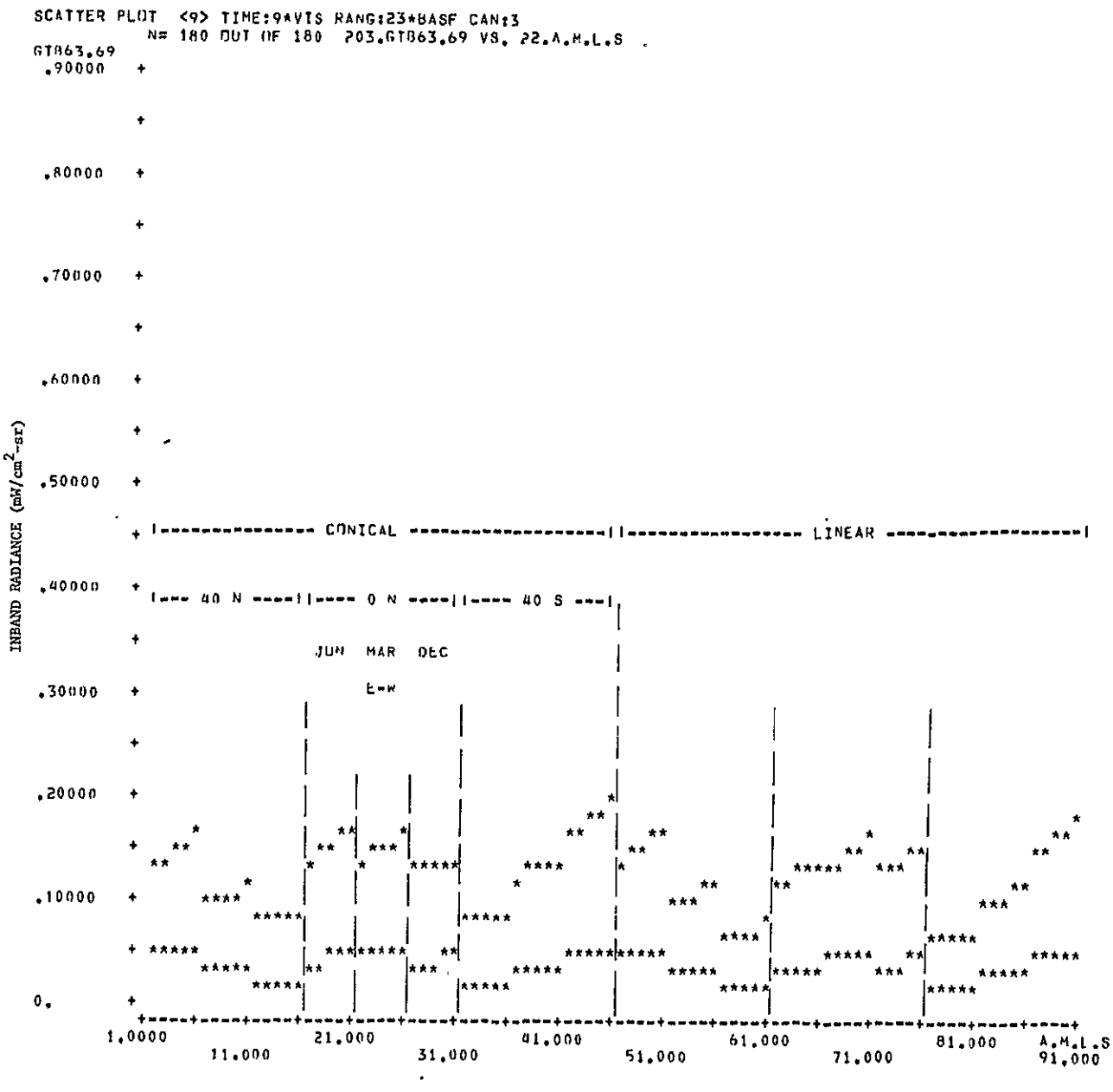

FIGURE 43. COMPARISON OF TOTAL AND GROUND RADIANCES; 0.63-0.69-μm BAND, V=23 KM, 9:30 AM

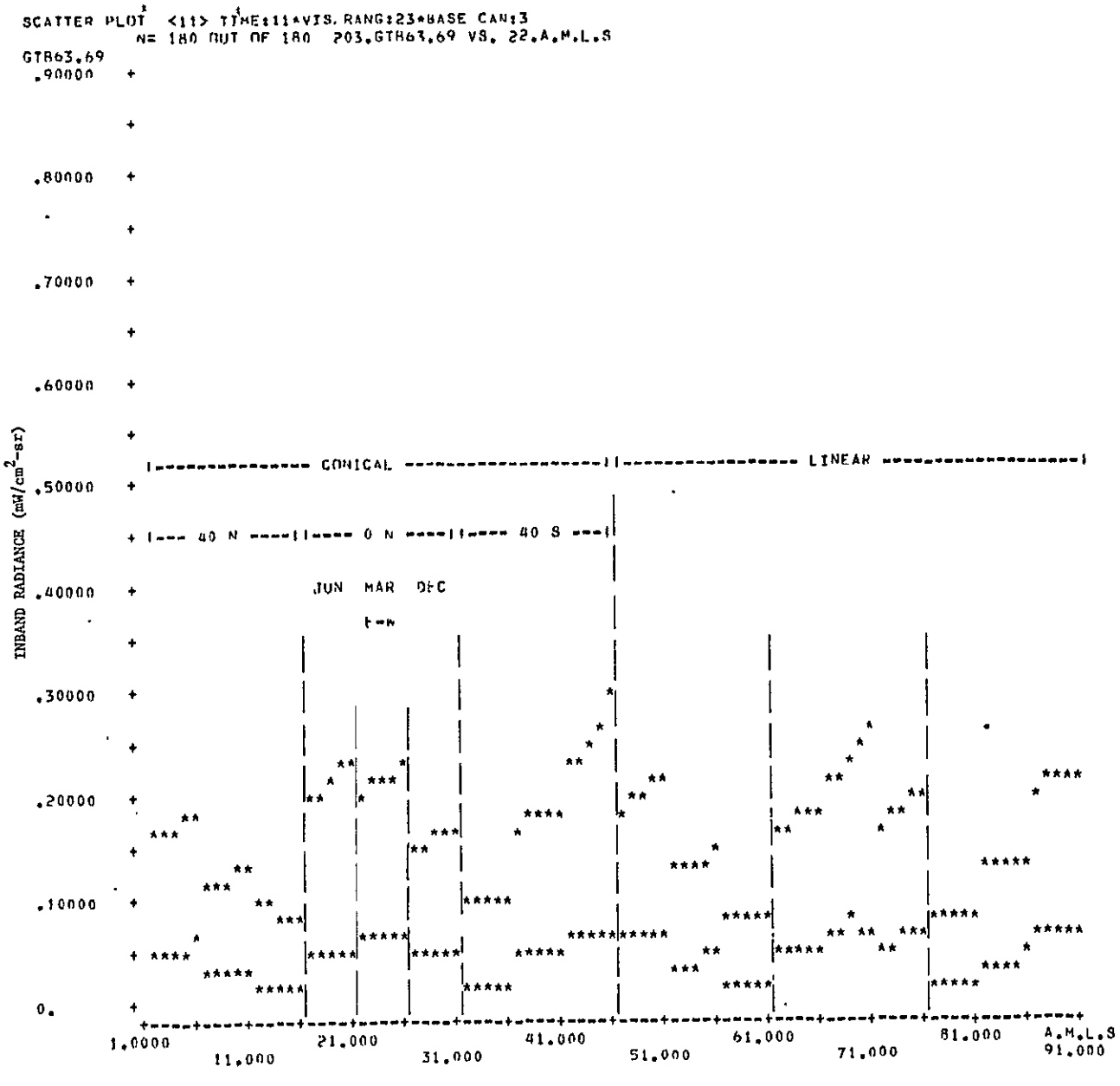

FIGURE 44. COMPARISON OF TOTAL AND GROUND RADIANCES; 0.63-0.69-μm BAND, V=23 KM, 11:00 AM

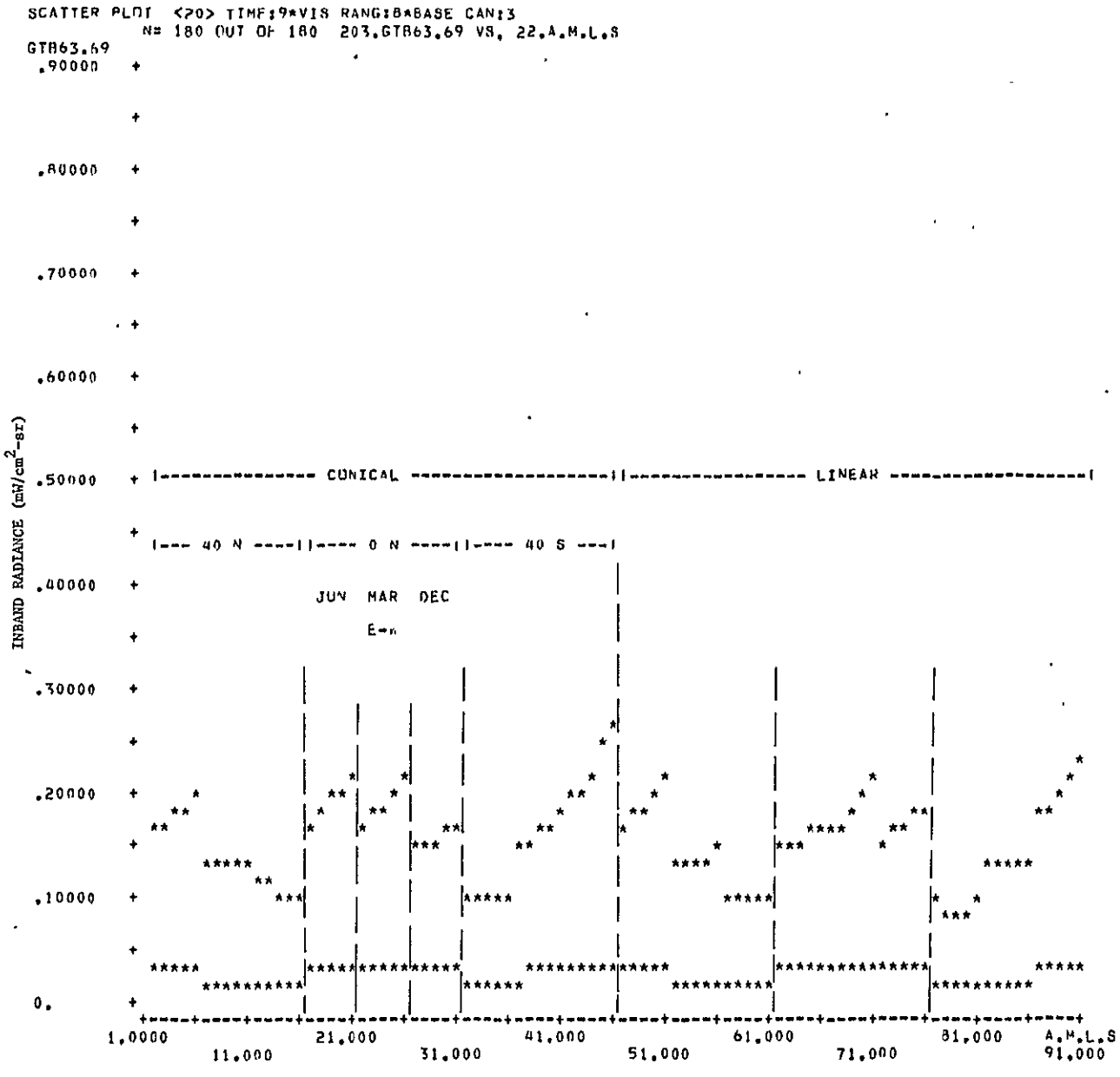

FIGURE 45. COMPARISON OF TOTAL AND GROUND RADIANCES; 0.63-0.69-μm BAND, V=8 KM, 9:30 AM

ERIM

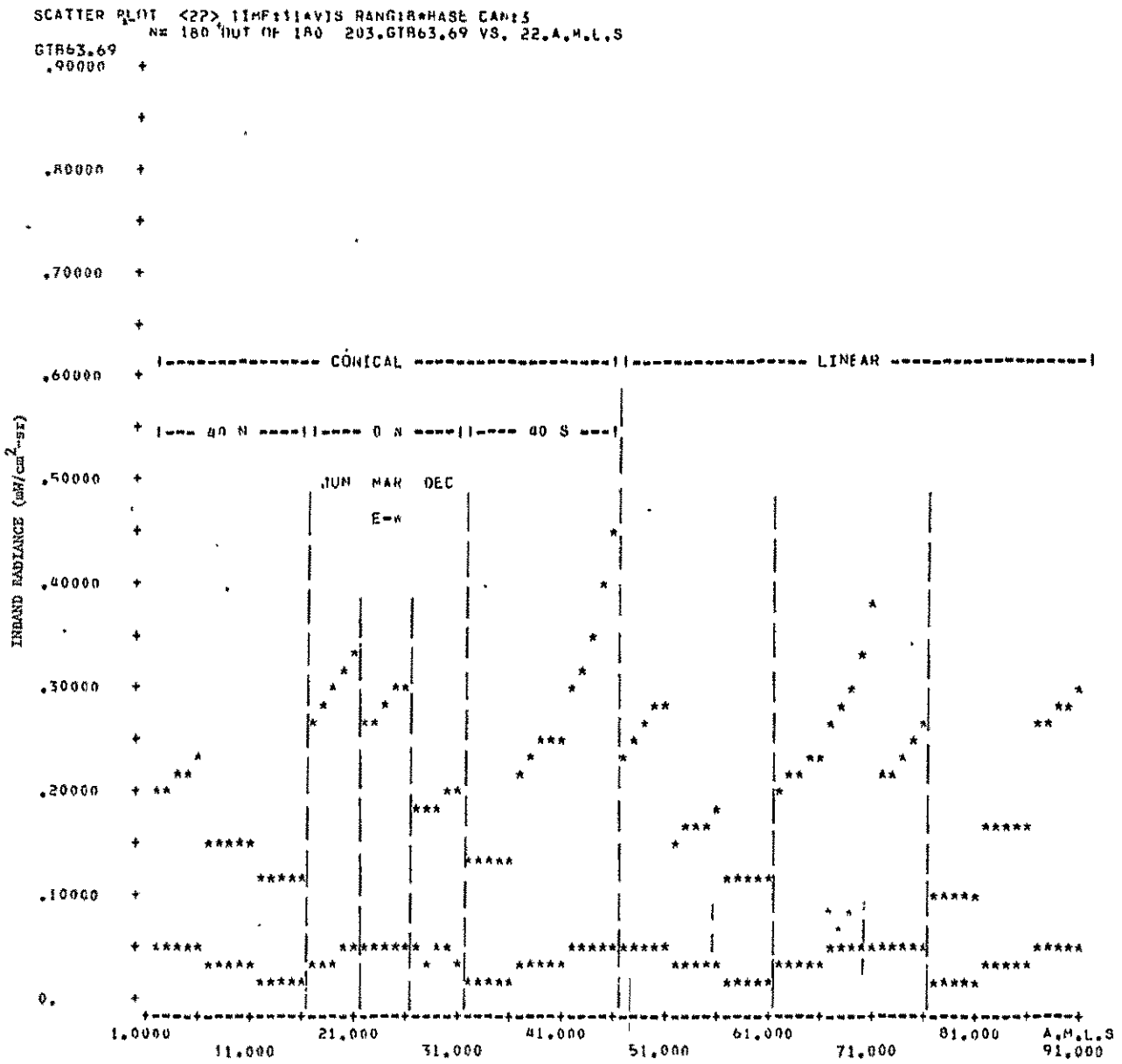

FIGURE 46. COMPARISON OF TOTAL AND GROUND RADIANCES; 0.63-0.69-μm BAND, V=8 KM, 11:00 AM

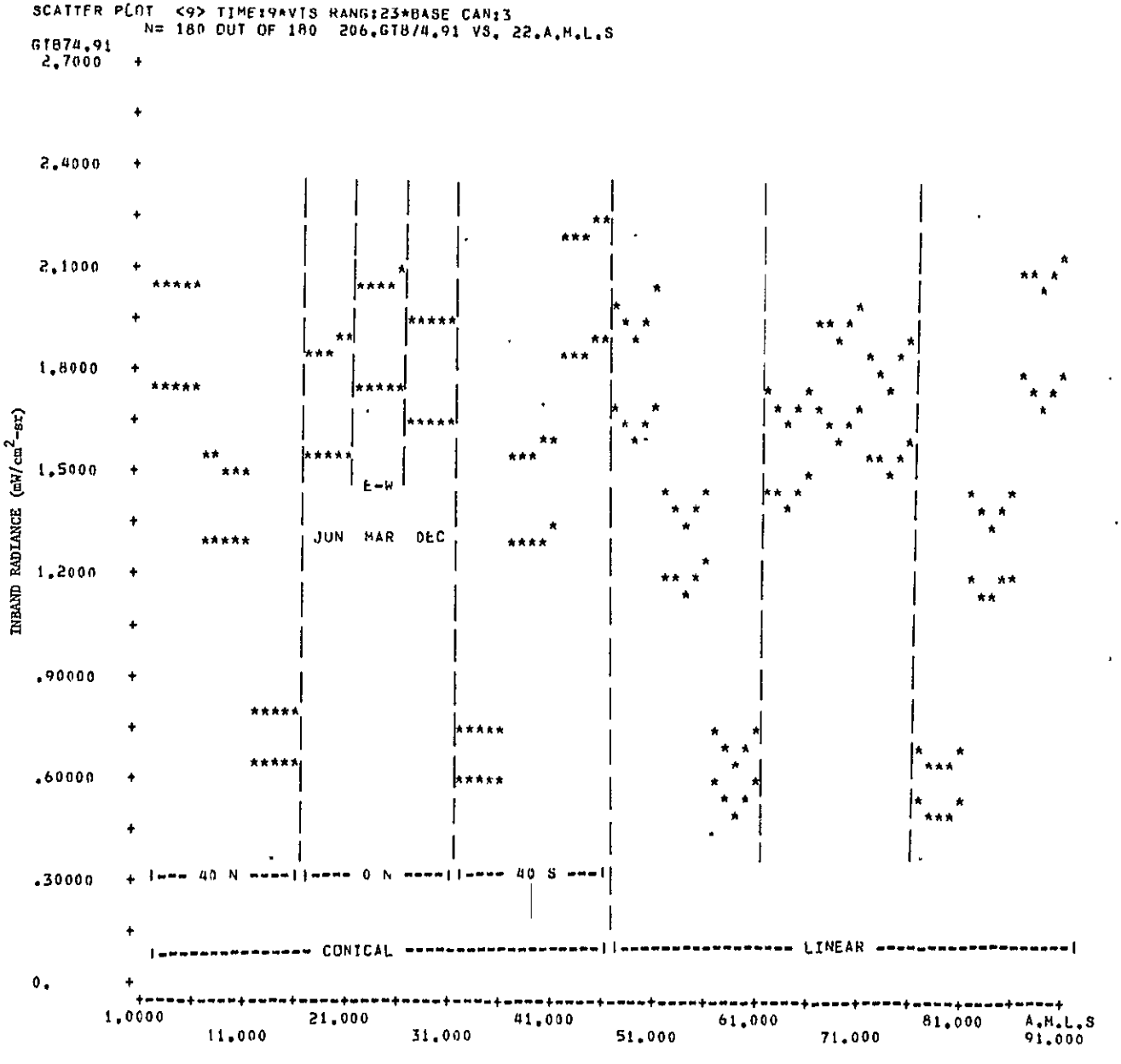

FIGURE 47. COMPARISON OF TOTAL AND GROUND RADIANCES; 0.74-0.91-μm BAND, V=23 KM, 9:30 AM

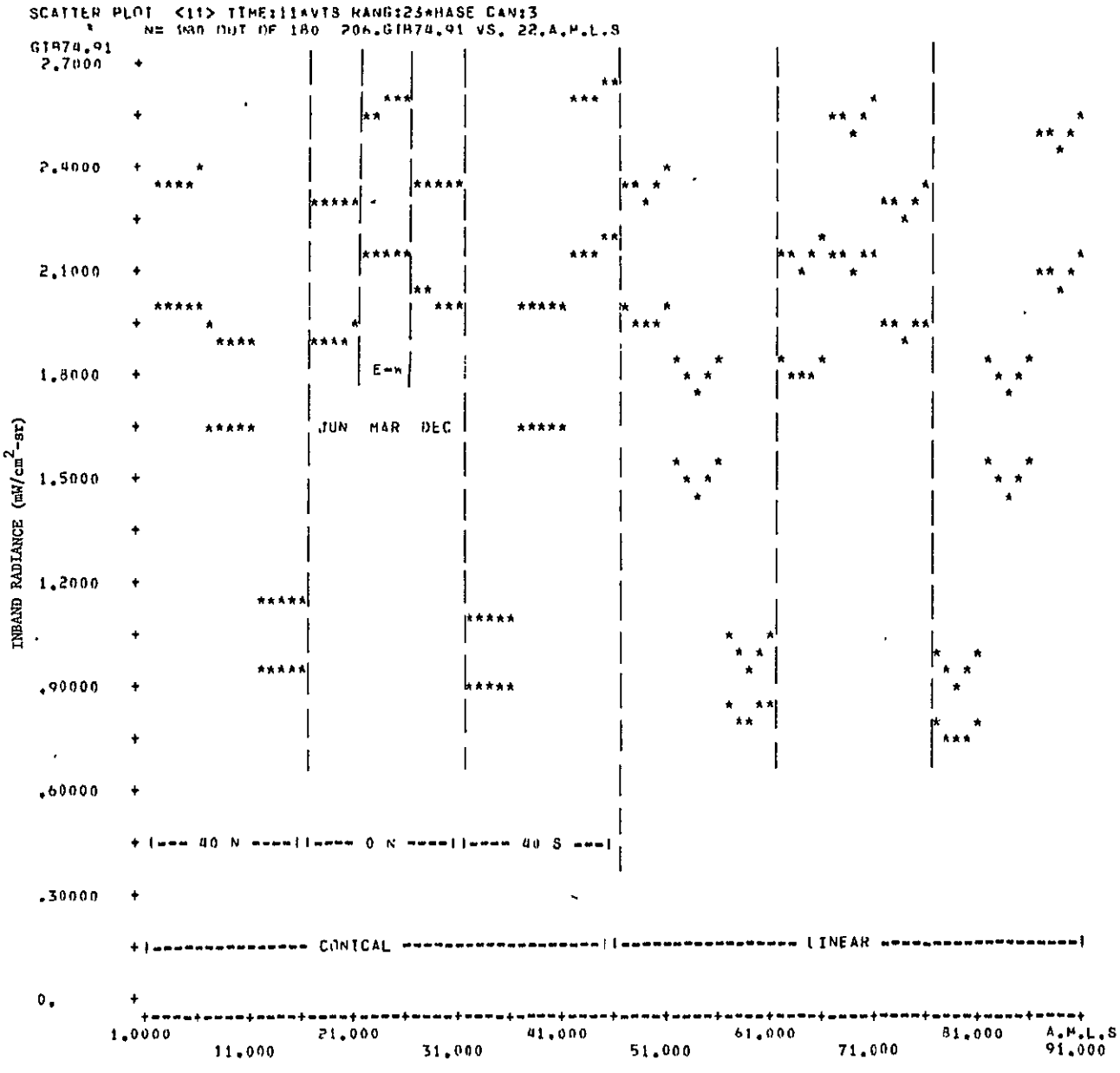

FIGURE 48. COMPARISON OF TOTAL AND GROUND RADIANCES; 0.74-0.91-μm BAND, V=23 KM, 11:00 AM

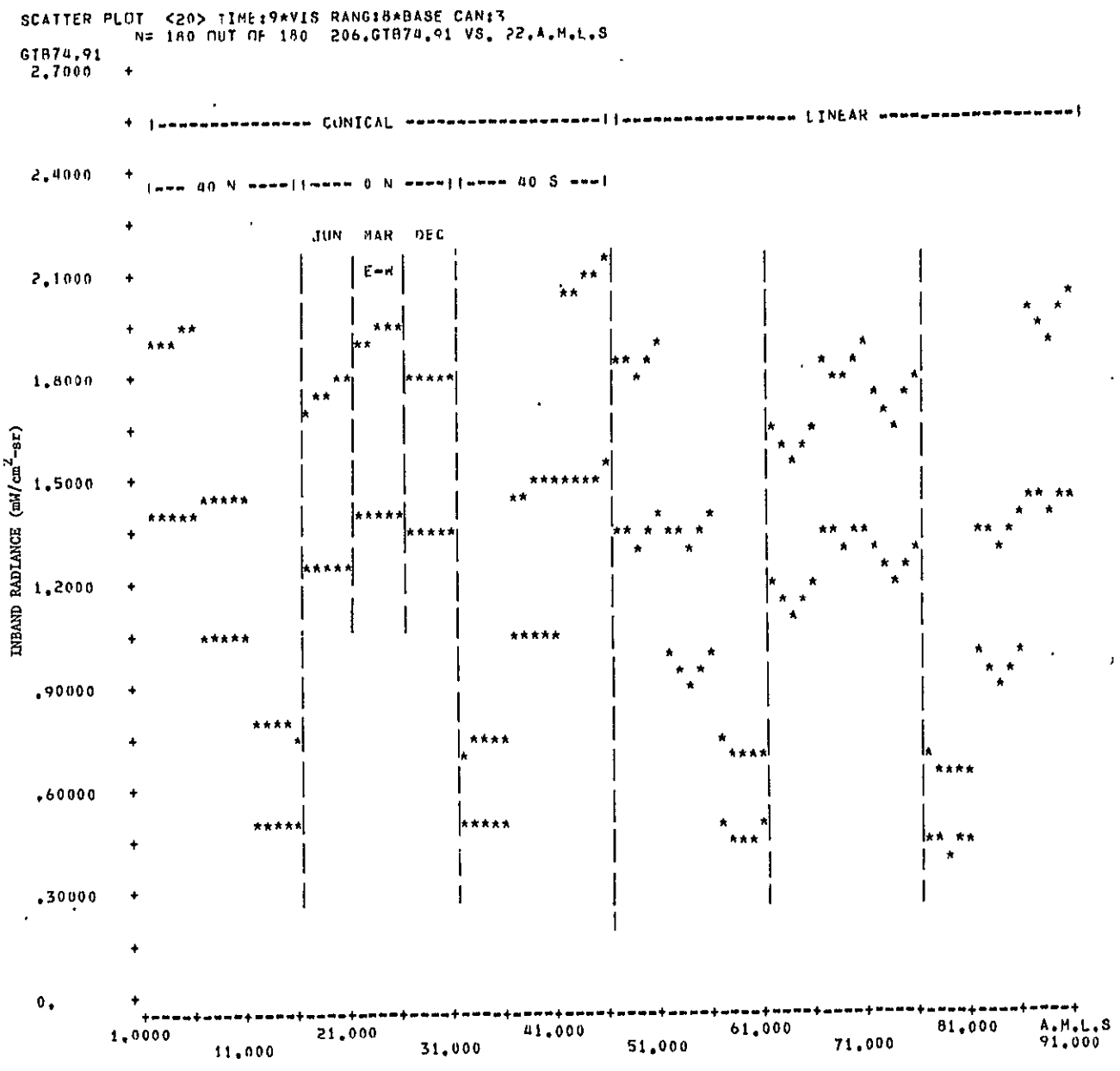

FIGURE 49. COMPARISON OF TOTAL AND GROUND RADIANCES; 0.74-0.91-μm BAND, V=8 KM, 9:30 AM

ERIM

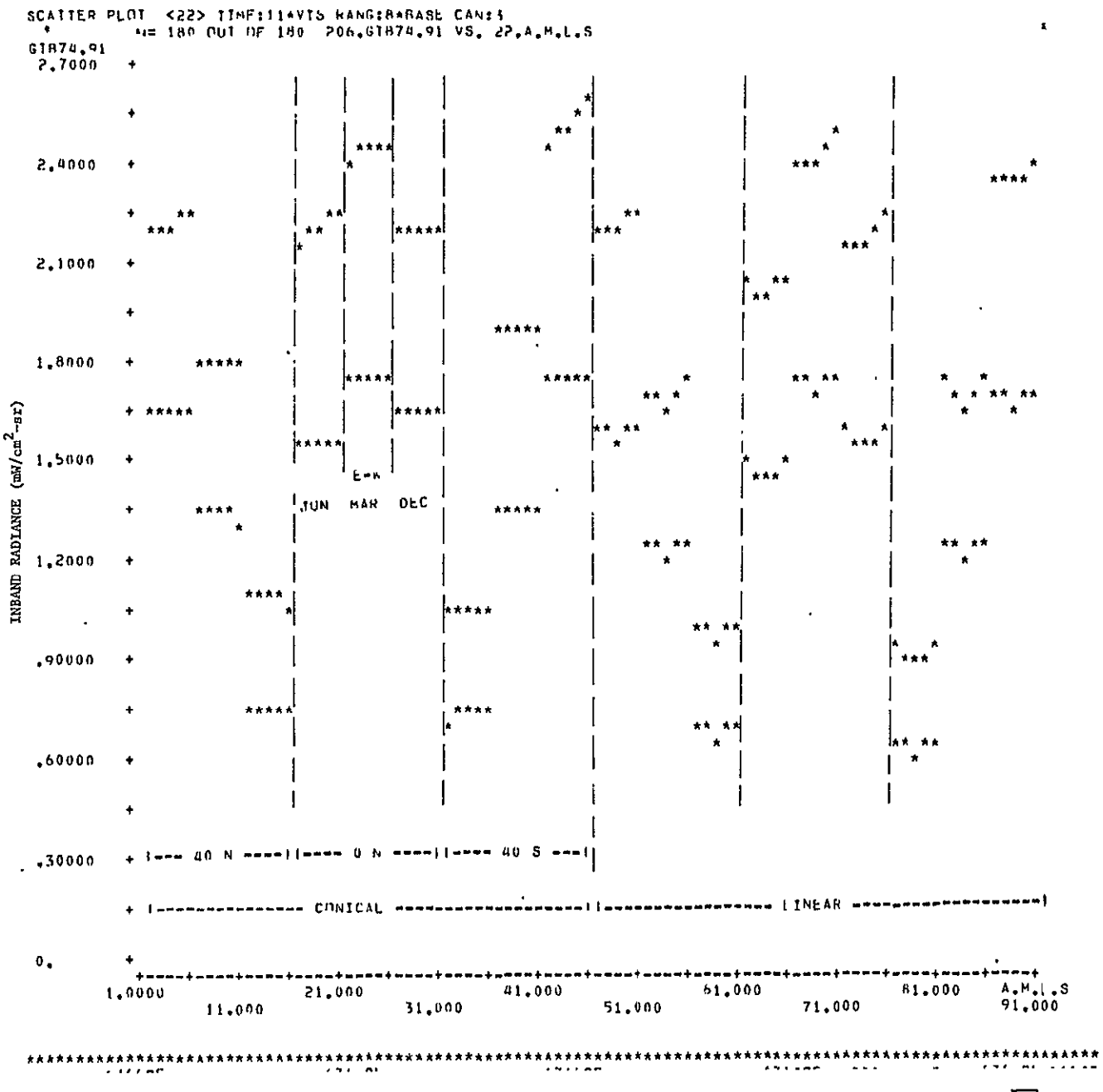

FIGURE 50. COMPARISON OF TOTAL AND GROUND RADIANCES; 0.74-0.91-μm BAND, V=8 KM, 11:00 AM

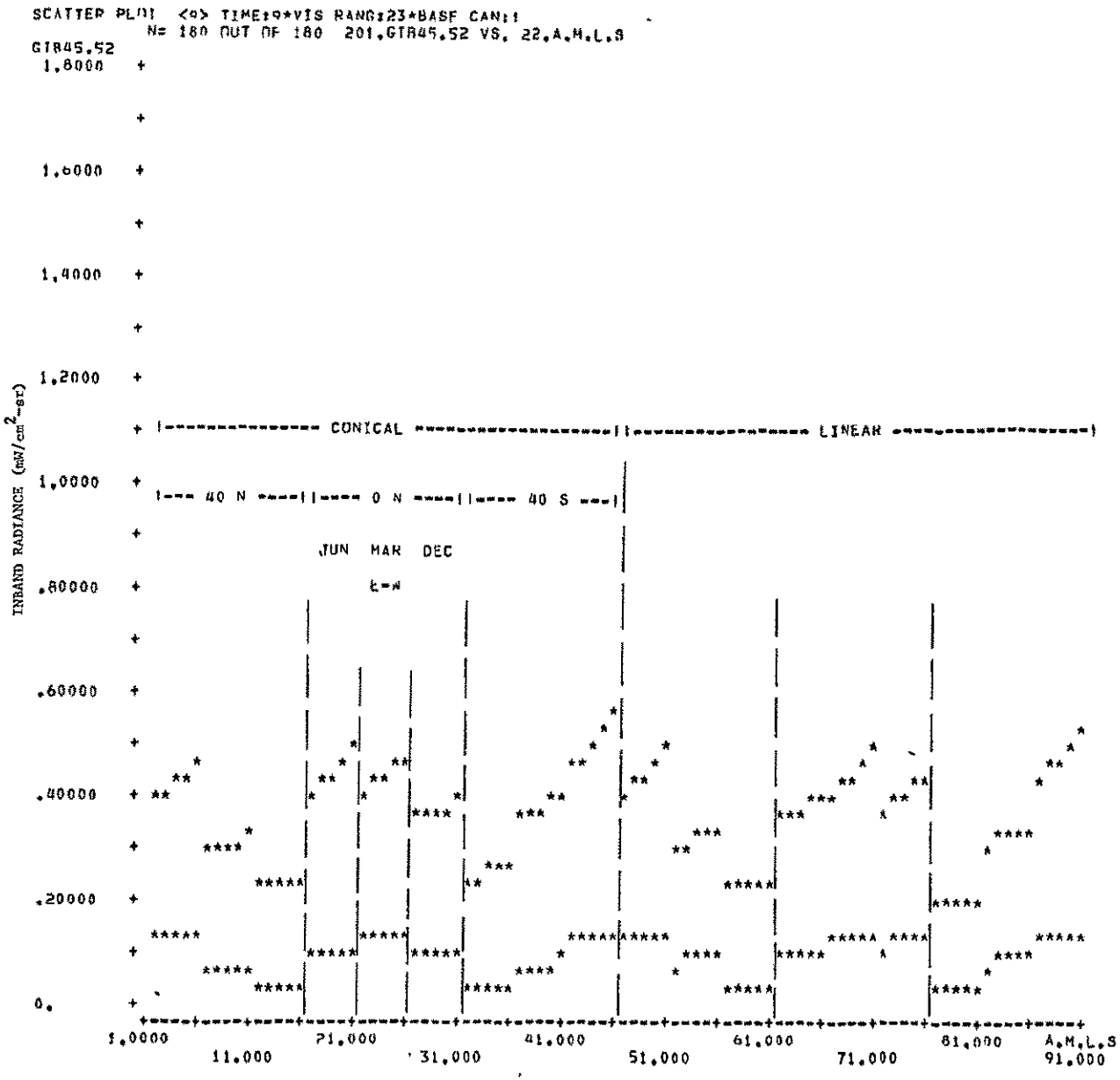

FIGURE 51. TOTAL AND GROUND RADIANCES FOR SPARSE GREEN VEGETATION; 9:30 AM, 0.45–0.52-μm BAND, V=23 KM

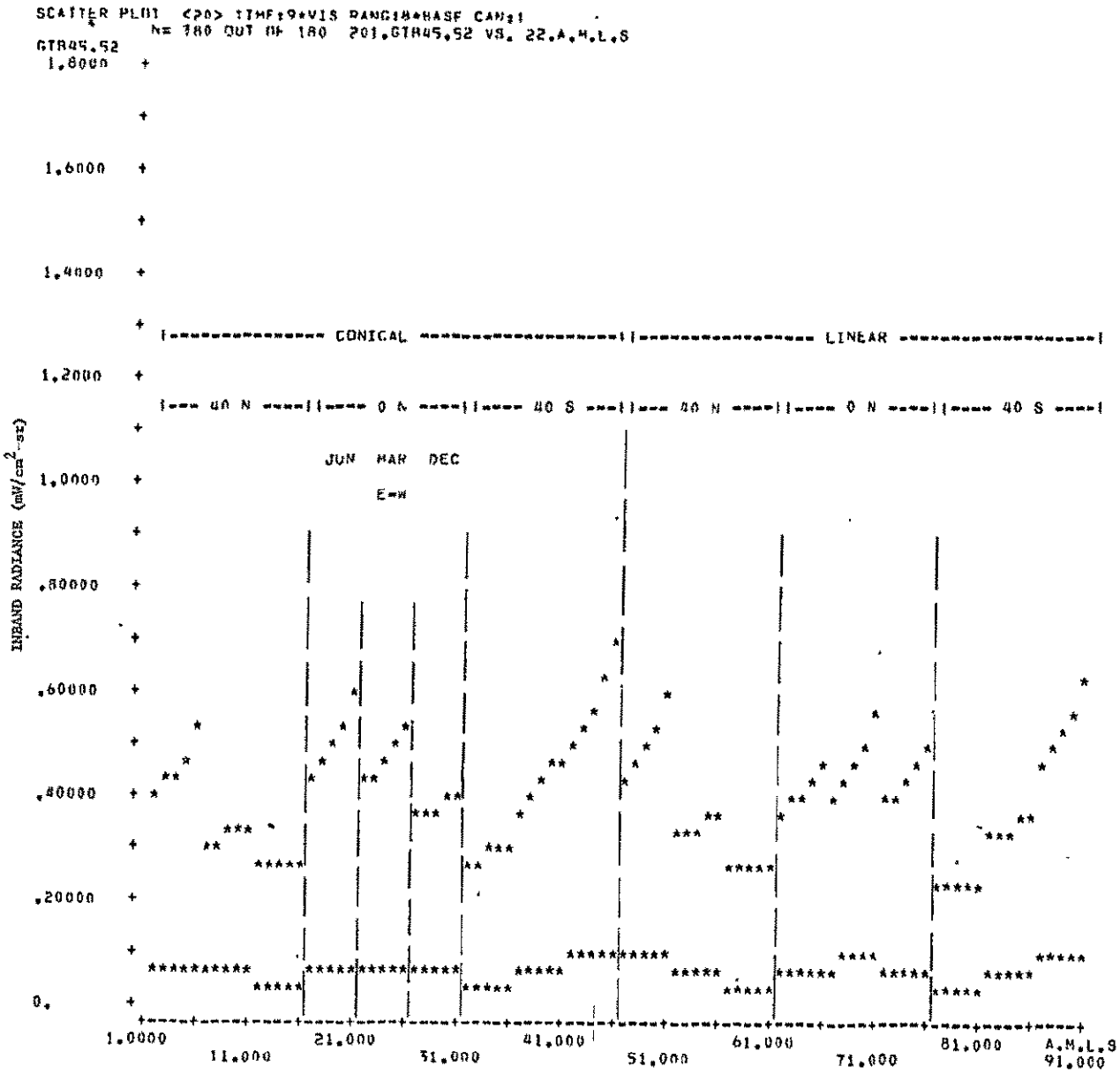

FIGURE 52. TOTAL AND GROUND RADIANCES FOR SPARSE GREEN VEGETATION; 9:30 AM, 0.45-0.52-μm BAND, V=8 KM

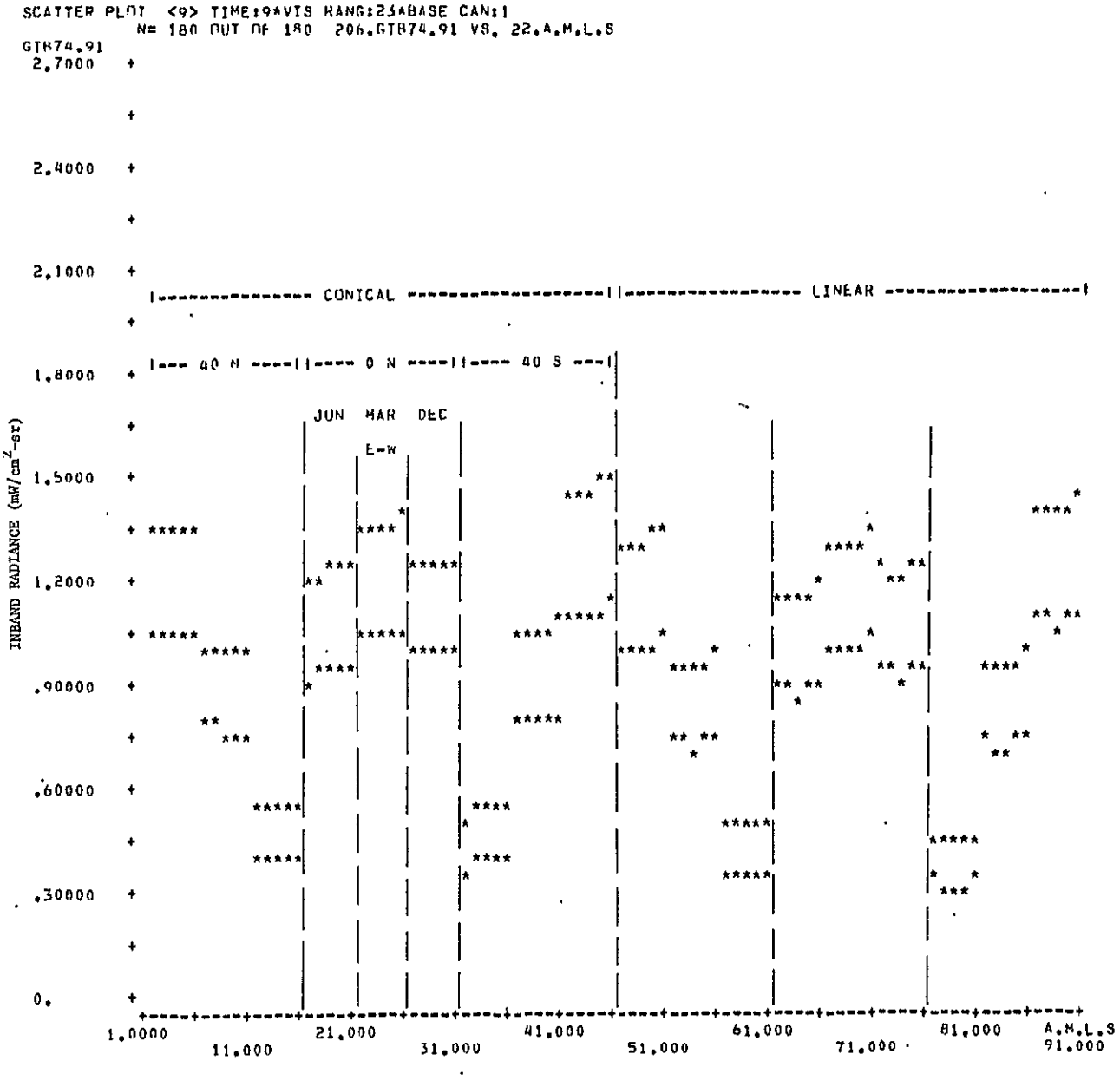

FIGURE 53. TOTAL AND GROUND RADIANCES FOR SPARSE GREEN VEGETATION; 9:30 AM, 0.74-0.91-μm BAND, V=23 KM

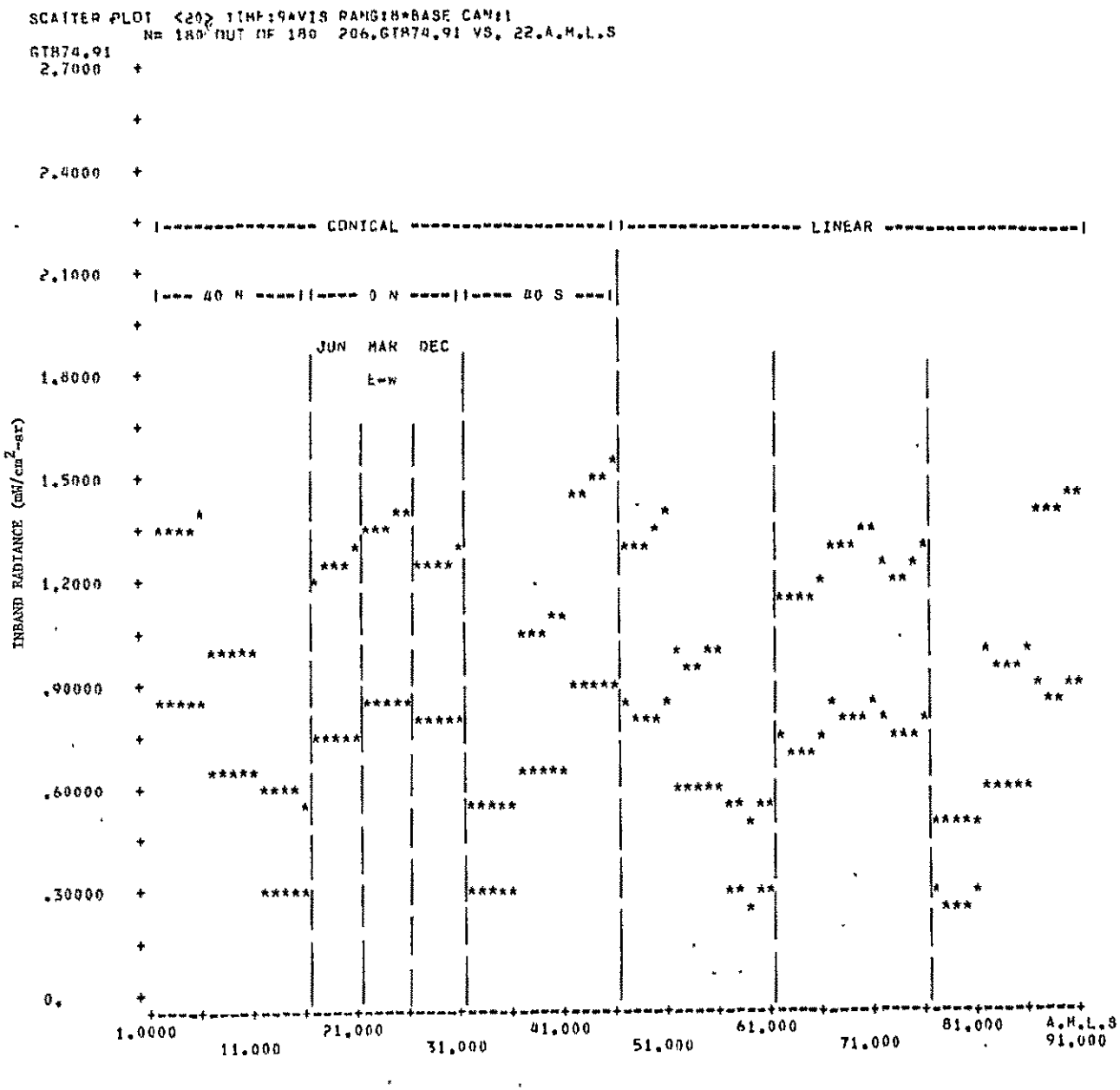

FIGURE 54. TOTAL AND GROUND RADIANCES FOR SPARSE GREEN VEGETATION; 9:30 AM, 0.74-0.91-μm BAND, V=8 KM

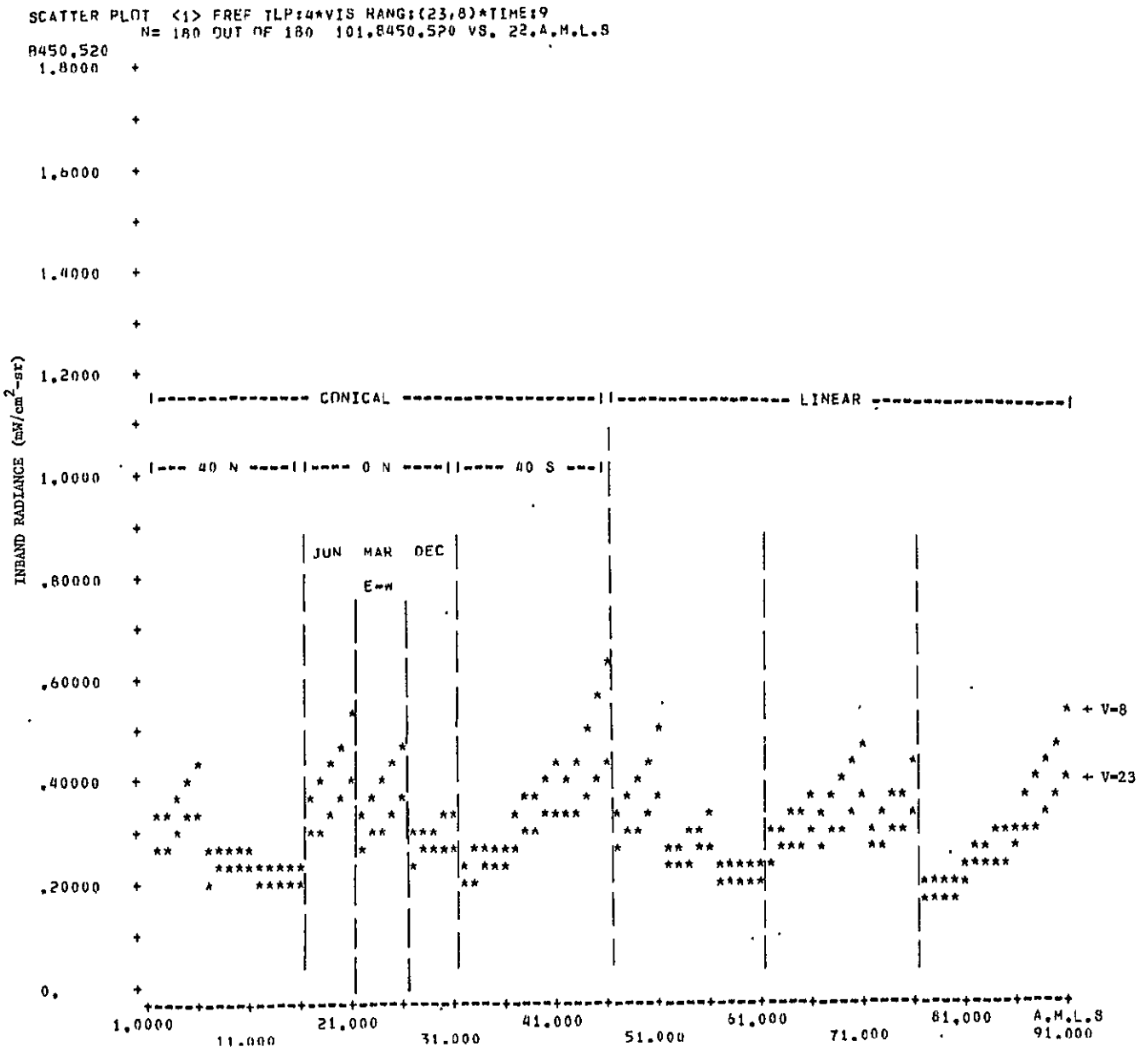

FIGURE 55. FACTORS AFFECTING PATH RADIANCE; 9:30 AM, V=8 AND 23 KM, 0.45-0.52-μm BAND

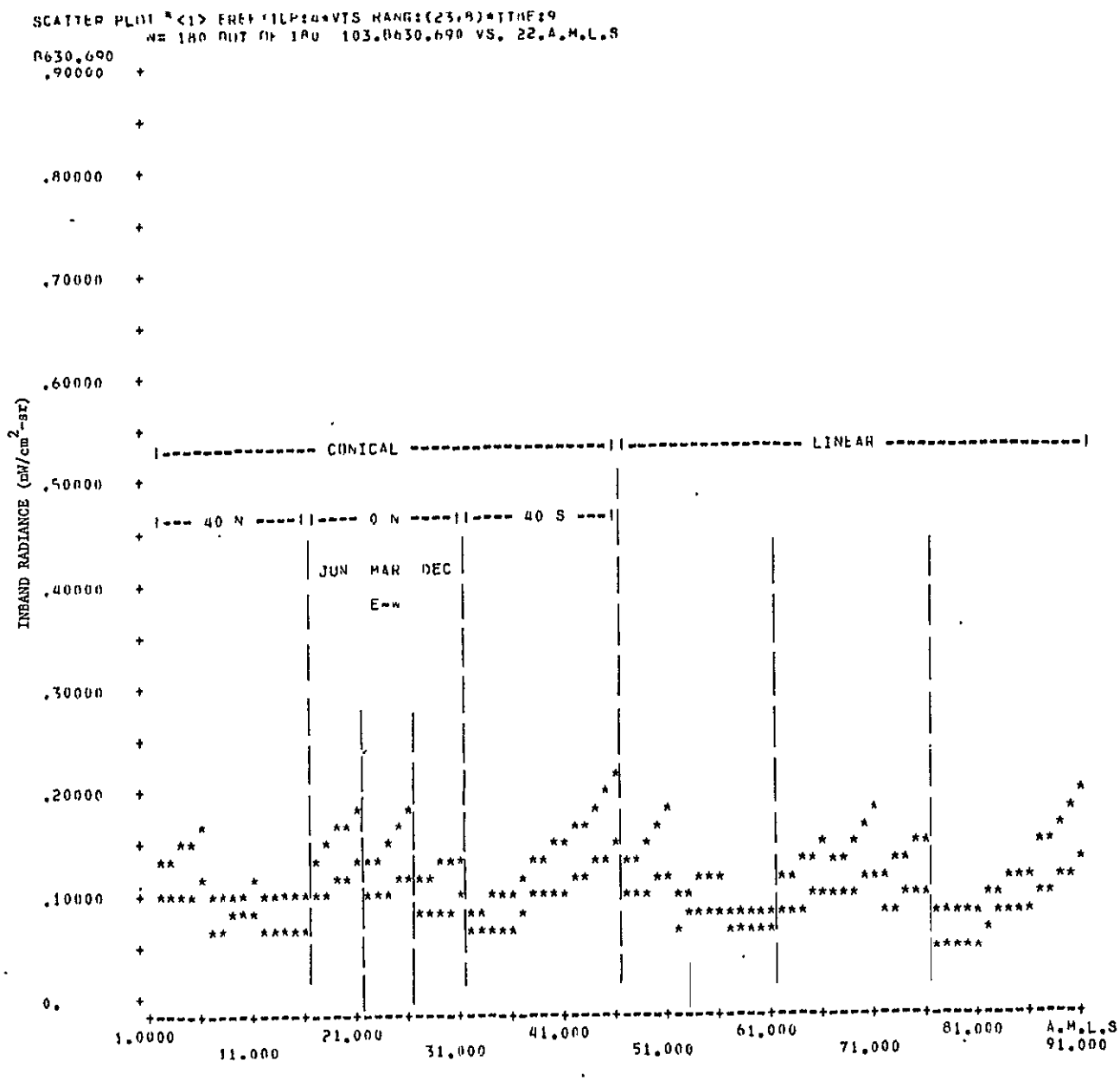

FIGURE 56. FACTORS AFFECTING PATH RADIANCE; 9:30 AM, V=8 AND 23 KM, 0.63-0.69-μm BAND

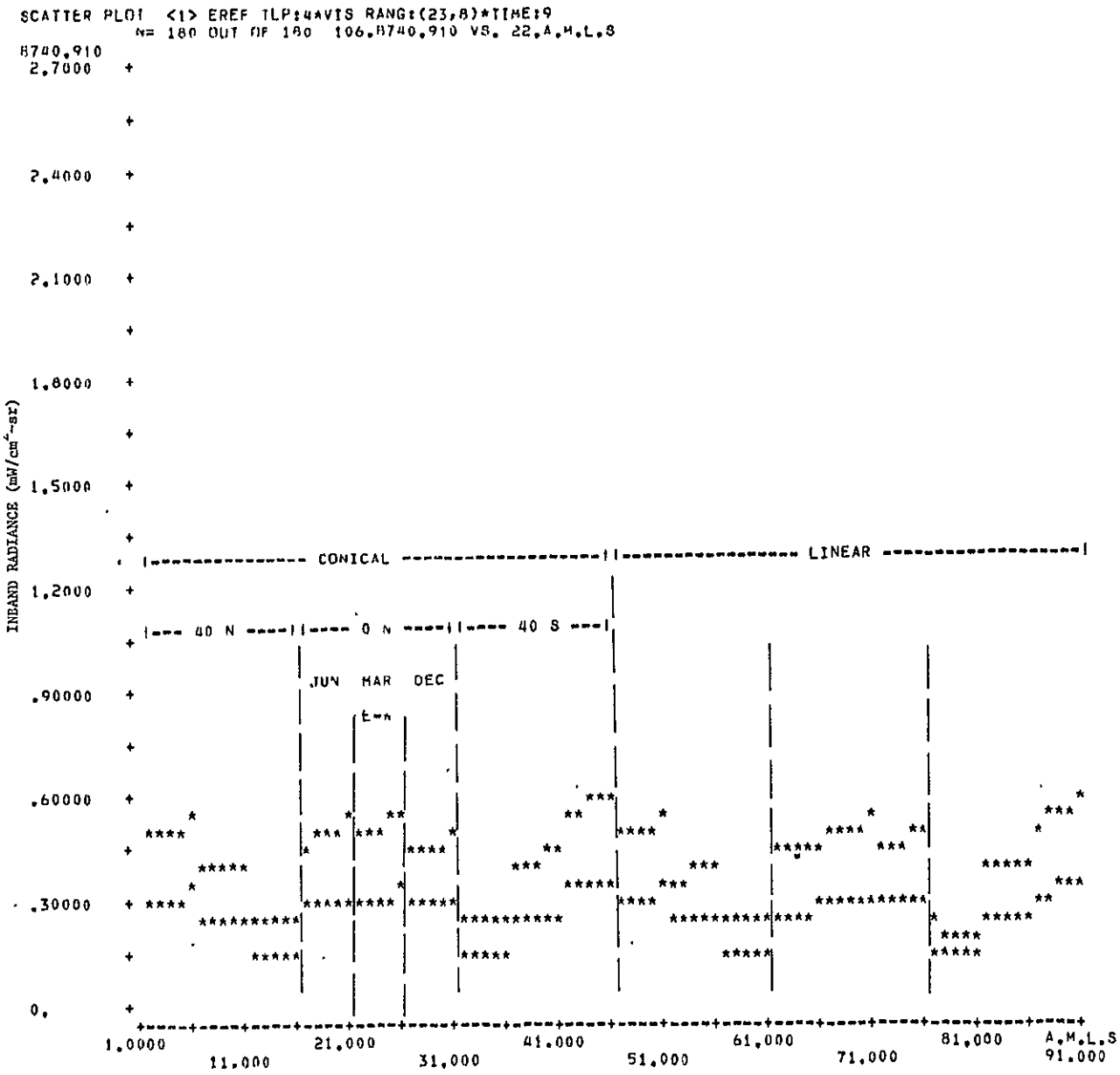

FIGURE 57. FACTORS AFFECTING PATH RADIANCE; 9;30 AM, V=8 AND 23 KM, 0.74-0.91-μm BAND

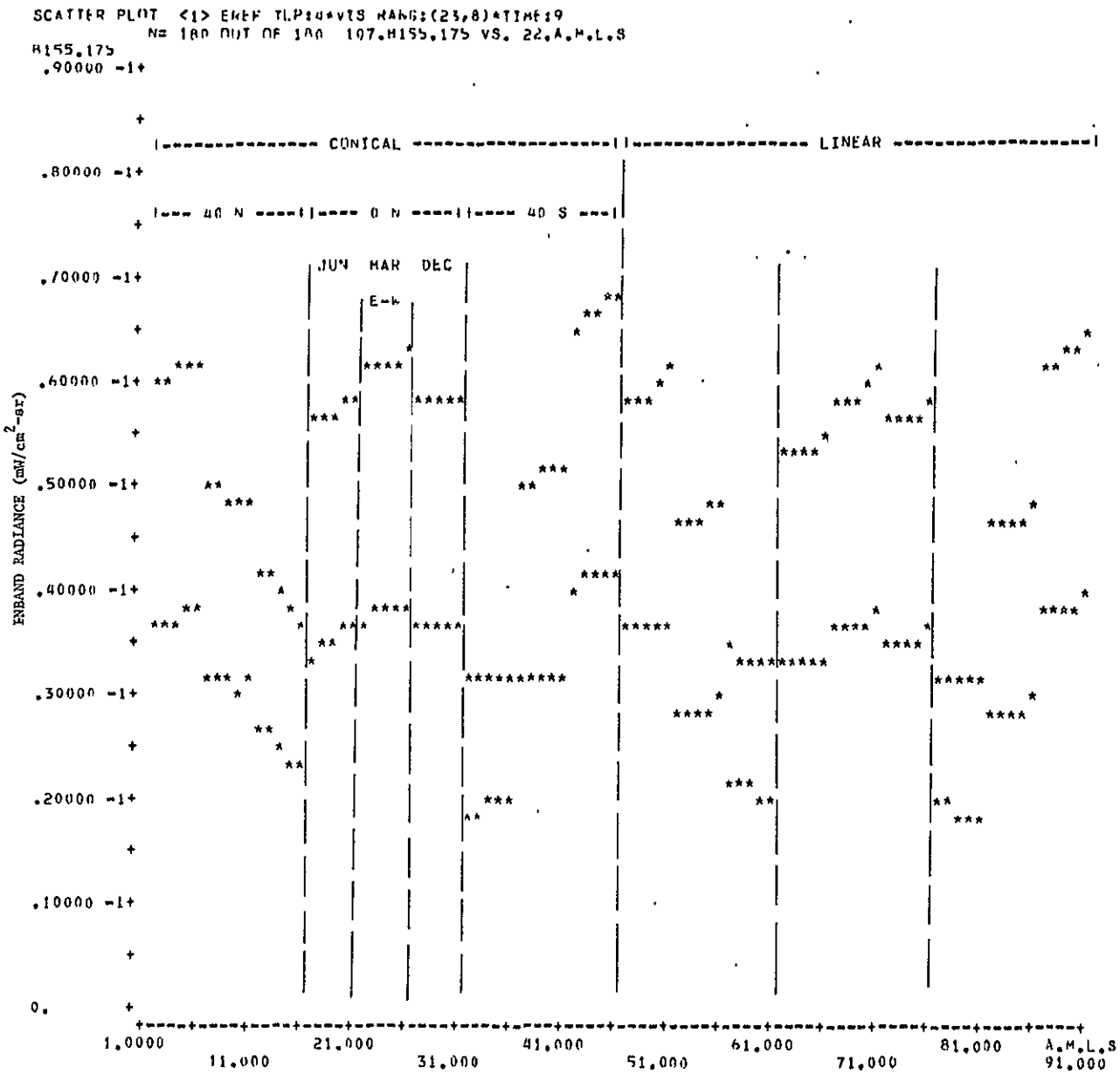

FIGURE 58. FACTORS AFFECTING PATH RADIANCE; 9:30 AM, V=8 AND 23 KM, 1.55-1.75-μm BAND

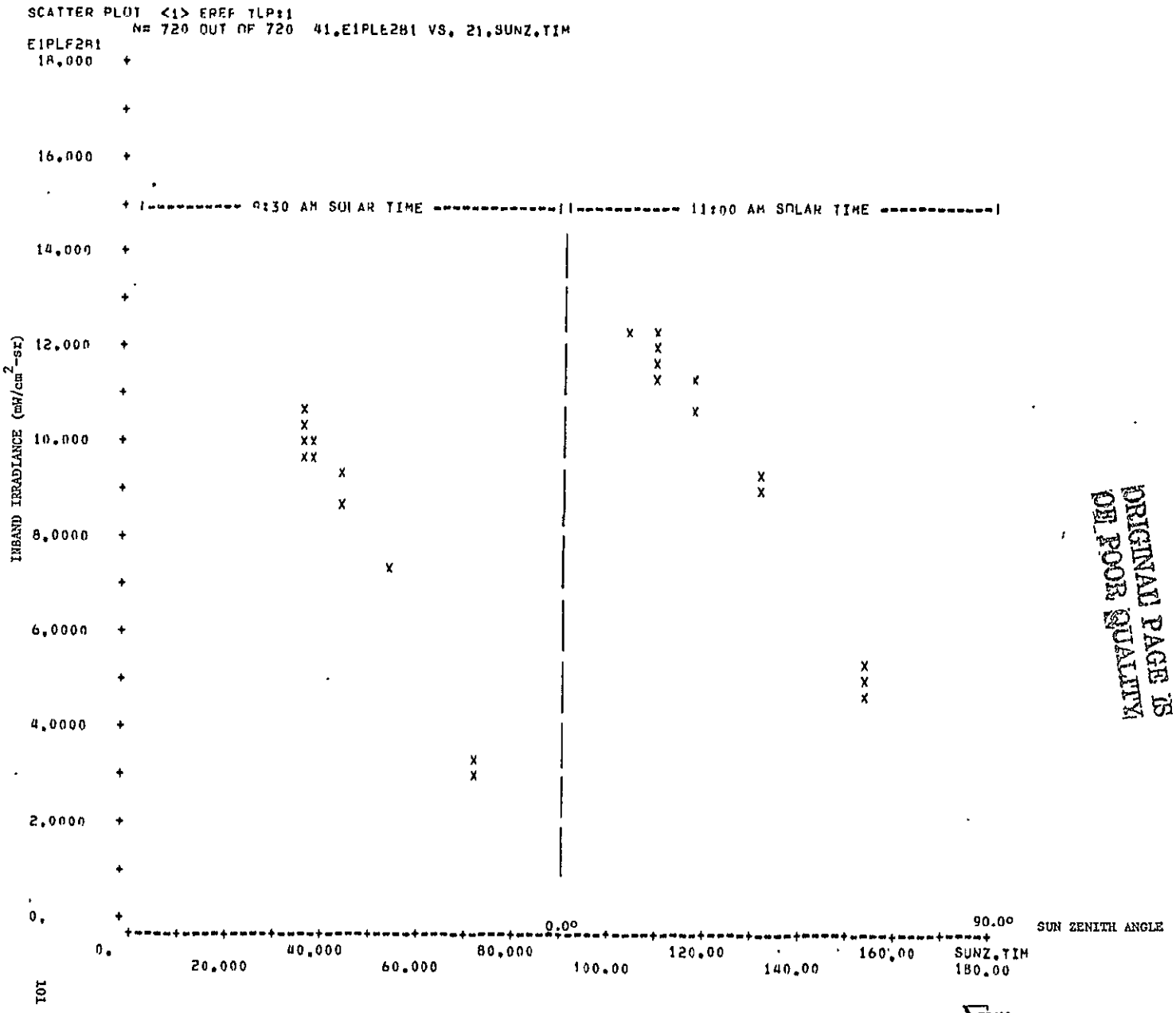

FIGURE 59. DEPENDENCE OF TOTAL IRRADIANCE ON SOLAR ZENITH ANGLE; ALL CONDITIONS, 0.45-0.52-μm BAND

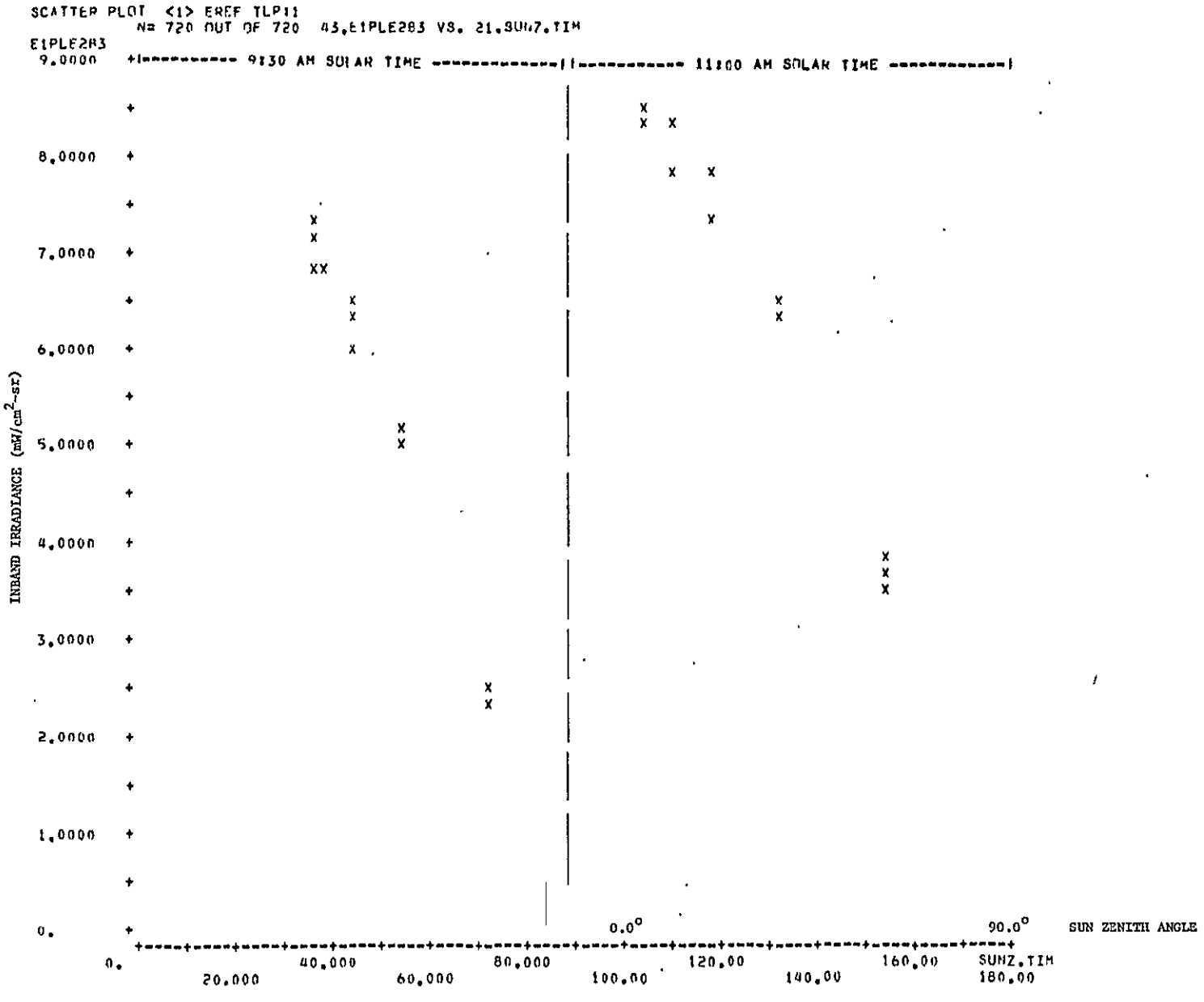

FIGURE 60. DEPENDENCE OF TOTAL IRRADIANCE ON SOLAR ZENITH ANGLE; ALL CONDITIONS, 0.63-0.69-MM BAND

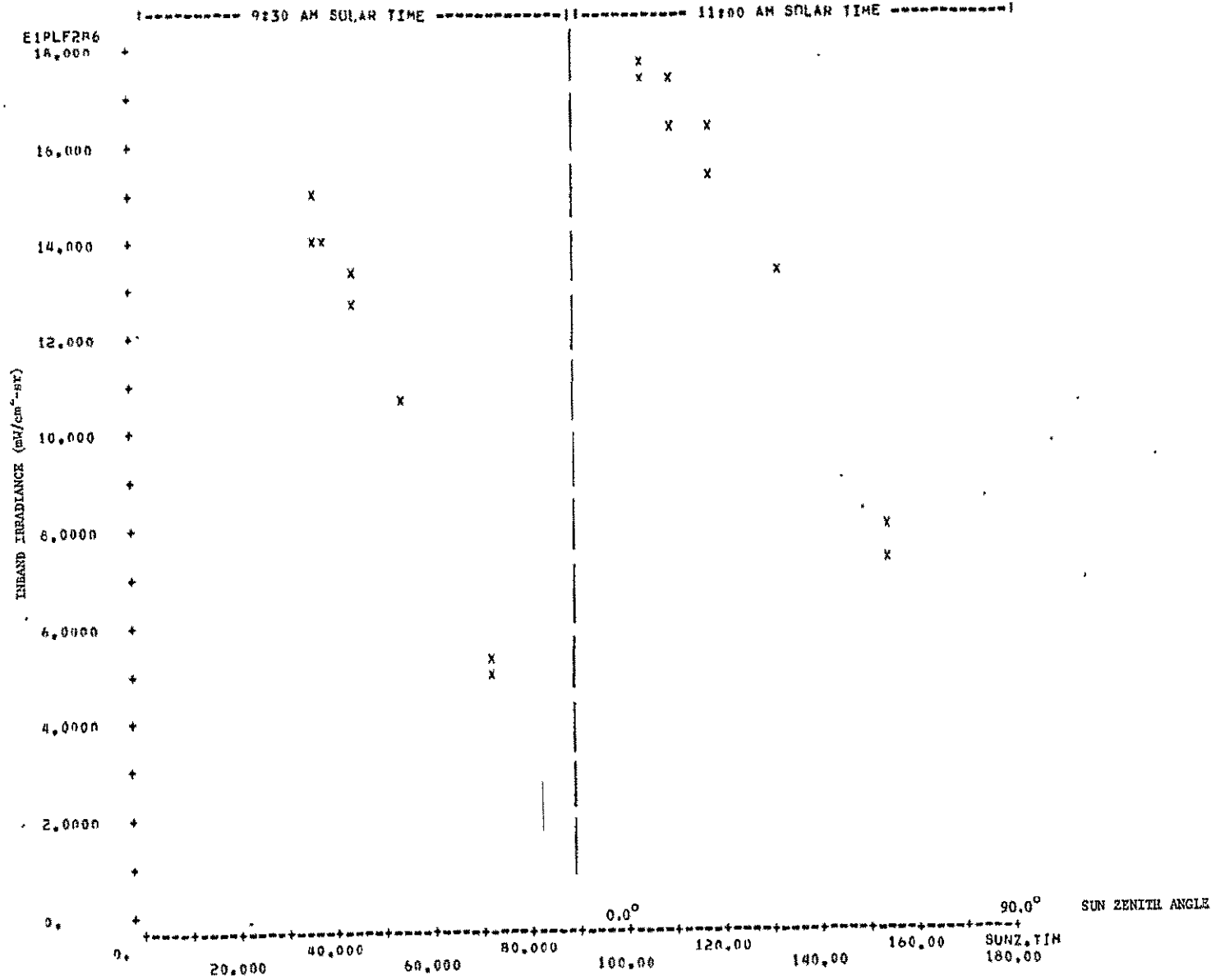

FIGURE 61. DEPENDENCE OF TOTAL IRRADIANCE ON SOLAR ZENITH ANGLE; ALL CONDITIONS, 0.74-0.91-MM BAND

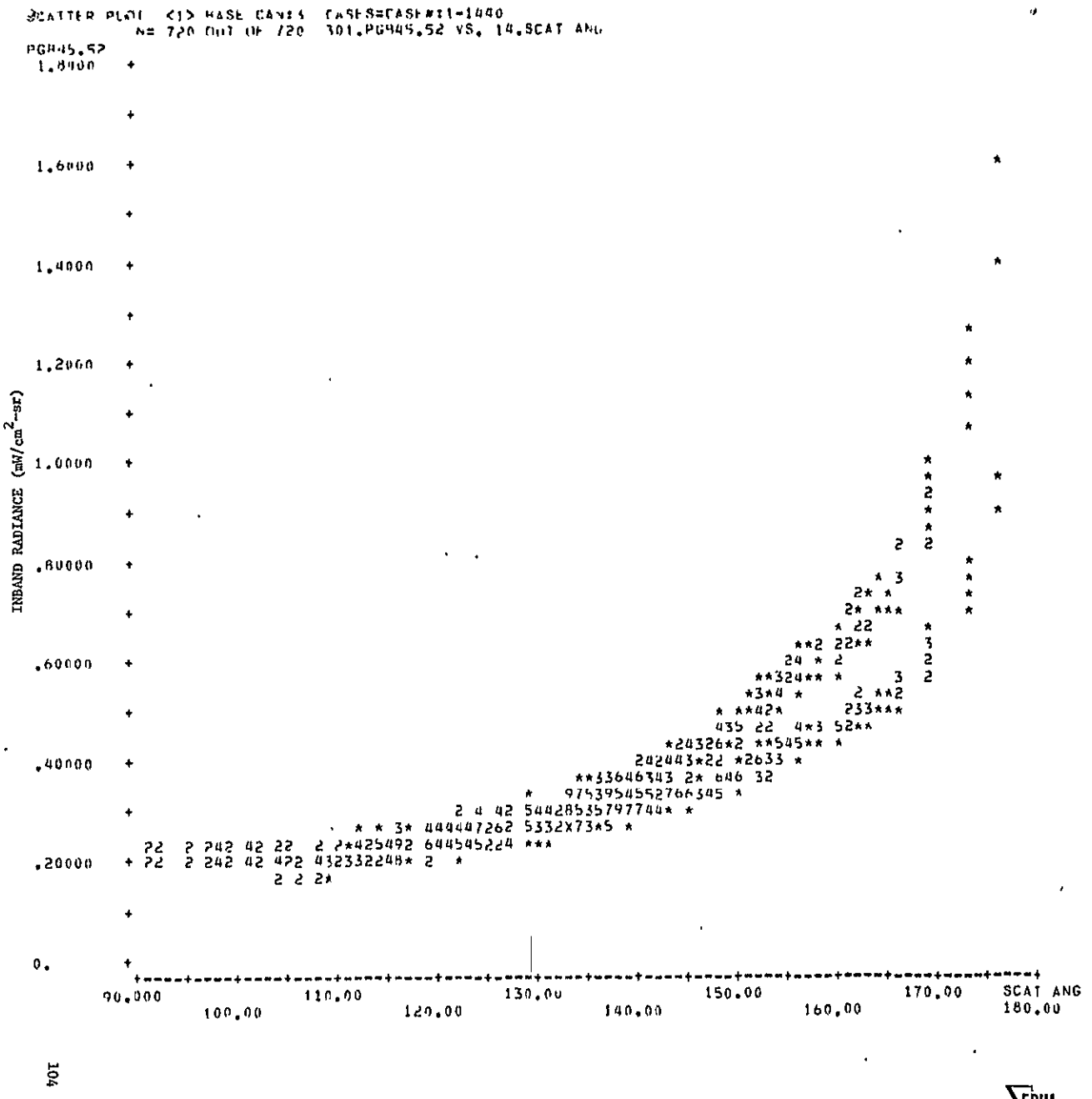

FIGURE 62. SCATTER DIAGRAM ILLUSTRATING THE CORRELATION BETWEEN PATH RADIANCE AND SCATTERING ANGLE; 0.45-0.52-μm BAND, BOTH TIMES, ALL FOUR VISUAL RANGES

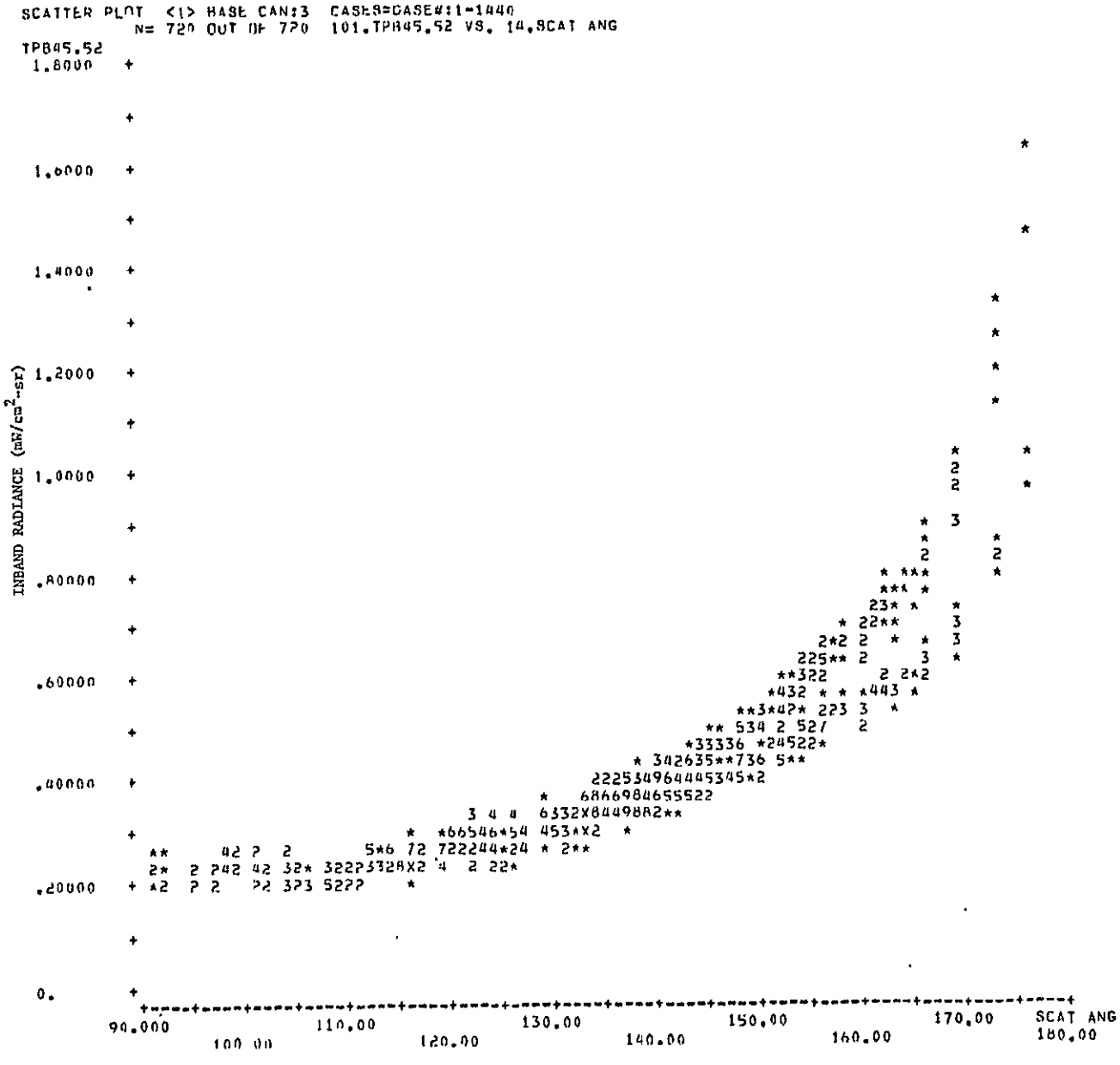

FIGURE 63. SCATTER DIAGRAM ILLUSTRATING THE CORRELATION BETWEEN TOTAL RADIANCE AND SCATTERING ANGLE; 0.45-0.52-μm BAND, BOTH TIMES, ALL FOUR VISUAL RANGES

TABLE 1. SUMMARY OF RADIATIVE TRANSFER MODEL CALCULATIONS FOR THEMATIC MAPPER THERMAL BAND
(λ = 10.29 to 12.50 μm, Sensor at Satellite Altitude)

Model Atmosphere	Off-Nadir Scan Angle	Atmos. Trans-mittance	Radiance (milliwatts/cm^2.sr) Atmos. Path	Total From 300°K Target	ΔL for ΔT = 0.5°K	For 300°K Target: L(0°)-L(8°)
Temperate, Summer	0°	0.6331	0.6122	1.921	0.010	-0.001
	4	0.6324	0.6133	1.921		
	8	0.6305	0.6164	1.920		
	12	0.6274	0.6217	1.919		
	18	0.6199	0.6342	1.916		
Temperate, Winter	0	0.8819	0.1330	1.951	0.013	--
	4	0.8817	0.1333	1.951		
	8	0.8810	0.1340	1.951		
	12	0.8800	0.1352	1.950		
	18	0.8774	0.1381	1.947		
Tropic	0	0.4803	0.9305	1.926	0.007	-0.001
	8	0.4771	0.9361	1.925		
	18	0.4638	0.9594	1.921		
Arctic, Summer	0	0.7567	0.3506	1.913	0.012	-0.001
	8	0.7549	0.3532	1.912		
	18	0.7475	0.3640	1.908		
Arctic, Winter	0	0.9205	0.0721	1.969	0.014	-0.001
	8	0.9199	0.0727	1.968		
	18	0.9175	0.0749	1.966		

TABLE 2. COMPARISON OF APPROXIMATE GEOMETRY USED FOR RADIANCE SIMULATIONS TO MORE PRECISE GEOMETRY BASED ON THEMATIC MAPPER ORBIT, 9:30 AM EQUATOR CROSSING

LATITUDE	DATE	TIME		SUN ZENITH		SUN AZIMUTH		LINEAR SCAN MODE			
								REL. AZIMUTH		SCAT. ANGLE	
		APPR.	ORBIT	APPR.	ORBIT	APPR.	ORBIT	APPR.	ORBIT	APPR.	ORBIT
40°N	JUN 21	9:30	9:20	35°	31°	105°	113°	4° 176	10° 170	153° 137	157° 141
	MAR/SEP 21	9:30	9:20	53	50	130	135	29 151	32 148	134 120	137 123
	DEC 21	9:30	9:20	72	69	145	151	44 136	47 133	114 102	116 105
0°	JUN 21	9:30	9:30	43	44	55	55	43 137	47 133	143 131	141 131
	MAR/SEP 21	9:30	9:30	38	39	90	90	8 172	12 168	150 134	148 133
	DEC 21	9:30	9:30	43	43	125	126	27 153	24 156	144 130	144 130
40°S	JUN 21	9:30	9:40	72	76	35	42	66 114	62 118	111 105	108 100
	MAR/SEP 21	9:30	9:40	53	58	50	58	51 129	45 135	132 122	127 116
	DEC 21	9:30	9:40	35	40	75	79	26 154	24 156	152 138	147 132

TABLE 3. COMPARISON OF APPROXIMATE GEOMETRY USED FOR RADIANCE SIMULATIONS TO MORE PRECISE GEOMETRY BASED ON THEMATIC MAPPER ORBIT, 11:00 AM EQUATOR CROSSING

LATITUDE	DATE	TIME		SUN ZENITH		SUN AZIMUTH		LINEAR SCAN MODE			
								REL. AZIMUTH		SCAT. ANGLE	
		APPR.	ORBIT	APPR.	ORBIT	APPR.	ORBIT	APPR.	ORBIT	APPR.	ORBIT
40°N	JUN 21	11:00	10:50	20°	18°	138°	154°	37°	50°	166°	166°
								143	130	153	156
	MAR/SEP 21	11:00	10:50	42	41	157	165	56	61	142	142
								124	119	133	135
	DEC 21	11:00	10:50	64	64	164	172	63	69	119	119
								117	111	112	113
0°	JUN 21	11:00	11:00	28	28	30	32	68	70	154	154
								112	110	148	149
	MAR/SEP 21	11:00	11:00	14	17	90	90	8	12	174	171
								172	168	158	155
	DEC 21	11:00	11:00	28	27	150	150	52	48	156	157
								128	132	147	147
40°S	JUN 21	11:00	11:10	64	67	16	22	85	81	116	114
								95	99	115	112
	MAR/SEP 21	11:00	11:10	42	46	23	34	78	69	139	137
								102	111	136	131
	DEC 21	11:00	11:10	20	25	42	54	59	49	163	160
								121	131	155	150

TIME OF EQUATORIAL CROSSING (GMT): 9 HOURS 30 MIN 0 SEC

TYPE OF SCAN: LINEAR

RUN DATE: 13:52:45 03-29-76

SIMULATION DATE: 6-21-78

LATITUDE (DEG N)	LONGITUDE (DEG W)	TIME D	MO	YR	HR	M	S	SUN POSITION ZEN	AZIM	SAT HEAD	GEOM	ZEN	R AZ	CON AZ	SCAT ANG
70.00	-27.87	21	6	78	9	11	53	47.	162.	26.	1	8.	46.	0.	138.
											2	8.	134.	0.	127.
60.00	-18.32	21	6	78	9	14	34	40.	145.	18.	1	8.	37.	0.	146.
											2	8.	143.	0.	133.
50.00	-13.10	21	6	78	9	17	11	34.	130.	15.	1	8.	25.	0.	153.
											2	8.	155.	0.	138.
40.00	-9.51	21	6	78	9	19	46	31.	113.	13.	1	8.	10.	0.	157.
											2	8.	170.	0.	141.
30.00	-6.69	21	6	78	9	22	20	30.	94.	13.	1	8.	-8.	0.	158.
											2	8.	172.	0.	142.
20.00	-4.29	21	6	78	9	24	53	33.	77.	12.	1	8.	-25.	0.	154.
											2	8.	155.	0.	140.
10.00	-2.10	21	6	78	9	27	27	37.	64.	12.	1	8.	-38.	0.	149.
											2	8.	142.	0.	136.
0.0	0.00	21	6	78	9	30	0	44.	55.	12.	1	8.	-47.	0.	141.
											2	8.	133.	0.	131.
-10.00	2.10	21	6	78	9	32	33	51.	49.	12.	1	8.	-53.	0.	133.
											2	8.	127.	0.	124.
-20.00	4.29	21	6	78	9	35	7	59.	45.	12.	1	8.	-58.	0.	125.
											2	8.	122.	0.	116.
-30.00	6.69	21	6	78	9	37	40	67.	42.	13.	1	8.	-60.	0.	116.
											2	8.	120.	0.	108.
-40.00	9.51	21	6	78	9	40	14	76.	42.	13.	1	8.	-62.	0.	108.
											2	8.	118.	0.	100.
-50.00	13.10	21	6	78	9	42	49	85.	43.	15.	1	8.	-62.	0.	99.
											2	8.	118.	0.	91.
-60.00	18.32	21	6	78	9	45	26	94.	47.	18.	1	8.	-62.	0.	90.
											2	8.	118.	0.	82.
-70.00	27.87	21	6	78	9	48	7	103.	56.	26.	1	8.	-60.	0.	81.
											2	8.	120.	0.	73.

TABLE 4. GEOMETRY SYNOPSIS; 9:30 AM ORBIT, JUNE, LINEAR SCANNER

TIME OF EQUATORIAL CROSSING (GMT): 9 HOURS 30 MIN 0 SEC

TYPE OF SCAN: LINEAR

RUN DATE: 13:52:45 03-29-76

SIMULATION DATE: 3-21-78

LATITUDE (DEG N)	LONGITUDE (DEG W)	TIME D	MO	YR	HR	M	S	SUN POSITION ZEN	AZIM	SAT HEAD	GEOM	ZEN	R	AZ	CON AZ	SCAT ANG
70.00	-27.87	21	3	78	9	11	55	71.	163.	26.	1	8.		47.	0.	115.
											2	8.		133.	0.	104.
60.00	-18.32	21	3	78	9	14	34	63.	152.	18.	1	8.		43.	0.	123.
											2	8.		137.	0.	111.
50.00	-13.10	21	3	78	9	17	11	56.	143.	15.	1	8.		38.	0.	130.
											2	8.		142.	0.	118.
40.00	-9.51	21	3	78	9	19	46	50.	135.	13.	1	8.		32.	0.	137.
											2	8.		148.	0.	123.
30.00	-6.69	21	3	78	9	22	20	44.	126.	13.	1	8.		23.	0.	143.
											2	8.		157.	0.	128.
20.00	-4.29	21	3	78	9	24	53	41.	115.	12.	1	8.		13.	0.	147.
											2	8.		167.	0.	131.
10.00	-2.10	21	3	78	9	27	27	39.	102.	12.	1	8.		0.	0.	149.
											2	8.		180.	0.	133.
0.0	0.00	21	3	78	9	30	0	39.	90.	12.	1	8.		-12.	0.	148.
											2	8.		168.	0.	133.
-10.00	2.10	21	3	78	9	32	33	42.	78.	12.	1	8.		-23.	0.	145.
											2	8.		157.	0.	131.
-20.00	4.29	21	3	78	9	35	7	46.	69.	12.	1	8.		-33.	0.	140.
											2	8.		147.	0.	127.
-30.00	6.69	21	3	78	9	37	40	52.	63.	13.	1	8.		-40.	0.	134.
											2	8.		140.	0.	122.
-40.00	9.51	21	3	78	9	40	14	58.	58.	13.	1	8.		-45.	0.	127.
											2	8.		135.	0.	116.
-50.00	13.10	21	3	78	9	42	49	65.	57.	15.	1	8.		-49.	0.	120.
											2	8.		131.	0.	109.
-60.00	18.32	21	3	78	9	45	26	73.	58.	18.	1	8.		-51.	0.	112.
											2	8.		129.	0.	102.
-70.00	27.87	21	3	78	9	48	7	81.	64.	26.	1	8.		-52.	0.	104.
											2	8.		128.	0.	94.

TABLE 5. GEOMETRY SYNOPSIS; 9:30 AM ORBIT, MARCH, LINEAR SCANNER

TIME OF EQUATORIAL CROSSING (GMT): 9 HOURS 30 MIN 0 SEC

TYPE OF SCAN: LINEAR

RUN DATE: 13:52:45 03-29-76

SIMULATION DATE: 12-21-77

LATITUDE (DEG N)	LONGITUDE (DEG W)	TIME D	MO	YR	HR	M	S	SUN POSITION ZEN	AZIM	SAT HEAD	GEOM	ZEN	R AZ	CON AZ	SCAT ANG
70.00	-27.87	21	12	77	9	11	53	94.	167.	26.	1	8.	52.	0.	91.
											2	8.	128.	0.	81.
60.00	-18.32	21	12	77	9	14	34	85.	159.	18.	1	8.	51.	0.	100.
											2	8.	129.	0.	89.
50.00	-13.10	21	12	77	9	17	11	77.	155.	15.	1	8.	49.	0.	108.
											2	8.	131.	0.	97.
40.00	-9.51	21	12	77	9	19	46	69.	151.	13.	1	8.	47.	0.	116.
											2	8.	133.	0.	105.
30.00	-6.69	21	12	77	9	22	20	62.	146.	13.	1	8.	44.	0.	124.
											2	8.	136.	0.	112.
20.00	-4.29	21	12	77	9	24	53	55.	141.	12.	1	8.	39.	0.	131.
											2	8.	141.	0.	119.
10.00	-2.10	21	12	77	9	27	27	48.	134.	12.	1	8.	32.	0.	138.
											2	8.	148.	0.	125.
0.0	0.00	21	12	77	9	30	0	43.	126.	12.	1	8.	24.	0.	144.
											2	8.	156.	0.	130.
-10.00	2.10	21	12	77	9	32	33	39.	115.	12.	1	8.	13.	0.	149.
											2	8.	167.	0.	133.
-20.00	4.29	21	12	77	9	35	7	37.	103.	12.	1	8.	1.	0.	151.
											2	8.	179.	0.	135.
-30.00	6.69	21	12	77	9	37	40	38.	90.	13.	1	8.	-12.	0.	150.
											2	8.	168.	0.	134.
-40.00	9.51	21	12	77	9	40	14	40.	79.	13.	1	8.	-24.	0.	147.
											2	8.	156.	0.	132.
-50.00	13.10	21	12	77	9	42	49	45.	72.	15.	1	8.	-34.	0.	141.
											2	8.	146.	0.	128.
-60.00	18.32	21	12	77	9	45	26	51.	68.	18.	1	8.	-41.	0.	135.
											2	8.	139.	0.	123.
-70.00	27.87	21	12	77	9	48	7	58.	70.	26.	1	8.	-46.	0.	127.
											2	8.	134.	0.	116.

TABLE 6. GEOMETRY SYNOPSIS; 9:30 AM ORBIT, DECEMBER, LINEAR SCANNER

TIME OF EQUATORIAL CROSSING (GMT): 11 HOURS 0 MIN 0 SEC

TYPE OF SCAN: LINEAR

RUN DATE: 13:52:45 03-29-76

SIMULATION DATE: 6-21-78

LATITUDE (DEG N)	LONGITUDE (DEG W)	TIME D	MO	YR	HR	M	S	SUN POSITION ZEN	AZIM	SAT HEAD	GEOM	ZEN R	AZ	CON SCAT AZ	ANG
70.00	-27.87	21	6	78	10	41	53	47.	190.	26.	1	8.	74.	0.	165.
											2	8.	106.	0.	131.
60.00	-18.32	21	6	78	10	44	34	37.	178.	18.	1	8.	70.	0.	145.
											2	8.	110.	0.	140.
50.00	-13.10	21	6	78	10	47	11	27.	169.	15.	1	8.	64.	0.	156.
											2	8.	116.	0.	149.
40.00	-9.51	21	6	78	10	49	46	18.	154.	13.	1	8.	50.	0.	166.
											2	8.	130.	0.	156.
30.00	-6.69	21	6	78	10	52	20	12.	122.	13.	1	8.	19.	0.	175.
											2	8.	161.	0.	161.
20.00	-4.29	21	6	78	10	54	53	12.	71.	12.	1	8.	-31.	0.	173.
											2	8.	149.	0.	161.
10.00	-2.10	21	6	78	10	57	27	19.	43.	12.	1	8.	-59.	0.	164.
											2	8.	121.	0.	156.
0.0	0.00	21	6	78	11	0	0	28.	32.	12.	1	8.	-70.	0.	154.
											2	8.	110.	0.	149.
-10.00	2.10	21	6	78	11	2	33	37.	26.	12.	1	8.	-76.	0.	144.
											2	8.	104.	0.	140.
-20.00	4.29	21	6	78	11	5	7	47.	23.	12.	1	8.	-79.	0.	134.
											2	8.	101.	0.	131.
-30.00	6.69	21	6	78	11	7	40	57.	22.	13.	1	8.	-80.	0.	124.
											2	8.	100.	0.	121.
-40.00	9.51	21	6	78	11	10	14	67.	22.	13.	1	8.	-81.	0.	114.
											2	8.	99.	0.	112.
-50.00	13.10	21	6	78	11	12	49	77.	24.	15.	1	8.	-81.	0.	104.
											2	8.	99.	0.	102.
-60.00	18.32	21	6	78	11	15	26	87.	27.	18.	1	8.	-81.	0.	94.
											2	8.	99.	0.	92.
-70.00	27.87	21	6	78	11	18	7	97.	35.	26.	1	8.	-80.	0.	84.
											2	8.	100.	0.	81.

TABLE 7. GEOMETRY SYNOPSIS; 11:00 AM ORBIT, JUNE, LINEAR SCANNER

TIME OF EQUATORIAL CROSSING (GMT): 11 HOURS 0 MIN 0 SEC

TYPE OF SCAN: LINEAR

RUN DATE: 13:52:45 03-29-76

SIMULATION DATE: 3-21-78

LATITUDE (DEG N)	LONGITUDE (DEG W)	TIME D	MO	YR	HR	M	S	SUN POSITION ZEN	AZIM	SAT HEAD	GEOM	ZEN	R	AZ	CON AZ	SCAT ANG
70.00	-27.87	21	3	78	10	41	53	70.	187.	26.	1	8.		71.	0.	112.
											2	8.		109.	0.	107.
60.00	-18.32	21	3	78	10	44	34	60.	177.	18.	1	8.		69.	0.	123.
											2	8.		111.	0.	117.
50.00	-13.10	21	3	78	10	47	11	50.	171.	15.	1	8.		66.	0.	133.
											2	8.		114.	0.	126.
40.00	-9.51	21	3	78	10	49	46	41.	165.	13.	1	8.		61.	0.	142.
											2	8.		119.	0.	135.
30.00	-6.69	21	3	78	10	52	20	32.	157.	13.	1	8.		54.	0.	152.
											2	8.		126.	0.	143.
20.00	-4.29	21	3	78	10	54	53	24.	144.	12.	1	8.		42.	0.	161.
											2	8.		138.	0.	150.
10.00	-2.10	21	3	78	10	57	27	18.	122.	12.	1	8.		20.	0.	169.
											2	8.		160.	0.	154.
0.0	0.00	21	3	78	11	0	0	17.	89.	12.	1	8.		-12.	0.	171.
											2	8.		168.	0.	155.
-10.00	2.10	21	3	78	11	2	33	21.	62.	12.	1	8.		-40.	0.	164.
											2	8.		140.	0.	153.
-20.00	4.29	21	3	78	11	5	7	28.	46.	12.	1	8.		-56.	0.	156.
											2	8.		124.	0.	147.
-30.00	6.69	21	3	78	11	7	40	37.	38.	13.	1	8.		-64.	0.	146.
											2	8.		116.	0.	139.
-40.00	9.51	21	3	78	11	10	14	46.	34.	13.	1	8.		-69.	0.	137.
											2	8.		111.	0.	131.
-50.00	13.10	21	3	78	11	12	49	55.	33.	15.	1	8.		-72.	0.	127.
											2	8.		108.	0.	122.
-60.00	18.32	21	3	78	11	15	26	65.	35.	18.	1	8.		-73.	0.	117.
											2	8.		107.	0.	113.
-70.00	27.87	21	3	78	11	18	7	75.	42.	26.	1	8.		-74.	0.	107.
											2	8.		106.	0.	103.

TABLE 8. GEOMETRY SYNOPSIS; 11:00 AM ORBIT, MARCH, LINEAR SCANNER

TIME OF EQUATORIAL CROSSING (GMT): 11 HOURS 0 MIN 0 SEC

TYPE OF SCAN: LINEAR

RUN DATE: 13:52:45 03-29-76

SIMULATION DATE: 12-21-77

LATITUDE (DEG N)	LONGITUDE (DEG W)	TIME D	MO	YR	HR	M	S	SUN POSITION ZEN	AZIM	SAT HEAD	GEOM	ZEN	R AZ	CON AZ	SCAT ANG
70.00	-27.87	21	12	77	10	41	53	94.	188.	26.	1	8.	72.	0.	89.
											2	8.	108.	0.	84.
60.00	-18.32	21	12	77	10	44	34	83.	180.	18.	1	8.	72.	0.	99.
											2	8.	108.	0.	94.
50.00	-13.10	21	12	77	10	47	11	74.	175.	15.	1	8.	70.	0.	109.
											2	8.	110.	0.	104.
40.00	-9.51	21	12	77	10	49	46	64.	172.	13.	1	8.	69.	0.	119.
											2	8.	111.	0.	113.
30.00	-6.69	21	12	77	10	52	20	54.	169.	13.	1	8.	66.	0.	129.
											2	8.	114.	0.	122.
20.00	-4.29	21	12	77	10	54	55	45.	165.	12.	1	8.	63.	0.	138.
											2	8.	117.	0.	131.
10.00	-2.10	21	12	77	10	57	27	36.	159.	12.	1	8.	57.	0.	148.
											2	8.	123.	0.	139.
0.0	0.00	21	12	77	11	0	0	27.	150.	12.	1	8.	48.	0.	157.
											2	8.	132.	0.	147.
-10.00	2.10	21	12	77	11	2	33	20.	133.	12.	1	8.	31.	0.	166.
											2	8.	149.	0.	152.
-20.00	4.29	21	12	77	11	5	7	17.	105.	12.	1	8.	3.	0.	171.
											2	8.	177.	0.	155.
-30.00	6.69	21	12	77	11	7	40	18.	74.	13.	1	8.	-29.	0.	168.
											2	8.	151.	0.	154.
-40.00	9.51	21	12	77	11	10	14	25.	54.	13.	1	8.	-49.	0.	160.
											2	8.	131.	0.	150.
-50.00	13.10	21	12	77	11	12	49	33.	45.	15.	1	8.	-60.	0.	151.
											2	8.	120.	0.	143.
-60.00	18.32	21	12	77	11	15	26	42.	42.	18.	1	8.	-66.	0.	141.
											2	8.	114.	0.	134.
-70.00	27.87	21	12	77	11	18	7	52.	46.	26.	1	8.	-70.	0.	131.
											2	8.	110.	0.	125.

TABLE 9. GEOMETRY SYNOPSIS; 11:00 AM ORBIT, DECEMBER, LINEAR SCANNER

TIME OF EQUATORIAL CROSSING (GMT): 9 HOURS 30 MIN 0 SEC

TYPE OF SCAN: CONICAL

RUN DATE: 13:52:45 03-29-76

SIMULATION DATE: 6-21-78

LATITUDE (DEG N)	LONGITUDE (DEG W)	TIME D	MO	YR	HR	M	S	SUN POSITION ZEN	AZIM	SAT HEAD	GEOM	ZEN R	AZ	CON SCAT AZ	ANG
70.00	-27.87	21	6	78	9	11	22	47.	161.	28.	1	18.	109.	24.	125.
											2	18.	157.	-24.	116.
60.00	-18.32	21	6	78	9	14	3	40.	145.	19.	1	18.	102.	24.	133.
											2	18.	150.	-24.	124.
50.00	-13.10	21	6	78	9	16	40	34.	130.	16.	1	18.	90.	24.	142.
											2	18.	138.	-24.	131.
40.00	-9.51	21	6	78	9	19	15	31.	113.	14.	1	18.	75.	24.	149.
											2	18.	123.	-24.	137.
30.00	-6.69	21	6	78	9	21	49	30.	94.	13.	1	18.	58.	24.	155.
											2	18.	106.	-24.	141.
20.00	-4.29	21	6	78	9	24	22	33.	77.	12.	1	18.	41.	24.	158.
											2	18.	89.	-24.	143.
10.00	-2.10	21	6	78	9	26	56	37.	64.	12.	1	18.	28.	24.	157.
											2	18.	76.	-24.	143.
0.0	0.00	21	6	78	9	29	29	44.	55.	12.	1	18.	19.	24.	153.
											2	18.	67.	-24.	140.
-10.00	2.10	21	6	78	9	32	2	51.	49.	12.	1	18.	13.	24.	146.
											2	18.	61.	-24.	136.
-20.00	4.29	21	6	78	9	34	35	59.	45.	12.	1	18.	9.	24.	139.
											2	18.	57.	-24.	129.
-30.00	6.69	21	6	78	9	37	9	67.	43.	12.	1	18.	6.	24.	130.
											2	18.	54.	-24.	122.
-40.00	9.51	21	6	78	9	39	43	76.	42.	13.	1	18.	5.	24.	122.
											2	18.	53.	-24.	114.
-50.00	13.10	21	6	78	9	42	18	85.	43.	15.	1	18.	5.	24.	113.
											2	18.	53.	-24.	106.
-60.00	18.32	21	6	78	9	44	55	94.	47.	17.	1	18.	5.	24.	104.
											2	18.	53.	-24.	97.
-70.00	27.87	21	6	78	9	47	36	103.	56.	24.	1	18.	8.	24.	95.
											2	18.	56.	-24.	87.

TABLE 10. GEOMETRY SYNOPSIS; 9:30 AM ORBIT, JUNE, CONICAL SCANNER

TIME OF EQUATORIAL CROSSING (GMT): 9 HOURS 30 MIN 0 SEC

TYPE OF SCAN: CONICAL

RUN DATE: 17:12:01 03-29-76

*SIMULATION DATE: 3-21-78

LATITUDE (DEG N)	LONGITUDE (DEG W)	TIME D	MO	YR	HR	M	S	SUN POSITION ZEN	AZIM	SAT HEAD	GEOM	ZEN	R AZ	CON AZ	SCAT ANG
70.00	-27.87	21	3	78	9	11	22	71.	163.	28.	1	18.	111.	24.	102.
											2	18.	159.	-24.	92.
60.00	-18.32	21	3	78	9	14	3	63.	152.	19.	1	18.	108.	24.	110.
											2	18.	156.	-24.	100.
50.00	-13.10	21	3	78	9	16	40	56.	143.	16.	1	18.	104.	24.	118.
											2	18.	152.	-24.	108.
40.00	-9.51	21	3	78	9	19	15	50.	135.	14.	1	18.	97.	24.	126.
											2	18.	145.	-24.	115.
30.00	-6.69	21	3	78	9	21	49	45.	126.	13.	1	18.	89.	24.	133.
											2	18.	137.	-24.	121.
20.00	-4.29	21	3	78	9	24	22	41.	115.	12.	1	18.	78.	24.	139.
											2	18.	126.	-24.	127.
10.00	-2.10	21	3	78	9	26	56	39.	102.	12.	1	18.	66.	24.	145.
											2	18.	114.	-24.	131.
0.0	0.00	21	3	78	9	29	29	40.	90.	12.	1	18.	54.	24.	148.
											2	18.	102.	-24.	134.
-10.00	2.10	21	3	78	9	32	2	42.	78.	12.	1	18.	43.	24.	149.
											2	18.	91.	-24.	135.
-20.00	4.29	21	3	78	9	34	35	46.	69.	12.	1	18.	33.	24.	148.
											2	18.	81.	-24.	134.
-30.00	6.69	21	3	78	9	37	9	52.	63.	12.	1	18.	26.	24.	144.
											2	18.	74.	-24.	131.
-40.00	9.51	21	3	78	9	39	43	58.	58.	13.	1	18.	21.	24.	138.
											2	18.	69.	-24.	126.
-50.00	13.10	21	3	78	9	42	18	65.	57.	15.	1	18.	18.	24.	132.
											2	18.	66.	-24.	121.
-60.00	18.32	21	3	78	9	44	55	73.	58.	17.	1	18.	16.	24.	124.
											2	18.	64.	-24.	114.
-70.00	27.87	21	3	78	9	47	36	81.	64.	24.	1	18.	16.	24.	116.
											2	18.	64.	-24.	106.

TABLE 11. GEOMETRY SYNOPSIS; 9:30 AM ORBIT, MARCH, CONICAL SCANNER

TIME OF EQUATORIAL CROSSING (GMT): 9 HOURS 30 MIN 0 SEC

TYPE OF SCAN: CONICAL

RUN DATE: 13:52:45 03-29-76

SIMULATION DATE: 12-21-77

LATITUDE (DEG N)	LONGITUDE (DEG W)	TIME D	MO	YR	HR	M	S	SUN POSITION ZEN	AZIM	SAT HEAD	GEOM	ZEN	R AZ	CON AZ	SCAT ANG
70.00	-27.87	21	12	77	9	11	22	94.	167.	28.	1	18.	115.	24.	79.
											2	18.	163.	-24.	69.
60.00	-18.32	21	12	77	9	14	3	86.	159.	19.	1	18.	116.	24.	87.
											2	18.	164.	-24.	77.
50.00	-13.10	21	12	77	9	16	40	77.	154.	16.	1	18.	115.	24.	95.
											2	18.	163.	-24.	85.
40.00	-9.51	21	12	77	9	19	15	69.	150.	14.	1	18.	113.	24.	103.
											2	18.	161.	-24.	93.
30.00	-6.69	21	12	77	9	21	49	62.	146.	13.	1	18.	109.	24.	111.
											2	18.	157.	-24.	101.
20.00	-4.29	21	12	77	9	24	22	55.	141.	12.	1	18.	105.	24.	119.
											2	18.	153.	-24.	109.
10.00	-2.10	21	12	77	9	26	56	48.	134.	12.	1	18.	98.	24.	127.
											2	18.	146.	-24.	116.
0.0	0.00	21	12	77	9	29	29	43.	126.	12.	1	18.	90.	24.	134.
											2	18.	138.	-24.	123.
-10.00	2.10	21	12	77	9	32	2	39.	115.	12.	1	18.	79.	24.	141.
											2	18.	127.	-24.	128.
-20.00	4.29	21	12	77	9	34	35	37.	103.	12.	1	18.	67.	24.	146.
											2	18.	115.	-24.	133.
-30.00	6.69	21	12	77	9	37	9	38.	90.	12.	1	18.	54.	24.	150.
											2	18.	102.	-24.	135.
-40.00	9.51	21	12	77	9	39	43	41.	80.	13.	1	18.	42.	24.	151.
											2	18.	90.	-24.	136.
-50.00	13.10	21	12	77	9	42	18	45.	72.	15.	1	18.	33.	24.	149.
											2	18.	81.	-24.	135.
-60.00	18.32	21	12	77	9	44	55	51.	68.	17.	1	18.	26.	24.	144.
											2	18.	74.	-24.	132.
-70.00	27.87	21	12	77	9	47	36	58.	70.	24.	1	18.	22.	24.	138.
											2	18.	70.	-24.	126.

TABLE 12. GEOMETRY SYNOPSIS; 9:30 AM ORBIT, DECEMBER, CONICAL SCANNER

TIME OF EQUATORIAL CROSSING (GMT): 11 HOURS 0 MIN 0 SEC

TYPE OF SCAN: CONICAL

RUN DATE: 13:52:45 03-29-78

STIMULATION DATE: 6-21-78

LATITUDE (DEG N)	LONGITUDE (DEG E)	TIME D	MO	YR	HR	M	S	SUN POSITION ZEN	AZIM	SAT HEAD	GEOM	ZEN	R AZ	CON AZ	SCAT ANG
70.00	-27.87	21	6	78	10	41	22	47.	190.	28.	1	18.	137.	24.	119.
											2	18.	175.	-24.	115.
60.00	-18.52	21	6	78	10	44	5	37.	178.	19.	1	18.	135.	24.	129.
											2	18.	177.	-24.	125.
50.00	-13.10	21	6	78	10	46	40	27.	168.	16.	1	18.	129.	24.	139.
											2	18.	177.	-24.	135.
40.00	-9.51	21	6	78	10	49	15	18.	154.	14.	1	18.	116.	24.	150.
											2	18.	164.	-24.	144.
30.00	-6.69	21	6	78	10	51	49	12.	122.	13.	1	18.	85.	24.	160.
											2	18.	133.	-24.	153.
20.00	-4.29	21	6	78	10	54	22	12.	71.	12.	1	18.	55.	24.	169.
											2	18.	83.	-24.	160.
10.00	-2.10	21	6	78	10	56	56	19.	43.	12.	1	18.	8.	24.	177.
											2	18.	56.	-24.	163.
0.0	0.00	21	6	78	10	59	29	28.	32.	12.	1	18.	-4.	24.	170.
											2	18.	44.	-24.	161.
-10.00	2.10	21	6	78	11	2	2	37.	26.	12.	1	18.	-10.	24.	160.
											2	18.	38.	-24.	155.
-20.00	4.29	21	6	78	11	4	35	47.	24.	12.	1	18.	-12.	24.	150.
											2	18.	36.	-24.	146.
-30.00	6.69	21	6	78	11	7	9	57.	22.	12.	1	18.	-14.	24.	140.
											2	18.	34.	-24.	137.
-40.00	9.51	21	6	78	11	9	45	67.	23.	13.	1	18.	-15.	24.	130.
											2	18.	33.	-24.	128.
-50.00	13.10	21	6	78	11	12	18	77.	24.	15.	1	18.	-15.	24.	120.
											2	18.	33.	-24.	118.
-60.00	18.52	21	6	78	11	14	55	87.	27.	17.	1	18.	-14.	24.	110.
											2	18.	34.	-24.	108.
-70.00	27.87	21	6	78	11	17	36	97.	36.	24.	1	18.	-12.	24.	100.
											2	18.	36.	-24.	97.

TABLE 13. GEOMETRY SYNOPSIS; 11:00 AM ORBIT, JUNE, CONICAL SCANNER

TIME OF EQUATORIAL CROSSING (GMT): 11 HOURS 0 MIN 0 SEC

TYPE OF SCAN: CONICAL

RUN DATE: 13:52:45 03-29-76

STMULATION DATE: 3-21-78

LATITUDE (DEG N)	LONGITUDE (DEG W)	TIME D	MO	YR	HR	M	S	SUN POSITION ZEN	AZIM	SAT HEAD	GEOM	ZEN	R AZ	CON AZ	SCAT ANG
70.00	-27.87	21	3	78	10	41	22	70.	187.	28.	1	18.	134.	24.	97.
											2	18.	178.	-24.	92.
60.00	-18.32	21	3	78	10	44	3	60.	177.	19.	1	18.	134.	24.	107.
											2	18.	178.	-24.	102.
50.00	-13.10	21	3	78	10	46	40	50.	171.	16.	1	18.	131.	24.	117.
											2	18.	179.	-24.	112.
40.00	-9.51	21	3	78	10	49	15	41.	164.	14.	1	18.	127.	24.	127.
											2	18.	175.	-24.	121.
30.00	-6.69	21	3	78	10	51	49	32.	156.	13.	1	18.	120.	24.	136.
											2	18.	168.	-24.	130.
20.00	-4.29	21	3	78	10	54	22	24.	144.	12.	1	18.	107.	24.	146.
											2	18.	155.	-24.	139.
10.00	-2.10	21	3	78	10	56	56	18.	121.	12.	1	18.	86.	24.	156.
											2	18.	134.	-24.	147.
0.0	0.00	21	3	78	10	59	29	17.	89.	12.	1	18.	54.	24.	164.
											2	18.	102.	-24.	153.
-10.00	2.10	21	3	78	11	2	2	21.	62.	12.	1	18.	26.	24.	171.
											2	18.	74.	-24.	157.
-20.00	4.29	21	3	78	11	4	35	28.	47.	12.	1	18.	11.	24.	169.
											2	18.	59.	-24.	156.
-30.00	6.69	21	3	78	11	7	9	37.	39.	12.	1	18.	2.	24.	161.
											2	18.	50.	-24.	152.
-40.00	9.51	21	3	78	11	9	43	46.	35.	13.	1	18.	-3.	24.	152.
											2	18.	45.	-24.	145.
-50.00	13.10	21	3	78	11	12	18	55.	33.	15.	1	18.	-5.	24.	143.
											2	18.	43.	-24.	137.
-60.00	18.32	21	3	78	11	14	55	65.	35.	17.	1	18.	-6.	24.	133.
											2	18.	42.	-24.	128.
-70.00	27.87	21	3	78	11	17	36	75.	42.	24.	1	18.	-6.	24.	123.
											2	18.	42.	-24.	118.

TABLE 14. GEOMETRY SYNOPSIS; 11:00 AM ORBIT, MARCH, CONICAL SCANNER

TIME OF EQUATORIAL CROSSING (GMT): 11 HOURS 0 MIN. 0 SEC

TYPE OF SCAN: CONICAL

RUN DATE: 13:52:45 03-29-76

STIMULATION DATE: 12-21-77

LATITUDE (DEG N)	LONGITUDE (DEG W)	TIME D	MO	YR	HR	M	S	SUN POSITION ZEN	AZIM	SAT HEAD	GEOM	ZEN	R AZ	CON AZ	SCAT ANG
70.00	-27.87	21	12	77	10	41	22	94.	188.	28.	1	18.	136.	24.	74.
											2	18.	176.	-24.	68.
60.00	-18.32	21	12	77	10	44	3	83.	180.	19.	1	18.	136.	24.	83.
											2	18.	176.	-24.	79.
50.00	-13.10	21	12	77	10	46	40	74.	175.	16.	1	18.	136.	24.	93.
											2	18.	176.	-24.	88.
40.00	-9.51	21	12	77	10	49	15	64.	172.	14.	1	18.	134.	24.	103.
											2	18.	178.	-24.	98.
30.00	-6.69	21	12	77	10	51	49	54.	169.	13.	1	18.	132.	24.	113.
											2	18.	180.	-24.	108.
20.00	-4.29	21	12	77	10	54	22	45.	165.	12.	1	18.	128.	24.	123.
											2	18.	176.	-24.	117.
10.00	-2.10	21	12	77	10	56	56	36.	159.	12.	1	18.	123.	24.	132.
											2	18.	171.	-24.	126.
0.0	0.00	21	12	77	10	59	29	27.	150.	12.	1	18.	114.	24.	142.
											2	18.	162.	-24.	135.
-10.00	2.10	21	12	77	11	2	2	20.	133.	12.	1	18.	97.	24.	151.
											2	18.	145.	-24.	143.
-20.00	4.29	21	12	77	11	4	35	17.	105.	12.	1	18.	69.	24.	160.
											2	18.	117.	-24.	150.
-30.00	6.69	21	12	77	11	7	9	19.	74.	12.	1	18.	58.	24.	168.
											2	18.	86.	-24.	155.
-40.00	9.51	21	12	77	11	9	43	25.	54.	13.	1	18.	17.	24.	171.
											2	18.	65.	-24.	157.
-50.00	13.10	21	12	77	11	12	18	33.	45.	15.	1	18.	6.	24.	165.
											2	18.	54.	-24.	154.
-60.00	18.32	21	12	77	11	14	55	42.	42.	17.	1	18.	1.	24.	156.
											2	18.	49.	-24.	148.
-70.00	27.87	21	12	77	11	17	36	52.	46.	24.	1	18.	-2.	24.	146.
											2	18.	46.	-24.	139.

TABLE 15. GEOMETRY SYNOPSIS; 11:00 AM ORBIT, DECEMBER, CONICAL SCANNER

TIME OF EQUATORIAL CROSSING (GMT): 9 HOURS 30 MIN 0 SEC

TYPE OF SCAN: CONICAL REAR

RUN DATE: 08:16:17 04-01-76

STMULATION DATE: 6-21-78

LATITUDE (DEG N)	LONGITUDE (DEG W)	TIME D	MO	YR	HR	M	S	SUN POSITION ZEN	AZIM	SAT HEAD	GEOM	ZEN	R AZ	CON AZ	SCAT ANG
70.00	-27.87	21	6	78	9	12	24	47.	162.	24.	1	18.	66.	24.	137.
											2	18.	18.	-24.	149.
60.00	-18.32	21	6	78	9	15	5	40.	146.	17.	1	18.	76.	24.	141.
											2	18.	28.	-24.	155.
50.00	-13.10	21	6	78	9	17	42	34.	130.	15.	1	18.	88.	24.	142.
											2	18.	40.	-24.	157.
40.00	-9.51	21	6	78	9	20	17	31.	113.	13.	1	18.	104.	24.	141.
											2	18.	56.	-24.	155.
30.00	-6.69	21	6	78	9	22	51	30.	95.	12.	1	18.	122.	24.	138.
											2	18.	74.	-24.	150.
20.00	-4.29	21	6	78	9	25	25	32.	77.	12.	1	18.	139.	24.	133.
											2	18.	91.	-24.	143.
10.00	-2.10	21	6	78	9	27	58	37.	64.	12.	1	18.	152.	24.	126.
											2	18.	104.	-24.	135.
0.0	0.00	21	6	78	9	30	31	44.	55.	12.	1	18.	161.	24.	119.
											2	18.	113.	-24.	127.
-10.00	2.10	21	6	78	9	33	4	51.	48.	12.	1	18.	167.	24.	111.
											2	18.	119.	-24.	119.
-20.00	4.29	21	6	78	9	35	38	59.	44.	12.	1	18.	172.	24.	103.
											2	18.	124.	-24.	110.
-30.00	6.69	21	6	78	9	38	11	67.	42.	13.	1	18.	174.	24.	95.
											2	18.	126.	-24.	101.
-40.00	9.51	21	6	78	9	40	45	76.	42.	14.	1	18.	176.	24.	86.
											2	18.	128.	-24.	93.
-50.00	13.10	21	6	78	9	43	20	85.	43.	16.	1	18.	177.	24.	77.
											2	18.	129.	-24.	84.
-60.00	18.32	21	6	78	9	45	57	94.	47.	19.	1	18.	177.	24.	68.
											2	18.	129.	-24.	75.
-70.00	27.87	21	6	78	9	48	38	103.	56.	28.	1	18.	177.	24.	59.
											2	18.	129.	-24.	66.

TABLE 16. GEOMETRY SYNOPSIS; 9:30 AM ORBIT, JUNE, CONICAL SCANNER (REARWARD LOOKING)

TIME OF EQUATORIAL CROSSING (GMT): 9 HOURS 30 MIN 0 SEC

TYPE OF SCAN: CONICAL REAR

RUN DATE: 08:10:17 04-01-76

SIMULATION DATE: 3-21-78

LATITUDE (DEG N)	LONGITUDE (DEG W)	TIME D	MO	YR	HR	M	S	SUN POSITION ZEN	AZIM	SAT HEAD	GEOM	ZEN	R AZ	CON AZ	SCAT ANG
70.00	-27.87	21	3	78	9	12	24	71.	163.	24.	1	18.	65.	24.	116.
											2	18.	17.	-24.	126.
60.00	-18.32	21	3	78	9	15	5	65.	152.	17.	1	18.	70.	24.	122.
											2	18.	22.	-24.	134.
50.00	-13.10	21	3	78	9	17	42	56.	144.	15.	1	18.	75.	24.	127.
											2	16.	27.	-24.	140.
40.00	-9.51	21	3	78	9	20	17	50.	135.	13.	1	18.	82.	24.	131.
											2	18.	34.	-24.	144.
30.00	-6.69	21	3	78	9	22	51	44.	126.	12.	1	18.	91.	24.	133.
											2	18.	43.	-24.	147.
20.00	-4.29	21	3	78	9	25	25	41.	115.	12.	1	18.	101.	24.	133.
											2	16.	53.	-24.	147.
10.00	-2.10	21	3	78	9	27	58	39.	102.	12.	1	18.	113.	24.	132.
											2	18.	65.	-24.	145.
0.0	0.00	21	3	78	9	30	31	39.	90.	12.	1	18.	126.	24.	128.
											2	18.	78.	-24.	141.
-10.00	2.10	21	3	78	9	33	4	42.	78.	12.	1	18.	138.	24.	124.
											2	18.	90.	-24.	135.
-20.00	4.29	21	3	78	9	35	38	46.	69.	12.	1	18.	147.	24.	118.
											2	18.	99.	-24.	129.
-30.00	6.69	21	3	78	9	38	11	52.	63.	13.	1	18.	154.	24.	112.
											2	16.	106.	-24.	122.
-40.00	9.51	21	3	78	9	40	45	58.	58.	14.	1	18.	159.	24.	105.
											2	18.	111.	-24.	114.
-50.00	13.10	21	3	78	9	43	20	65.	56.	16.	1	18.	163.	24.	97.
											2	18.	115.	-24.	106.
-60.00	18.32	21	3	78	9	45	57	73.	58.	19.	1	18.	166.	24.	90.
											2	18.	118.	-24.	98.
-70.00	27.87	21	3	78	9	48	38	81.	64.	28.	1	18.	168.	24.	81.
											2	18.	120.	-24.	90.

TABLE 17. GEOMETRY SYNOPSIS; 9:30 AM ORBIT, MARCH, CONICAL SCANNER (REARWARD LOOKING)

TIME OF EQUATORIAL CROSSING (GMT): 9 HOURS 30 MIN 0 SEC

TYPE OF SCAN: CONICAL REAR

RUN DATE: 08:16:17 04-01-76

SIMULATION DATE: 12-21-77

LATITUDE (DEG N)	LONGITUDE (DEG W)	TIME D	MO	YR	HR	M	S	SUN POSITION ZEN	AZIM	SAT HEAD	GEOM	ZEN	R AZ	CON AZ	SCAT ANG
70.00	-27.87	21	12	77	9	12	24	94.	167.	24.	1	18.	60.	24.	95.
											2	18.	12.	-24.	104.
60.00	-18.32	21	12	77	9	15	5	85.	159.	17.	1	18.	62.	24.	103.
											2	18.	14.	-24.	112.
50.00	-13.10	21	12	77	9	17	42	77.	155.	15.	1	18.	64.	24.	110.
											2	18.	16.	-24.	120.
40.00	-9.51	21	12	77	9	20	17	69.	151.	13.	1	18.	67.	24.	117.
											2	18.	19.	-24.	128.
30.00	-6.69	21	12	77	9	22	51	62.	146.	12.	1	18.	70.	24.	123.
											2	18.	22.	-24.	135.
20.00	-4.29	21	12	77	9	25	25	55.	141.	12.	1	18.	75.	24.	128.
											2	18.	27.	-24.	141.
10.00	-2.10	21	12	77	9	27	58	48.	134.	12.	1	18.	81.	24.	132.
											2	18.	33.	-24.	146.
0.0	0.00	21	12	77	9	30	31	43.	126.	12.	1	18.	90.	24.	134.
											2	18.	42.	-24.	149.
-10.00	2.10	21	12	77	9	33	4	39.	115.	12.	1	18.	101.	24.	135.
											2	18.	53.	-24.	149.
-20.00	4.29	21	12	77	9	35	38	37.	103.	12.	1	18.	113.	24.	133.
											2	18.	65.	-24.	147.
-30.00	6.69	21	12	77	9	38	11	38.	90.	13.	1	18.	126.	24.	130.
											2	18.	78.	-24.	142.
-40.00	9.51	21	12	77	9	40	45	40.	79.	14.	1	18.	138.	24.	125.
											2	18.	90.	-24.	136.
-50.00	13.10	21	12	77	9	43	20	45.	71.	16.	1	18.	148.	24.	119.
											2	18.	100.	-24.	129.
-60.00	18.32	21	12	77	9	45	57	51.	68.	19.	1	18.	156.	24.	112.
											2	18.	108.	-24.	122.
-70.00	27.87	21	12	77	9	48	38	58.	70.	28.	1	18.	162.	24.	105.
											2	18.	114.	-24.	113.

TABLE 18. GEOMETRY SYNOPSIS; 9:30 AM ORBIT, DECEMBER, CONICAL SCANNER (REARWARD LOOKING)

TIME OF EQUATORIAL CROSSING (GMT): 11 HOURS 0 MIN 0 SEC

TYPE OF SCAN: CONICAL REAR

RUN DATE: 08:16:17 04-01-76

SIMULATION DATE: 6-21-76

LATITUDE (DEG N)	LONGITUDE (DEG W)	TIME D	MO	YR	HR	M	S	SUN POSITION ZEN	AZIM	SAT HEAD	GEOM	ZEN	R AZ	CON AZ	SCAT ANG
70.00	-27.87	21	6	78	10	42	24	47.	190.	24.	1	18.	58.	24.	146.
											2	16.	10.	-24.	151.
60.00	-18.32	21	6	78	10	45	5	37.	179.	17.	1	18.	43.	24.	154.
											2	18.	5.	-24.	161.
50.00	-13.10	21	6	78	10	47	42	27.	169.	15.	1	18.	50.	24.	160.
											2	18.	2.	-24.	171.
40.00	-9.51	21	6	78	10	50	17	18.	154.	13.	1	18.	63.	24.	161.
											2	18.	15.	-24.	175.
30.00	-6.69	21	6	78	10	52	51	11.	122.	12.	1	18.	94.	24.	158.
											2	18.	46.	-24.	167.
20.00	-4.29	21	6	78	10	55	25	12.	71.	12.	1	18.	145.	24.	151.
											2	18.	97.	-24.	157.
10.00	-2.10	21	6	78	10	57	58	19.	43.	12.	1	18.	173.	24.	143.
											2	18.	125.	-24.	147.
0.0	0.00	21	6	78	11	0	31	28.	31.	12.	1	18.	184.	24.	134.
											2	18.	136.	-24.	137.
-10.00	2.10	21	6	78	11	3	4	37.	26.	12.	1	18.	190.	24.	125.
											2	18.	142.	-24.	128.
-20.00	4.29	21	6	78	11	5	38	47.	23.	12.	1	18.	193.	24.	115.
											2	16.	145.	-24.	118.
-30.00	6.69	21	6	78	11	8	11	57.	22.	13.	1	18.	195.	24.	106.
											2	18.	147.	-24.	108.
-40.00	9.51	21	6	78	11	10	45	67.	22.	14.	1	18.	195.	24.	96.
											2	18.	147.	-24.	98.
-50.00	13.10	21	6	78	11	13	20	77.	24.	16.	1	18.	196.	24.	86.
											2	18.	148.	-24.	88.
-60.00	18.32	21	6	78	11	15	57	87.	27.	19.	1	18.	196.	24.	76.
											2	18.	148.	-24.	78.
-70.00	27.87	21	6	78	11	18	38	97.	35.	28.	1	18.	197.	24.	65.
											2	18.	149.	-24.	67.

TABLE 19. GEOMETRY SYNOPSIS; 11:00 AM ORBIT, JUNE, CONICAL SCANNER (REARWARD LOOKING)

TIME OF EQUATORIAL CROSSING (GMT): 11 HOURS 0 MIN 0 SEC

TYPE OF SCAN: CONICAL REAR

RUN DATE: 08:16:17 04-01-76

SIMULATION DATE: 3-21-78

LATITUDE (DEG N)	LONGITUDE (DEG W)	TIME D	MO	YR	HR	M	S	SUN POSITION ZEN	AZIM	SAT HEAD	GEOM	ZEN	R AZ	CON AZ	SCAT ANG
70.00	-27.87	21	3	78	10	42	24	70.	187.	24.	1	18.	41.	24.	123.
											2	18.	7.	-24.	128.
60.00	-18.32	21	3	78	10	45	5	60.	177.	17.	1	18.	44.	24.	132.
											2	18.	4.	-24.	138.
50.00	-13.10	21	3	78	10	47	42	50.	171.	15.	1	18.	48.	24.	140.
											2	18.	0.	-24.	148.
40.00	-9.51	21	3	78	10	50	17	41.	165.	13.	1	18.	52.	24.	147.
											2	18.	4.	-24.	157.
30.00	-6.69	21	3	78	10	52	51	32.	157.	12.	1	18.	60.	24.	153.
											2	18.	12.	-24.	165.
20.00	-4.29	21	3	78	10	55	25	24.	144.	12.	1	18.	72.	24.	155.
											2	18.	24.	-24.	170.
10.00	-2.10	21	3	78	10	57	58	18.	122.	12.	1	18.	94.	24.	154.
											2	18.	46.	-24.	166.
0.0	0.00	21	3	78	11	0	31	17.	89.	12.	1	18.	126.	24.	149.
											2	18.	78.	-24.	158.
-10.00	2.10	21	3	78	11	3	4	21.	62.	12.	1	18.	154.	24.	142.
											2	18.	106.	-24.	149.
-20.00	4.29	21	3	78	11	5	38	28.	46.	12.	1	18.	170.	24.	134.
											2	18.	122.	-24.	140.
-30.00	6.69	21	3	78	11	8	11	37.	38.	13.	1	18.	179.	24.	125.
											2	18.	131.	-24.	130.
-40.00	9.51	21	3	78	11	10	45	46.	34.	14.	1	18.	183.	24.	116.
											2	18.	135.	-24.	120.
-50.00	13.10	21	3	78	11	13	20	55.	33.	16.	1	18.	186.	24.	107.
											2	18.	138.	-24.	111.
-60.00	18.32	21	3	78	11	15	57	65.	35.	19.	1	18.	188.	24.	97.
											2	18.	140.	-24.	101.
-70.00	27.87	21	3	78	11	18	38	75.	42.	28.	1	18.	190.	24.	87.
											2	18.	142.	-24.	91.

TABLE 20. GEOMETRY SYNOPSIS; 11:00 AM ORBIT, MARCH, CONICAL SCANNER (REARWARD LOOKING)

TIME OF EQUATORIAL CROSSING (GMT): 11 HOURS 0 MIN 0 SEC

TYPE OF SCAN: CONICAL REAR

RUN DATE: 08:15:17 04-01-78

SIMULATION DATE: 12-21-77

LATITUDE (DEG N)	LONGITUDE (DEG W)	TIME D	MO	YR	HR	M	S	SUN POSITION ZEN	AZIM	SAT REAR	GEOM	ZEN	R AZ	LOS AZ	SCAT ANG
70.00	-27.47	21	12	77	10	42	24	94.	188.	28.	1	18.	40.	24.	100.
											2	18.	8.	-24.	104.
60.00	-18.32	21	12	77	10	45	5	83.	180.	17.	1	18.	42.	24.	110.
											2	18.	6.	-24.	114.
50.00	-13.10	21	12	77	10	47	42	74.	176.	15.	1	18.	43.	24.	119.
											2	18.	5.	-24.	124.
40.00	-9.51	21	12	77	10	50	17	64.	172.	13.	1	18.	45.	24.	128.
											2	18.	3.	-24.	134.
30.00	-6.69	21	12	77	10	52	51	54.	169.	12.	1	18.	47.	24.	136.
											2	18.	1.	-24.	144.
20.00	-4.29	21	12	77	10	55	25	45.	165.	12.	1	18.	51.	24.	144.
											2	18.	3.	-24.	153.
10.00	-2.10	21	12	77	10	57	58	36.	159.	12.	1	18.	57.	24.	151.
											2	18.	9.	-24.	162.
0.0	0.00	21	12	77	11	0	31	27.	150.	12.	1	18.	66.	24.	155.
											2	18.	18.	-24.	169.
-10.00	2.10	21	12	77	11	3	4	20.	133.	12.	1	18.	82.	24.	155.
											2	18.	34.	-24.	169.
-20.00	4.29	21	12	77	11	5	38	17.	105.	12.	1	18.	111.	24.	152.
											2	18.	63.	-24.	162.
-30.00	6.69	21	12	77	11	8	11	18.	74.	13.	1	18.	143.	24.	146.
											2	18.	95.	-24.	153.
-40.00	9.51	21	12	77	11	10	45	25.	54.	14.	1	18.	164.	24.	138.
											2	18.	116.	-24.	144.
-50.00	13.10	21	12	77	11	13	20	33.	45.	16.	1	18.	175.	24.	129.
											2	18.	127.	-24.	134.
-60.00	18.32	21	12	77	11	15	57	42.	42.	19.	1	18.	181.	24.	120.
											2	18.	135.	-24.	125.
-70.00	27.87	21	12	77	11	18	38	52.	46.	28.	1	18.	186.	24.	111.
											2	18.	138.	-24.	114.

TABLE 21. GEOMETRY SYNOPSIS; 11:00 AM ORBIT, DECEMBER, CONICAL SCANNER (REARWARD LOOKING)

TABLE 22. SUMMARY OF SCATTERING ANGLE STATISTICS; FOR LATITUDES FROM 70°N TO 70°S, IN INCREMENTS OF 5°

	9:30 AM ORBIT			11:00 AM ORBIT		
MODE OF SCAN	LINEAR	CONICAL	REARWARD CONICAL	LINEAR	CONICAL	REARWARD CONICAL
SCATTER ANGLE EXTREMES						
• MAX.	157.8	157.9	156.6	177.1	177.4	175.4
• MIN.	73.2	68.9	66.4	84.0	68.4	67.4
AVG. SCATTER ANGLE DURING ONE SCAN						
• MEAN OVER LATITUDES	125.2	125.5	122.2	136.4	135.6	133.9
RANGE OF SCATTER ANGLES DURING ONE SCAN						
• MEAN OVER LATITUDES	12.3	11.2	10.8	7.6	7.0	6.7
• MAX	16.0	14.5	14.5	16.0	14.4	14.5
• MIN	7.5	7.1	6.6	2.4	2.6	1.9

TABLE 23. FACTORS AND LEVELS FOR REFLECTIVE-BAND RADIANCE SIMULATIONS

FACTOR	NO. LEVELS	LEVELS
SCAN MODE	2	LINEAR and CONICAL
SCAN ANGLE	5	LINEAR: 0°, $\pm 4^{\circ}$, $\pm 8^{\circ}$ zenith CONICAL: 0°, $\pm 12^{\circ}$, $\pm 24^{\circ}$ azimuth
TIME OF DAY	2	9:30 AND 11:00 AM SOLAR TIME
DAY OF YEAR	3	21st of JUN, MAR/SEP, and DEC
ATMOSPHERIC HAZE (Visual Range)	4	20 and 23 KM (Clear), and 8 and 10 KM (Hazy)
SPECTRAL BAND	7	For atmospheric effects simulations: 0.45-0.52 μm 0.52-0.60 0.63-0.69 0.74-0.80 0.80-0.91 0.74-0.91 1.55-1.75
	6	For total radiance simulations (1.55-1.75 μm excluded)
SURFACE VEGETATION	2	Dense green wheat (79% ground cover) Sparse green wheat (14% ground cover)

TABLE 24. REFLECTANCE VALUES USED IN THE SIMULATIONS

QUANTITY	AVERAGE REFLECTANCE IN DESIGNATED SPECTRAL BAND						
	0.45 to 0.52	0.52 to 0.60	0.63 to 0.69	0.74 to 0.80	0.80 to 0.91	0.74 to 0.91	1.55 to 1.75
1. DENSE GREEN VEGETATION							
a. Relative Bidirectional Reflectance	0.030	0.051	0.032	0.467	0.484	0.478	N/A
b. Diffuse Reflectance	0.023	0.042	0.025	0.441	0.457	0.452	N/A
2. SPARSE GREEN VEGETATION							
a. Relative Bidirectional Reflectance	0.068	0.106	0.128	0.283	0.294	0.290	N/A
b. Diffuse Reflectance	0.054	0.086	0.099	0.270	0.280	0.276	N/A
3. BACKGROUND ALBEDO, (Average Green Leaf Reflectance)	0.082	0.138	0.120	0.46	0.50	0.48	0.320
4. SOIL REFLECTANCE (Condit's Mean Spectrum)	0.111	0.163	0.223	0.262	0.273	0.269	N/A

TABLE 25. CORRELATION MATRICES FOR TOTAL RADIANCES; BETWEEN SPECTRAL BANDS AND SCATTERING ANGLE

A. BOTH HAZY AND CLEAR CONDITIONS

VARIABLE							
TPB45.52	1.0000						
TPB52.60	.9519	1.0000					
TPB63.69	.8057	.9360	1.0000				
TPB74.80	.4822	.6399	.6051	1.0000			
TPB80.91	.4595	.6215	.5922	.9996	1.0000		
TPB74.91	.4682	.6285	.5972	.9998	.9999	1.0000	
SCAT ANG	.8161	.7730	.6156	.3854	.3635	.3719	1.0000
	TPB45.52	TPB52.60	TPB63.69	TPB74.80	TPB80.91	TPB74.91	SCAT ANG

B. HAZY CONDITIONS (V = 8 AND 10 KM)

TPB45.52	1.0000						
TPB52.60	.9611	1.0000					
TPB63.69	.8257	.9386	1.0000				
TPB74.80	.4805	.6298	.6255	1.0000			
TPB80.91	.4497	.6034	.6059	.9993	1.0000		
TPB74.91	.4615	.6136	.6135	.9997	.9999	1.0000	
SCAT ANG	.8457	.8394	.7019	.4300	.4011	.4122	1.0000
	TPB45.52	TPB52.60	TPB63.69	TPB74.80	TPB80.91	TPB74.91	SCAT ANG

C. CLEAR CONDITIONS (V = 20 AND 23 KM)

TPB45.52	1.0000						
TPB52.60	.9426	1.0000					
TPB63.69	.8018	.9407	1.0000				
TPB74.80	.5240	.6777	.5916	1.0000			
TPB80.91	.5085	.6665	.5842	.9998	1.0000		
TPB74.91	.5144	.6708	.5870	.9999	1.0000	1.0000	
SCAT ANG	.8536	.7405	.5477	.3486	.3323	.3385	1.0000
	TPB45.52	TPB52.60	TPB63.69	TPB74.80	TPB80.91	TPB74.91	SCAT ANG

REFERENCES

1. LaRocca, A. J., and R. E. Turner, Atmospheric Transmittance and Radiance: Methods of Calculation, IRIA State-of-the-Art Report No. 107600-10-T, Environmental Research Institute of Michigan, Ann Arbor, June 1975.

2. Turner, R. E., Radiative Transfer in Real Atmospheres, Report No. NASA CR ERIM 190100-24-T, Environmental Research Institute of Michigan, 1974.

3. Suits, G. H., "The Calculation of the Directional Reflectance of a Vegetative Canopy", Remote Sensing of Environment, Vol. 2: 117-125, 1972.

4. Smithsonian Meteorological Tables, R. J. List, Preparer, Smithsonian Institution Press, Washington, D.C., 6th Ed., 1971.

5. Turner, R. E., W. A. Malila, and R. F. Nalepka, "The Importance of Atmospheric Scattering in Remote Sensing...", Proceedings of Seventh International Symposium on Remote Sensing of Environment, Publication No. 10259-1-X, Willow Run Laboratories, The University of Michigan, Ann Arbor, Mich., May 1971.

6. Condit, H. R., "The Spectral Reflectance of American Soils", Photogrammetric Engineering, Vol. XXXVI, No. 9:955-966, Sept. 1970.

7. Malila, W. A., and R. F. Nalepka, "Atmospheric Effects in ERTS-1 Data, and Advanced Information Extraction Techniques", Proceedings of Symposium on Significant Results Obtained from the Earth Resources Technology Satellite-1, NASA SP-327, pp. 1097-1104, Mar. 1973.

DISTRIBUTION LIST

NASA/GODDARD SPACE FLIGHT CENTER, GREENBELT, MD 20771

Dr. Lou Walter, Code 920.0	(25)
Dr. William Nordberg, Code 900.0	(1)
Dr. Stan Freden, Code 902.0	(1)
William Stroud, Code 110.0	(1)
Dr. Charles Schnetzler, Code 923.0	(1)
Dr. John Barker, Code 923.0	(1)
Marvin Maxwell, Code 943.0	(1)
Oscar Weinstein, Code 726.0	(1)

NASA HEADQUARTERS, WASHINGTON, D.C. 20546

William Stoney, Code ER	(1)
Ruth Whitman, Code ERR	(1)
Jim Morrison, Code ERR	(1)

NASA/JOHNSON SPACE CENTER, HOUSTON, TX 77058

Clifford Charlesworth, Code HA	(1)
R. M. Elder, Code BB63	(1)
Jay Harnage, Jr., Code HC	(25)
Richard Moke, Code HC	(1)
Retha Shirkey, Code JM6	(1)
Dr. Glenn Smith, Code HD	(1)
Robert MacDonald, Code TF	(1)
Ted Sampsel, Code ED6	(1)